Simultaneous Serologic and Phenotypic Analyses of Blood on Silicon Photonics

Pakapreud Khumwan

A dissertation

submitted in partial fulfillment of the

requirements for the degree of

Doctor of Philosophy

University of Washington

2018

Reading Committee:

Daniel Ratner, Chair

Barry Lutz

Mark Wener

Program Authorized to Offer Degree:

Bioengineering

University of Washington

Abstract

Simultaneous Serologic and Phenotypic Analyses of Blood on Silicon Photonics

Pakapreud Khumwan

Chair of the Supervisory Committee:
Associate Professor Daniel Ratner
Bioengineering

Blood loss is one of the leading causes of hospital-related mortality. Severe degree of exsanguination of trauma patients requires massive blood transfusion in which multiple units of blood products are administered for the fluid resuscitation. Despite our good understanding of blood group compatibility in transfusion medicine, the process of transfusion in the emergent scenarios is still challenged by the underrepresentation of competitive technologies commercialized specifically to perform rapid blood testing at the site of transfusion. Racing against time, trauma physicians are constrained by urgency to administering universal blood units, such as type-O red blood cells, to the patients. Given the diversity of blood groups and their different prevalence across demographic backgrounds, a lack of thorough profiling of patients' red blood cell phenotypes and plasma antibodies prior to transfusion could ensue both acute and chronic adverse side effects that may further complicate their possible transfusions and pregnancy in the future.

The ultimate goal of the research described in this dissertation is to expedite the process of serologic and phenotypic characterizations of blood to determine the patient's blood type, allowing for better matched blood products to be delivered. With its emerging roles in rapid, real-time biosensing applications, silicon photonics has actively been explored in the development of various clinical assays following both label-based and label-free strategies. To address the aforementioned unmet need for reduced transfusion turnaround time, we took advantage of the multiplexed feature of silicon photonic sensors for simultaneous serologic and phenotypic analyses of ABO/RhD blood group systems by combining the forward and reverse typing assays on a single sensor chip. The first two chapters of this dissertation provide necessary backgrounds in silicon photonics and blood transfusion. The third and fourth chapters are dedicated to laying the groundwork for the method development of forward and reverse typing assays and discussing preliminary results. Lastly, the final chapter, built upon the previous chapters, describes the process of developing multiplexed sensors capable of performing both forward and reverse typing. Based on our current accomplishments, future improvements upon assay optimization and device miniaturization could undoubtedly help translate this technology into the clinical use.

TABLE OF CONTENTS

LIST OF FIGURES

LIST OF TABLES

ACKNOWLEDGEMENTS

The beginning of a story of this dissertation is traced back to a genuine need for a more rapid blood typing by Dr. Jill Johnsen who, together with my advisor, Prof. Daniel Ratner, has been trying to realize her envision of an ideal bedside typing technology. Throughout my involvement in the LSDF project, I have learned a great deal of knowledge that covers not only science, but also work ethics from Dr. Johnsen. As a physician, she also saved my life once from deep vein thrombosis, which coincidentally is her medical specialty. I could not express enough gratitude for her helps and guidance. This work, nevertheless, could not be completed without collaborative efforts of Kerry Lannert, who has been involved in the process of tube testing and data analysis, Dr. Jing Shang, who established the initial testing paradigm based on the methods pioneered by Dr. James Kirk, and lastly Dr. Adam Munday, who devoted his time to the anti-RhD functionalization strategy.

I would like to thank my committee members: Prof. Valerie Daggett, Prof. Lih Lin, Prof. Barry Lutz and Dr. Mark Wener for your continuous supports since my qualifying exam. I truly appreciate the Molecular Medicine Certificate Program (MMTP) for the unique opportunity to shadow physicians at the Seattle's Children Hospital and the Department of Medical Genetics. My study at the university of Washington, like other fellow graduate students', had gone through an emotional rollercoaster, but in the end I could always see myself standing on the bright side thanks to the comradeship and moral supports from my colleagues at the Department of Bioengineering, particularly Nuttada Panpradist, and a chosen family of international students who periodically gathered to uplift one another. I would like to thank my parents, who gave me a freedom to pursue the education I wanted and always tried to offer their helps to make my life seven thousand miles away from home progress as smoothly as it can.

Above all, I am deeply indebted to Prof. Daniel Ratner who gave this opportunity to me to work on this translational research project that has a positive impact on the current care of patients. Words cannot describe how fortunate I am to be under your mentorship, and I do appreciate everything you have done to me. Your caring nature is felt by everyone around your presence. Beyond work, I also feel privileged that we share similar interests in music, food and cultures that have strengthened our bonds over the course of my Ph.D. journey.

This ten-year stretch of my higher education in the United States is made possible by a ceaseless support from the Royal Thai Government and National Science and Development Agency of Thailand (NSTDA). I would like to express my sincere gratitude towards all staff at the Office of Educational Affairs of the Royal Thai Embassy for your services and integrity. I also appreciate other funding sources, particularly LSDF, NSF, Coulter Foundation and HHMI, that have helped contribute to the completion of my study. Finally, I would like to thank the German Academic Exchange Service (DAAD) for an undeniable, life-changing internship opportunity in Dresden, Germany.

DEDICATION

To both of my grandmothers who passed away during my academic pursuit in the United States, your teaching and nurture are the most valuable assets I could ever be endowed with. To Ronnie Houchin, the friendship and solidarity we share have shaped me into who I currently am. To Nils Frahm, your blessing verbal support: “See things in a positive light,” has solemnly carried me through my doctorate.

Chapter 1 : The Clinical Significance of *In Vitro* Diagnostics and Emerging Role of Silicon Photonic Biosensors in Point-of-Care Testing

1.1 Significance of *In Vitro* Diagnostics in Patient Care

In vitro diagnostics (IVD) are medical tests, assays or equipment used for the purpose of evaluating patient's bodily fluids, e.g. blood, urine, saliva, etc., outside his or her body. In contrast to *in vivo* diagnostics, such as the skin test for tuberculosis, that is performed inside the body, IVD offers minimally invasive or noninvasive alternatives to diagnosing diseases and monitoring patient's conditions. Over the years, IVD tests have become a vital part of patient care and disease management due to the abundance of commercially available options that span nearly all major medical specialties, such as biochemistry, immunoassays, transfusion medicine, hematology, coagulation, microbiology, molecular diagnostics and cytology. IVD industry has been active and continues to grow at a 4% annual growth rate with a projected market worth of $65 billion in 2018 (**Table 1-1**).[1] This lucrative potential growth and market competition have driven new innovations and improvement upon the sensitivity, accuracy and user-oriented design of IVD products. In developed countries, one key aspect of IVD instrumentation is the focus upon assay automation aimed to be installed in core, centralized laboratories in hospitals. This automated streamline of assays not only reduces clerical errors in sample handling, but also trims down the cost-per-assay due to its high throughput. In addition, there is a cost incentive in health care expenditure associated with using IVD to determine the early onset of treatable diseases that helps foster the adoption of standard IVD tests in the process of patient care.[2]

However, recent technological advances in wireless communication, data processing, device miniaturization and microfluidics have shifted disease diagnoses to decentralized services that may not require high-end instruments and experienced medical technicians.[1] The lateral flow

technology on paper-based diagnostics and related microfluidic platforms is the important factor that generates a large demand for diagnostic test decentralization.[3] Thus, it is highly possible that the IVD manufacturers will focus their efforts on producing tests or instruments that can be readily used in the point of care or resource-limited settings in the near future to expand their supply simultaneously in both developed and developing countries with emerging IVD markets.[1]

Table 1-1. Sales of in vitro diagnostic reagents in 2013 and 2018.[1]

Test Segment	Sales in 2013	% Mkt	Sales in 2018	% Mkt
Clinical chemistry	7,725	14	8,325	13
Immunoassay				
• Infectious disease	6,230	11	7,400	11
• Other immunoassays	7,675	14	8,525	13
• Blood bank Screening	690	1	740	1
• Diabetes HbA1c	350	1	690	1
Hematology	2,840	5	3,100	5
Microbiology (ID/AST)	3,795	7	4,790	7
Microbiology, molecular	2,445	4	3,430	5
Radioimmunoassay	300	1	300	-
Coagulation	1,200	2	1,360	2
Histology/Cytology	2,455	4	3,510	5
HPV, molecular	370	1	550	1
Nucleic acid assay	670	1	1,230	2
Blood typing	690	1	780	1
Blood bank molecular	990	2	1,300	2
Flow cytometry	1,170	2	1,280	2
Circulating tumor cells	23	0	75	0
POC, OTC diabetes	7,897	15	9,100	14
POC, OCT other	987	2	1,071	2
POC, professional/ hospital	6,053	11	7,410	12
Total	54,557	100	64,966	100

1.1.1 Point-of-Care Diagnostics in Near-Patient Settings

Decentralization of diagnostic tests has been ongoing since 1960s-1980s after the advent of over-the-counter pregnancy test strip and blood glucose sensor capable of providing instantaneous

results.[4,5] Point-of-care (POC) devices by their virtue convey a notion of portability that permits them to be utilized in various places where access to core laboratory is limited. The term of "point-of-care" can refer to multiple settings where care takes place, such as patient bedsides, doctor's offices, emergency rooms, operating rooms, critical care units or even at sites of disaster. Similar to IVD, the goal of POC diagnostics is to provide accurate and rapid tests to improve patient care.[4] Patients can now easily access a more variety of POC tests for drugs of abuse and sexually transmitted diseases (STDs) from drugstores or online marketplaces. The marketing target of POC devices is not limited only to patients. In many hospitals, in-patients are monitored for blood electrolytes and hematocrits at the bedside by handheld devices (e.g. Abbot's iStat or Roche's Cobas systems). A newer generation of hospital POC devices are microfluidics-integrated and capable of performing more advanced assays in molecular biology, such as isothermal nucleic acid amplification, quantitative polymerase chain reaction (qPCR) and sequencing.[6] All POC devices mentioned above are a subtype of IVD that enables *in vitro* diagnostic tests to be performed closer to patients, leading to a change in the patient management.[7]

The most important driving attribute unique to POC devices in the patient care process is a rapid turnaround time (TAT or time-to-result) of the test that allows patients to receive results during a doctor visit, thereby helping providers make appropriate clinical decisions faster.[8,9] Rapid TAT can undoubtedly be a desirable aspect in time-sensitive situations such as blood transfusion in trauma care. A retrospective study conducted in the United Kingdom has shown that patients who received an anticoagulant (Coumadin) therapy had benefited from POC devices that reduced the clinic visit time by 35 minutes on average and prevented possible delays from a core laboratory.[10] Other drivers in the POC industry include (1) new detection techniques that permit tests to be performable on POC platform, (2) increasing importance of personalized medicine in certain disease contexts, (3) expansion of small clinics and laboratories, (4) diseases, treatments

or acute conditions that require immediate monitoring and responses, and (5) miniaturization and microfluidic integration that improve device's throughput and multiplex.[4,11]

While blood glucose, cholesterol and blood electrolytes are still the staples of POC tests in the market, other options for analyzing coagulation, cardiac markers, urine and fecal occult blood, infectious diseases, C-reactive protein (CRP), D-Dimer, whole blood lactate, B-type Natriuretic Peptide (BNP) and HbA1c are available.[1] The world's market of POC devices is largest in the United States, growing by 2.8% from 2010 to 2011 with a projected worth of $16.5 billion in 2016 (**Table 1-2**).[8] In 2011, the market worth of POC tests was estimated at $16.7 billion worldwide, of which $10.7 billion went to self-testing devices and the remainder went to professional use.[11] The market for POC is expected to expand with the annual growth rate of 4% from 2013 onward, making it $17.6 billion in worth in 2018.[1]

Table 1-2. Global POC market forecast through 2016 ($ millions).[8]

Test type	2009	2010	2011	2016
Glucose monitoring	7,760	7,650	7,503	7,600
Blood chemistry and electrolyte	2,185	2,210	2,251	2,850
Pregnancy and fertility	793	815	851	100
Cardiac markers	619	801	1,025	2,010
Drug and alcohol	503	490	498	565
Infectious disease	391	284	412	687
Cholesterol	367	372	387	470
Hemoglobin/hemostasis	360	375	409	585
Urine chemistry	215	233	258	370
Tumor marker	196	203	215	350
Total	13,389	13,434	13,809	16,537

Despite their potential advantages in reducing hospital facility cost and offering a rapid turnaround time of test results, POC tests are often criticized for an insufficient reimbursement[6,12] and their higher per-test costs compared to their standard IVD counterparts that are automated.[10,11] However, the use of point-of-care blood analyzer in pediatrics unit has shown

otherwise that a fast TAT could help reduce the number of neonates requiring transfusion, hence, saving the cost of care by 8.3%.[13] Clinical benefits in other scenarios may include accuracy from using fresh specimens from patients that in turn brings about a better decision on the treatment regiments for patients, particularly in hematology and thrombosis. In resource-limited settings and developing countries, POC devices can alleviate the cost obstacles associated with a lack of access to expensive instruments that are only available in the centralized labs, skilled technicians and instrument maintenance services.[9,14] Thus, the advantages of POC devices in developed and developing worlds come from a different angle. In response to the remaining cost concern, device miniaturization and lab-on-a-chip technology can be leveraged in the manufacture of affordable multiplexed sensor arrays that have sufficient sensitivity for performing clinical assays in various disease contexts.[15–20] In the next section, a type of silicon photonic cavity sensors will be discussed for its emerging role in biosensing and applications in medical POC tests.

1.2 Label-Free Microring Resonator Sensors

Despite their current application in biosensing, silicon photonic devices are originally invented for optical manipulation purposes in telecommunication, such as spectral filters and switches,[21–23] and they are still being used nowadays in data centers and mobile companies. Although their emerging role as a biosensor has only been largely explored and researched in the previous decade, the first observation of label-free “biosensing” on metal surface was first reported in 1937 in an attempt to quantify the thickness of adsorbed biomolecule monolayers based on the change in the colors of surface.[24] Owing to the present established CMOS fabrication techniques, silicon photonic devices can be designed to have complex architectures that support multiplexing by combining a large number of devices into arrays. Individual photonic sensors can be interrogated in real-time, offering a unique functionality that may not always exist in other label-free test platforms.[25] The silicon photonic device that will be discussed in this dissertation is a type of a

microcavity resonator called microring resonator or sometimes ring resonator for brevity. Microring resonator is a ring shaped circular waveguide that serves as an optical path for near-infrared (NIR) laser light to propagate through in the resonance condition. The principle of operation of microring resonators as a biosensor is discussed in the following section.

1.2.1 Principle of Photonics

The biosensing application of silicon photonics is enabled by near-infrared (NIR) light that propagates inside a silicon waveguide via total internal reflection (**Figure 1-1**). A guiding layer with a refractive index, n, lies on top of the substrate later with a refractive index, n_s. Air, water and other surrounding media with a refractive index, n_a, are represented as the superstrate layer beyond the boundary of a guiding layer. When the light is introduced into a waveguide such that the angle (θ) is larger than the critical angle of the waveguide-superstrate interface, light will be in a total internal reflection and continue to propagate along the waveguide. Waveguides can be integrated with other optic elements, such as prism, grating or mode couplers, etc., to couple the light into a waveguide.[25] Grating couplers used on our biosensing platform are often preferred over other types of the couplers for their low back-scattering and small footprints. Although the optical mode (oscillating electromagnetic field) is mostly confined in the core of the waveguide after total internal reflection takes place, a portion of it referred to as the evanescent field does not propagate along with the light, but rather are concentrated on the waveguide's interface.

Owing to the intensity of the evanescent field that decays exponentially with respect to the distance from the waveguide boundary, this gives the waveguide the ability to interact with molecules that bind to its surface and increase the effective refractive index of the local medium surrounding the waveguide. While there are several types of sensor devices that are sufficiently sensitive for performing label-free detection, silicon photonic sensors are more appealing than

other competitive technologies, e.g. surface plasmonic, mechanical and electrochemical sensing, because photonic devices (1) have high manufactural reproducibility, (2) can be designed into arrays owing to their small footprints for high throughput and multiplexed screening, and (3) gain benefits from the economy of scale of the well-established CMOS fabrication processes. Silicon photonic devices are available in various types with different physical and optical characteristics that lend themselves utilizable in different sensing applications. Some of the high-performance devices include Fabry-Perot oscillator,[26–28] micro-disks[29], photonic crystal cavities,[30,31] and microring resonators.

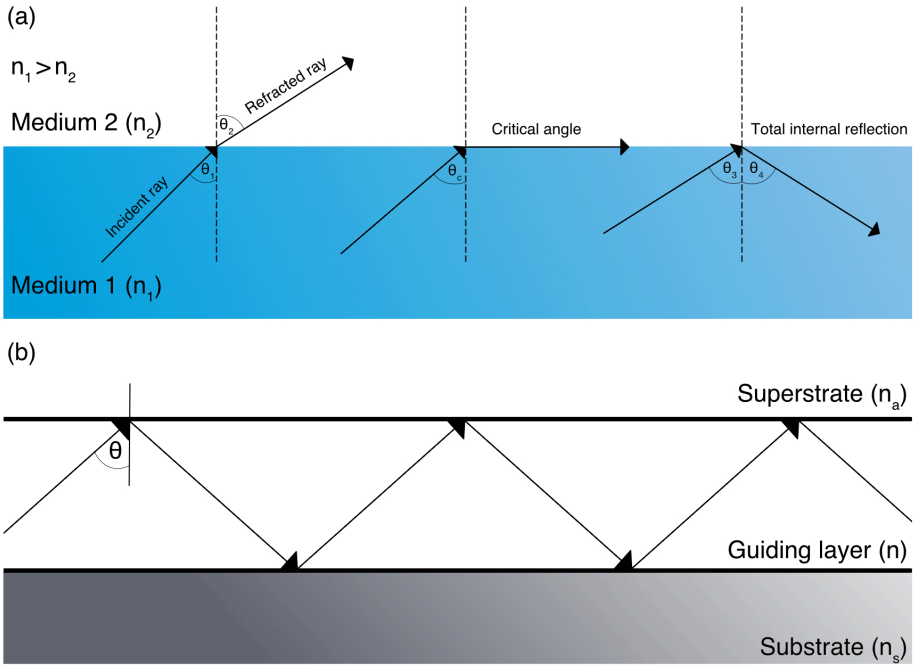

Figure 1-1. Schematic illustration of the light refraction from a slow medium to a fast medium (**a**). The light ray bends away from the normal towards the interface of the two media. Total internal refraction occurs when the incident angle is larger than the critical angle (θ_c). Light propagates through a guiding layer (e.g. silicon) between the superstrate (e.g. water, air) and substrate (e.g. buried oxide) layers by total internal reflection when the refractive index of the guiding layer (n) is larger than the refractive index of the superstrate layer (n_a) (**b**).

For a microring resonator, light can be coupled into the microring via evanescent field from the linear bus waveguide positioned in a close proximity to the microring. Propagating light completes its loop around the circular path length with the phase shift of wavelength equivalent to integer multiples of 2π. The wavelength will interfere constructively resulting in a cavity in resonance, which takes place when the circumference of the microring is a multiple of the wavelength (**Equation 1-1**).[32] The resonance condition in the microring resonator is very sensitive to the refractive index change of the medium surrounding the waveguide. This is useful for biosensing because deposition or binding of biomolecules can result in a local mass accumulation above the sensor, producing the change in refractive index that increases the resonance wavelength, or deceases it when the mass is depleted (**Figure 1-2**). Critical coupling occurs when the tunable laser's wavelength matches the resonance wavelength, causing light to be "trapped" inside the microring resonator and creating an observable dip in the spectrum of the output power of the linear waveguide. Three factors that influence the strength of the coupling are, (1) the tangential spacing between the microring and the linear bus waveguide (typically around 180-240 nm), (2) dielectric constant of the medium surrounding the cladding and (3) refractive index contrast of the waveguide.[33]

As light travels through the waveguides and microring resonators, there are two modes at which the electromagnetic field can be polarized. For a common microring resonator whose width is greater than height, the ground mode will be a quasi-transverse electric (TE) polarization where strong discontinuity is observed on the sidewall of the surface. The transverse magnetic (TM) mode, on the other hand, has a strong discontinuity on the top and bottom surface of a waveguide (**Figure 1-3**). The type of microring resonator used to perform biological assays in this dissertation operates exclusively based on the transverse electric (TE) polarization.

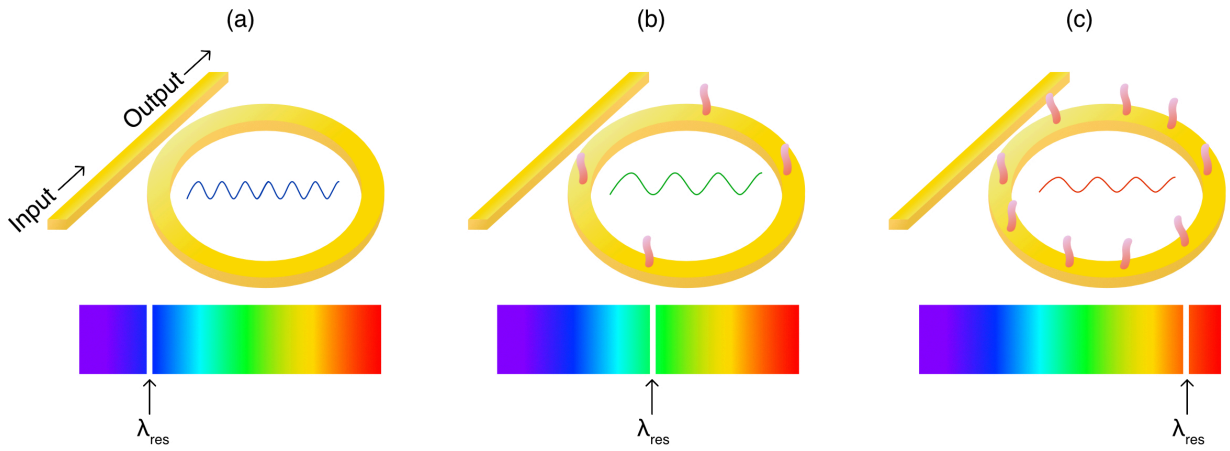

Figure 1-2. Operating principle of microring resonators. Microring resonator couples light from the waveguide and resonates light at particular wavelength (**a**). Mass accumulation increases the local refractive index around the microring resonator, causing the resonance wavelenth to red-shift towards a higher wavelength (**b**). Resonance wavelength continues to increase as higher masses accumulate over the sensor (**c**).

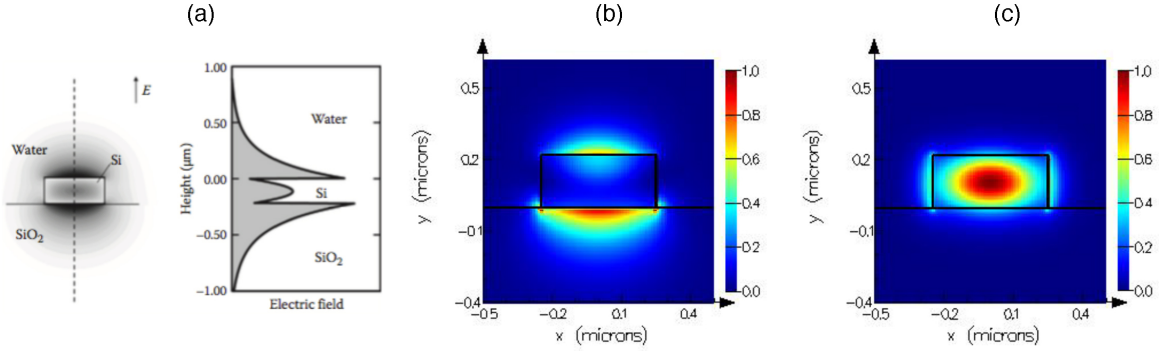

Figure 1-3. Evanescent field profiles of TE and TM waveguides. Evanescent field decays exponentially outside the boundary of silicon waveguide (**a**).[25] Simulations of the intensity of electric field for the transverse magnetic (TM) waveguide (**b**) and the transverse electric (TE) waveguide (**c**). (Figure courtesy of Dr. Shon Schmidt).

$$\lambda_{res} = \frac{2\pi r n_{eff}}{m} \qquad \text{(Equation 1-1)}$$

Equation 1-1 shows that the resonance wavelength (λ_{res}) is influenced by the circumference of the microring resonator and the effective refractive index (n_{eff}) where *m* is a positive integer. The refractive index is induced by the amount of mass deposition or depletion that occurs on the sensor surface. The change in the effective refractive index can be influenced by a small

perturbation of the local refractive index induced by the binding of molecules to the surface according to perturbation theory proposed by Kogelnik.[25,34] The effective refractive index, n_{eff}, can be mathematically determined in various ways, but it is simply also the ratio of the wavelength in vacuum and the wavelength of the waveguide mode.

$$n_{eff} = \frac{\lambda_0}{\lambda_{res}} \qquad \text{(Equation 1-2)}$$

For silicon on insulator (SOI) wafer, with the refractive indices of a silicon core and a silicon oxide cladding of 3.47 and 1.44, respectively, the resulting effective index is 2.34 with the confinement factors of 0.7624, 0.1193, 0.1088 and 0.0094 for silicon, buried oxide, bulk and sensing regions respectively.[35] Given the importance of how the local refractive index change can induce the sensor response measured by the resonance wavelength shift, it is important to design the waveguide to produce evanescent field that extends into the cladding at the right level. If the evanescent field is too localized to the sensor surface, the sensor would then not be able to interact much with the medium. If it is too far extending into the cladding, on the other hand, the sensor's response will mostly dominated by the bulk properties of the medium instead of molecular interactions that take place at the interface.

In a sensing application, the characteristics and performance of microring resonator and other photonic devices can be determined in a number of ways. Here, four figures of merit that are meaningful for sensors are the following: full width at half maximum (FWHM), Q-factor, FSR and sensitivity. FWHM describes the extent of the output spectrum between the two extreme values (minimum and maximum). FWHM can be mathematically expressed as shown in **Equation 1-3**, or directly measured from the width of the spectrum at half maximum.

$$FWHM = \frac{(1-ra)\lambda_{res}^{2}}{\pi n_g L\sqrt{ra}} \quad \text{(Equation 1-3)}$$

Where *r* denotes the self-coupling coefficient of microring, *a* denotes a single-pass amplitude transmission, and *L* denotes a circumference of the microring. Another related parameter used for describing the bandwidth of the spectrum in relative to the resonance wavelength is the Q-factor. In a physical sense, Q-factor is the oscillation in the field before the energy is depleted to 1/e of its starting energy. Q-factor can be defined as:

$$Q = \frac{\lambda_{res}}{FWHM} \quad \text{(Equation 1-4)}$$

For peak tracking, the extinction ratios (ratio of optical power when the light source is on and off) of greater than -10 dB provide enough good signal for tracking locations of the peak over the course of the assay.[32] The free spectral range (FSR) defined by spacing between peaks in the output spectrum is determined by the circumference of the microring resonator (L) and the group refractive index of the waveguide (n_g). FSR can be expressed as:

$$FSR = \frac{\lambda^2}{n_g L} \quad \text{(Equation 1-5)}$$

Where the group index (n_g) is defined as:

$$n_g = n_{eff} - \lambda_0 \frac{dn_{eff}}{d\lambda} \quad \text{(Equation 1-6)}$$

Sensitivity is defined as the change in the resonance wavelength (λ_{res}) with respect to a certain parameter of interest. For example, it can be defined in the context of the resonance wavelength

change influenced by the change in the local refractive index around the waveguide. Thus, **Equation 1-1** can be modified as,

$$\Delta\lambda_{res} = \frac{2\pi r \Delta n_{eff}}{m} \qquad \text{(Equation 1-7)}$$

In some biosensing applications, it might be useful to know the limit of detection (LoD) of the sensors. The limit of detection can be calculated from the limit of blank (LoB), which is average response of the negative control plus three times its standard deviation, and the standard deviation of the lowest concentration of a sample (SD_S) as seen from the following expression,

$$LoD = LoB + (c_\beta \times SD_S) \qquad \text{(Equation 1-8)}$$

Where c_β is approximately 1.65 for a type II error of 5%.[36]

1.2.2 Maverick M1 Biosensing System

The fabrication of silicon waveguides and microring resonators is compatible with techniques and instruments used in CMOS foundries, i.e. e-beam or photolithography. In the Ratner lab, we purchased silicon photonic microring resonator chips and the Maverick M1 optical reader from Genalyte, Inc., (San Diego, CA).[37] The current generation of Genalyte's microring resonator (IMEC-3) were fabricated by IMEC (Heverlee, Belgium). The microring resonator is designed to accommodate the center wavelength of 1,550 nm which is widely used in telecommunication. The resonator and other waveguides on the chip are 200×500 nm in height and width, respectively. The 1/e decay length of the evanescent field from the sensor surface on the chip was empirically determined at 63 nm, making it suitable for detecting analytes in tens of nanometers whereas that of a more sensitive SPR system typically extends out in hundred nanometers.[35] This value also

agrees with the empirically determined surface sensitivity of 64 nm/RIU based on a salt step characterization (**Figure 1-4**). The limit of detection in terms of mass per area is 1.5 pg/mm^2 or the total of 125 attograms for the total surface area of 66 μm^2 equivalent to putting down 500 IgG molecules.[35]

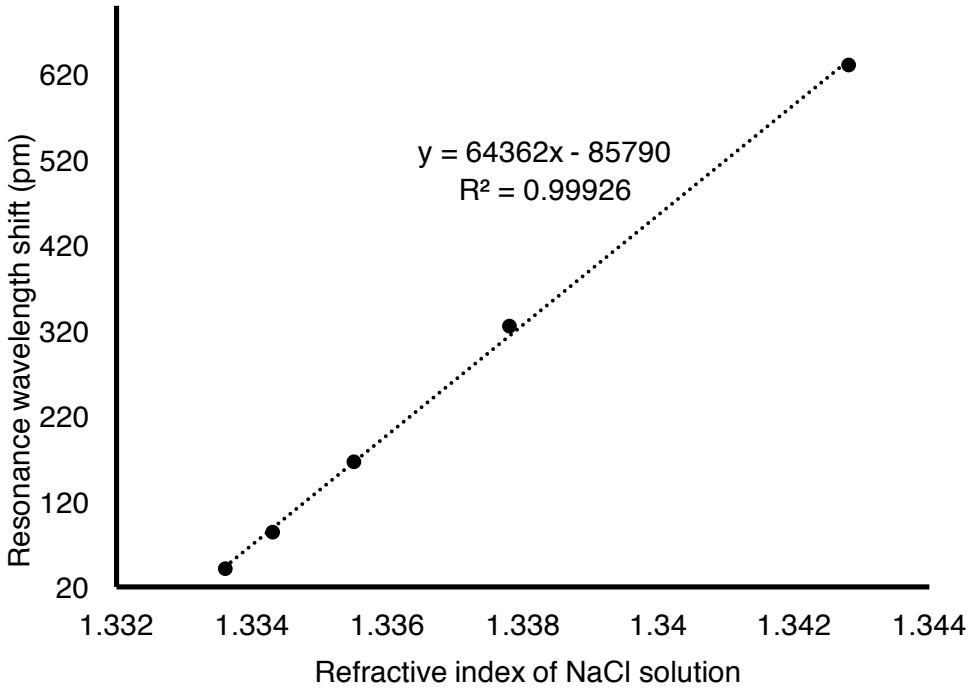

Figure 1-4. Salt step characterization of the IMEC-3 sensor chip. The surface sensitivity of 64 nm/RIU is determined from the slope of the sensor's response plotted with respect to the refractive index of each NaCl standard.

Genalyte's microring resonator exhibits favorable optical properties that make them utilizable in biosensing application owing to a high cavity Q-factor of more than 43,000 and an extinction ratio (ER) of higher than -10 dB with FSR of 5.98 nm (**Figure 1-5**).[33,38] There are 136 microring devices on the IMEC-3 chip where 128 devices can be used as sensors while the remainder serves as temperature and leak controls. These 128 functionalizable sensors are organized into clusters of four microring devices, and patterned into arrays forming two separate channels. Each channel or sensor array consists of 16 sensor clusters (**Figure 1-6**). During the

fabrication process, opening annular window features are created over clusters of four microring resonators by etching a wafer previously spin-coated with a chemically inert perflouropolymer cladding.

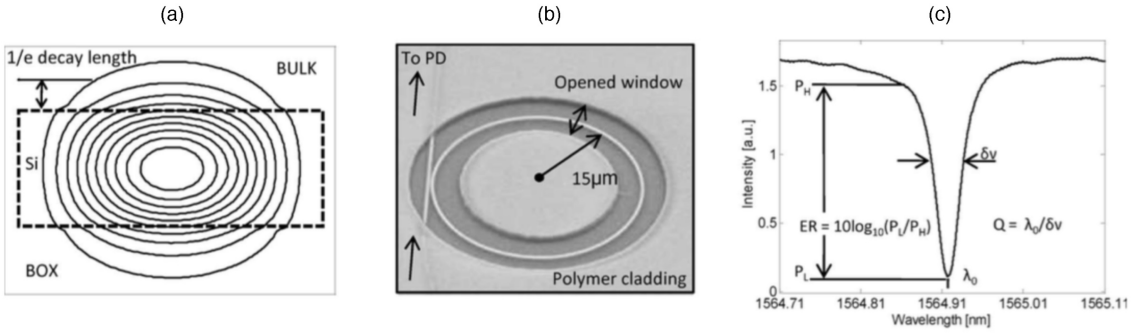

Figure 1-5. Physical characteristics of a microring resonator. FDTD mode profile of a silicon waveguide operated in a single-mode (**a**). Microring resonator has a diameter of 30 μm, but most of the sensor surface is clad under a protective layer with a 6-μm opening annular window that exposes microring resonator (**b**). The output spectrum has a dip corresponding to the resonance wavelength of the microring resonator (**c**).[39]

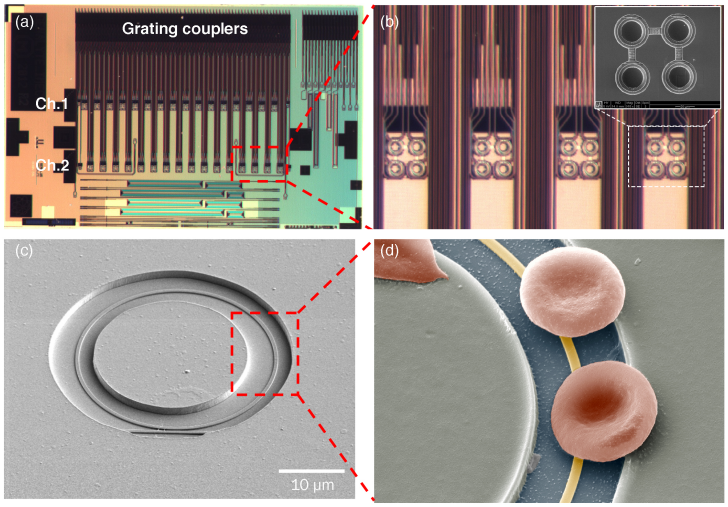

Figure 1-6. The architecture of an IMEC-3 chip. IMEC-3 chip consists of 128 individually addressable microring resonators. Microring resonators are organized into two sensor arrays forming separate channels with grating couples located on the top edge of the chip (**a**). Four microring resonators form individual clusters of sensors. There are 16 sensor clusters in each channel (**b**). Scanning electron micrograph of an individual microring resonator clad under a chemically inert polymer (**c**). Red blood cells (RBCs) are shown for scale in relative to the opening window of the silicon waveguide (**d**).

The user-oriented design of the Maverick M1 optical system genuinely answers the need for POC devices to require no highly-trained personnel. In its current and past designs, the instrument optically accesses the sensor chip via an opening space on the top side of the chip where input and output grating couplers for individual microring resonators are located and scanned via tunable laser. Genalyte's automated chip alignment algorithm helps reduce vibrations associated with unstable manual chip handling during the chip registration (**Figure 1-7**). During this process, a scanner consisting of two tip-tilt mirrors will raster across the grating coupler array on the top side of the chip. When the beam finds grating couplers, the light will travel along the waveguide in the optical loop and exits at the output grating coupler also located on the same array, allowing the automated software to determine the positions of grating couplers assigned to each microring device.

During data acquisition, the laser beam will excite each sensor device by entering the optical loop via the input grating coupler. Output light from the output grating coupler is captured by the scanner and directed to a photodetector. The laser is set to trigger the sensor at specific time interval before the spectra of output signal is captured and processed by the data acquisition electronics. The scanner will move along grating coupler array to scan the next sensor until all devices are scanned in one round of read. Samples are prepared in the 96-well plate that can be loaded onto a 3-axis robotic stage. Fluid is introduced and flowed across the two channels of the sensor chip via tubes connected to syringe pumps controlled by software. Data are acquired and processed in the controller board and visualized in the application software as resonance wavelength shifts with respect to time.

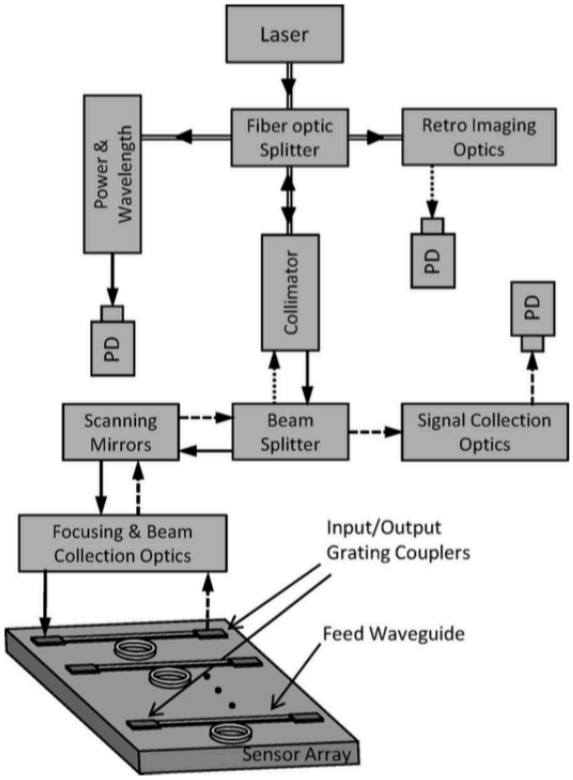

Figure 1-7. Schematic of the Maverick M1 optical scanner's chip registration and data acquisition processes.[39]

The idea of using microring resonators as biosensors was first proposed in 2001.[29,40] The silicon photonic Maverick M1 system currently being used in the Ratner Lab was designed and distributed by Genalyte, Inc., that pioneered and marketed silicon photonics as a commercial biosensing platform. Genalyte initially reported that the primary binding curve of 1 μg/mL protein concentration, or higher, could be observed on the system.[33] The silicon dioxide passivation layer on the sensor surface is compatible with well-characterized surface modification techniques, such as silane and coupling chemistries, that allow the sensor to be functionalized with appropriate capture molecules. With the intrinsically multiplexed feature of the IMEC-3 chip consisting of 128 individually addressable microring devices, Genalyte has since their early successes been developing high-throughput assays that address clinical needs in various specific medical areas.

As of 2018, Genalyte has been pursuing a rapid blood test for hematology, pathogen screening and immunology aimed to be used in decentralized or mobile laboratories. One of the commercially available products is the anti-adalimumab antibody (ADA) test for rheumatoid arthritis and Crohn's patients that detects multiple subclasses of antibodies, particularly IgG4 in which traditional bridging assay can sometimes give false negative results. In addition to developing their own commercial tests, Genalyte previously also distributed unfunctionalized sensor chips to their academic partners for research purposes. This contributes greatly to their publicity that demonstrates the suitability of the Maverick M1 system in detecting diverse types of biomolecules, from small to large, as it has been used for capturing nucleic acid,[41–43] cytokines,[44–46] viral particles,[33,47] and other disease antigens.[48–50] To maintain or improve the sensor's compatibility with complex biological fluids, several attempts were made in the field of biosensing research to improve the signal-to-noise ratio either by coating the surface with anti-fouling materials[51–56] or by amplifying signals with secondary antibody, precipitated products of an enzymatic reaction[45,48] or polymer beads.[33,57] **Table 1-3** provides a summary of assays that are developed on the microring resonator platform on the Maverick M1 system and other similar non-commercial setups.

Table 1-3. Biosensing applications of microring resonators on the Maverick M1 and other non-commercial platforms.

Application	Surface functionalization technique	Signal amplification	Limit of detection	Ref
Detection of interleukin-2 (IL-2) secreted by T-cells	Antibody on HyNic silane and S-4FB	Secondary antibody	0.1 ng/mL	44
Detection of C-reactive protein in serum and plasma	Antibody (surface conjugation not reported)	Secondary antibody and ~100-nm beads	$3x10^{-5}$ μg/mL or 200 fM	57
Detection of IL-2, IL-4, IL-5 and TNFa	Antibody and HyNic silane and S-4FB	Label-free	100 pM	46
Detection of bean pod mottle virus (BPMV)	Antibody and HyNic silane and S-4FB	Label-free	Not reported	47
Detection of microRNAs via recognition of DNA:RNA heteroduplexs	cDNA and HyNic silane and S-4FB	Secondary antibody	350 aM	41
Detection of IL-2, IL-6, IL-8 in undiluted cerebrospinal fluid	Antibody and HyNic silane and S-4FB	HRP and 4-CN	≤1 pg/mL	45
Detection of carcinoembryonic antigen (CEA)	Antibody on APTES, HyNic silane and S-4FB	Label-free	2 ng/mL	49
Protein-lipid bilayer nanodisc interactions	Adsorption of nanodiscs	Label-free	Not reported	58
Detection of Zaire Ebola, Marburg, dengue and malaria recombinant antigens in human blood, serum and saliva	Antibody (surface conjugation not reported)	Beads	37.0 ng/mL (ZEBOC rdGP), 1000 ng/mL (MARV Angola), 37.0 ng/mL (Dengue NS1) in blood	33
Detection of monocyte chemotactic protein 1 in serum	Antibody on APTES and BS3	HRP and 4-CN	0.5 pg/mL	48
Detection of human immunoglobulin E (IgE) and human thrombin	DNA aptamer on APTES and glutaraldehyde	Label-free	33 pM (IgE) and 1.4 nM (thrombin)	59
Detection Aleuria Aurantia Lection (AAL) and Sambucus Nigra Lectin (SNA)	Amine-derivatized glycan on MPTMS and SM(PEG)12 linker and NHS esters	Label-free	10 pM	60
Detection of aflatoxin M1	DNA-Aptamer on GPTMS and Fab' on MPTMS	Label-free	5 nM for Fab'	61

Abbreviations

APTES 3-aminopropyltriethoxysilane
4-CN 4-chloro-1-napthol
GPTMS 3-glycidoxypropyltrimethoxysilane
HRP Horseradish peroxidase
HyNic 3-*N*-((6-(*N'*-Isopropylidene-hydrazino))nicotinamide)propyltriethyoxysilane
MPTMS 3-mercaptopropyltrimethoxysilane
NHS N-Hydroxysuccinimide
PEG Polyethylene glycol
S-4FB Succinimidyl 4-formyl benzoate

Chapter 2 : The Past, Current and Future of Transfusion Medicine

2.1 A Brief History of Blood Transfusion

Blood, like other parts of the body, is vital for sustaining life. It carries and supplies nutrients, ions and gases to every part of the body. Human blood consists of four major components: red blood cells (RBCs), white blood cells (WBCs), plasma and platelets. Red blood cells contain hemoglobin molecules that capture oxygen required for cellular respiration and deliver it to the tissues. RBCs are produced in the bone marrow, and have a life cycle of approximately 120 days. White blood cells are members of the immune system. Depending on their types and clonality, they can play different roles towards fighting infections caused by foreign pathogens. Plasma comprises mostly water and carries nutrients, ions, hormones and wastes. Most importantly, plasma contains coagulation factors that, together with platelets, are necessary for blood clotting. A significant loss of blood from serious injuries or traumas, therefore, can put the human body under a life-threatening danger. Ironically, the era of modern blood banking and research did not begin until the turn of the twentieth century, right at the outbreak of World War I, a period in which a countless number of soldiers were suffering from blood loss from severe open wounds.

A large number of casualties from the two world wars had ushered in a series of ground-breaking discoveries in transfusion medicine.[62,63] Among these findings was the first use of sodium citrate as a nontoxic anticoagulant in 1914 that served as a stepping stone for other investigations to be made. Shortly after that, the blood donor services in London, the Soviet Union and the United States were initiated between the 1920s and 30s.[64] However, the most important breakthrough was made by an Austrian physician, Karl Landsteiner, who was awarded the Nobel Prize in 1930 for his discovery of the ABO blood system and adverse outcomes of incompatible blood transfusions. After 1954, new blood group antigens had been continually identified by either an immunization of rabbits, guinea pigs and rhesus monkeys with human red blood cells or a

direct detection of antibodies in human sera.[65] There are currently 30 distinct blood groups, which encompass more than 300 blood group associated genotypes identified to date.[66]

Whole blood or components of blood is used for various medical procedures, e.g. cardiovascular and transplant surgeries, operations for life-threatening trauma[67] and treatment of chronic anemia or hematological cancers.[68,69] Each medical procedure may require different quantities of blood components (**Figure 2-1**). Human blood and blood component market is expanding due to a growing number of aging populations among developed nations. According to the World Health Organization (WHO), the annual donation of blood worldwide has reached 112.5 million units. The demand for RBCs alone was estimated at 105 million pints in 2012, and is projected to reach 140 million units in 2018.[70] Transfusion can be administered to patients in a form of whole blood, which is unseparated blood stored in appropriate anticoagulants and preservatives, or blood components, such as packed RBCs, plasma, platelets, autologous leukocytes, immunoglobulins or cryoprecipitate.[71] As blood transfusion has been increasingly given therapeutically, it is estimated that there were 12 million medical procedures performed, requiring more than 35 million red blood cell units (**Table 2-2**).[70]

Table 2-1. Blood and blood components required for different medical procedures.[70]

Cause of blood need	Average number of units required
Automobile accident	50 units of blood
Heart surgery	6 units of blood 6 units of platelets
Organ transplant	40 units of blood 30 units of platelets 20 bags of cryoprecipitate 25 units of fresh frozen plasma
Bone marrow transplant	120 units of platelets 20 units of blood
Burn	20 units of platelets

Table 2-2. Estimated RBC unit required for high blood loss surgical procedures.[70]

Type of surgery	Number of procedures	Units of RBCs/procedure	Total units transfused
Gastrointestinal	3,218,396	3.6	11,586,224
Cardiovascular	3,036,700	3.8	11,539,459
Orthopedic	2,038,456	2.7	5,503,830
Urologic	1,022,234	2.6	2,657,809
Thoracic	402,881	3.3	1,329,506
Other	1,315,291	2.5	3,288,229
Total	11,033,958	3.3	35,905,057

2.2 Blood Group Antigens

Landsteiner's important discovery of the ABO blood group and the adverse effects of transfusion emphasizes the fact that red blood cells cannot be imprudently used in every transfusion due to hemolytic reactions triggered by the incompatibility of blood types. This very first step in the modern blood transfusion history also brought fourth other significant discoveries of the human blood systems. In a molecular level, blood group antigens are surface antigens on red blood cells. They can be carbohydrates that are an integral part of glycoproteins or glycolipid, or membrane proteins that are expressed to serve certain cellular functions (**Figure 2-1**). The three most immunogenic blood group antigens in transfusion, namely ABO, RhD and Kell, will be discussed in this section along with other clinically important blood group systems.

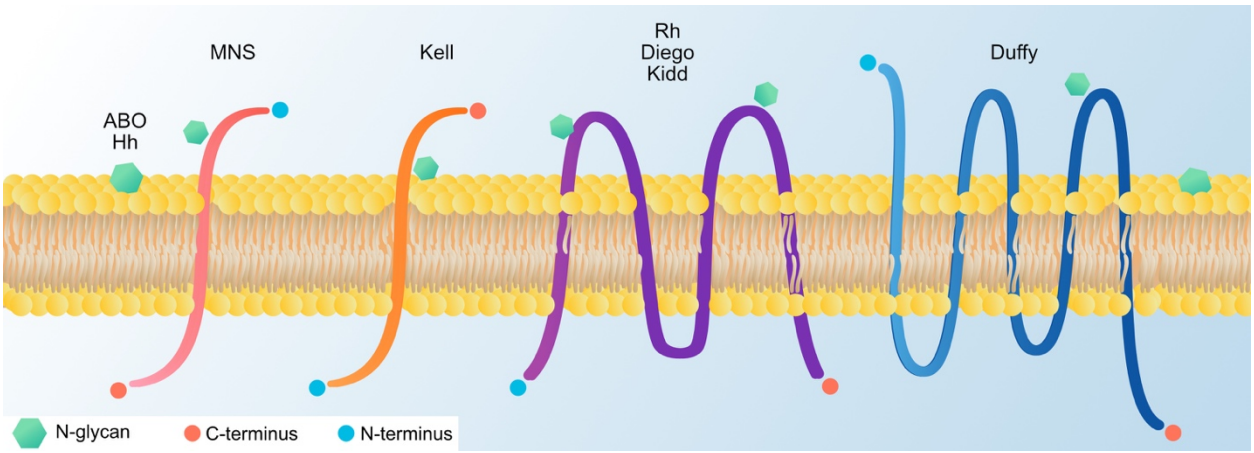

Figure 2-1. Schematic illustration of blood group antigens on red blood cells. Blood group antigens are surface- or membrane-associated glycoproteins or glycolipids. MNS and Kell antigens are single-pass transmembrane proteins, while Rh, Diego, Kidd and Duffy are complex, multi-pass transmembrane proteins.

2.2.1 The ABO Blood Group

The ABO blood group is most important blood type in transfusion medicine owing to their high immunogenicity. There are four major phenotypes in the ABO system that are differentiated by their carbohydrate makeups: A, B, O and AB. In the ABO system, a person with type-A blood has the A antigens expressed on the RBC surface, and carries natural antibodies (isohemagglutinins) against the B antigen in plasma. Conversely, a person with type-B blood has the B antigens expressed on the RBC surface, and carries antibodies against the A antigen in plasma. A person with type-O blood lacks both A and B antigens on RBCs, and thus carries antibodies against A and B antigens in plasma. A person with type-AB blood carries antibodies against neither A nor B antigen due to the presence of both antigens on the RBC surface (**Figure 2-2**).

Antigenically, the A and B antigens are based on a simpler H antigen (type-O) that structurally serves as a precursor for both antigens. Three important genes, ABO, Hh and Se, play a crucial role in the formation of ABH antigens by making specific glycosyltransferases that transfer terminal sugars to the precursor structure. The H gene is responsible for the expression of A and B antigens on RBCs, while the Se gene regulates the expression of A and B antigens in biological secretions. ABH antigens expressed on the RBC surface are constructed by using a type-2 precursor substance, which has the terminal galactose attached to N-acetylglucosamine (GlcNAc) via a beta 1→4 linkage. This initial precursor is called the h antigen. The H gene encodes for a transferase that adds fucose (Fuc) to this precursor (h) to produce an H antigen that is present in type-O blood. The A and B genes encode different transferases that attach N-acetylgalactosamine (GalNAc) and D-galactose (Gal) to the H antigen, respectively. There exists a rare blood group (h, Bombay) resulting from the absence of fucose linked to the type-2 precursor substance in individuals who have an hh genotype.

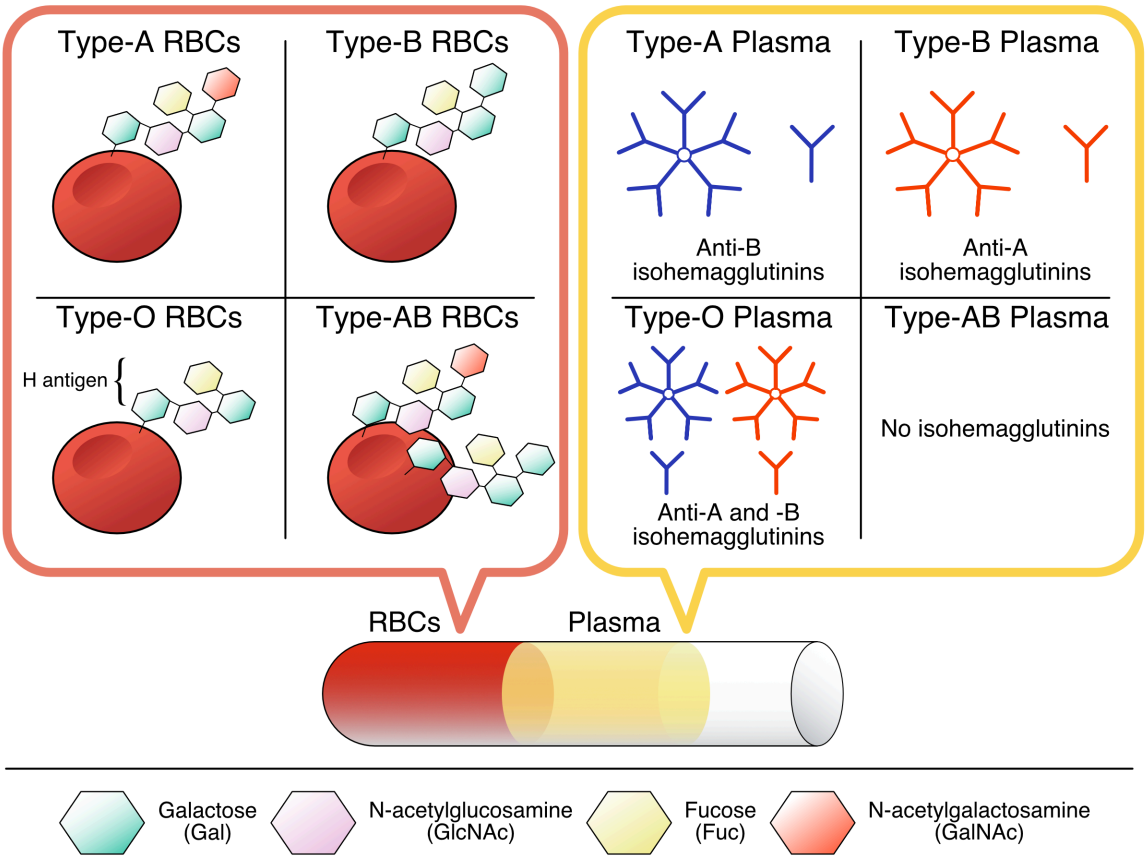

Figure 2-2. Schematic illustration of ABO blood group antigens and antibodies. (**Left**) ABO blood group antigens are glycoproteins expressed on the surface of red blood cells. Type-O RBCs express the H antigen constructed from a primary h antigen (Gal-GlcNAc-Gal) by the addition fucose (Fuc) to the terminal galactose (Gal). In addition to fucose, the A and B antigens also have N-acetylgalactosamine (GalNAc) and galactose added to the terminal galactose, respectively. Type-AB RBCs express both A and B antigens. (**Right**) ABO blood type is the only blood group system where isohemagglutinins against a missing A or B antigen from RBCs are naturally present in plasma. Type-O blood carries RBCs expressing only the H antigen, therefore natural anti-A and anti-B antibodies can be found in the plasma. Type-AB blood, on the other hand, lacks both ABO isohemagglutinins because the A and B antigens are present on RBCs.

In terms of expression levels, the A gene produces more transferases than the B gene, leading to a higher concentration or density of A antigens on the RBC surface. It is estimated that there are 810,000-1,170,000 sites available for the A antigens, whereas the B antigens occupy approximately 610,000-830,000 sites.[72,73] However, when both A and B genes are present in AB adult individuals, both transferases will compete for available H antigens, therefore the density of A and B antigens may vary among individuals with an AB blood type. Some diseases can alter

the expressions of A and B antigens on red blood cells. During infection, certain bacteria can secrete an enzyme that converts an A1 to a B-like antigen.[74] Thalassemia patients whose bodies exert a lot of demands on red blood cells can lose the ABO phenotypes by suppressing the expression. Hematological malignancies such as acute myeloid leukemia, myeloproliferative disorders or myelodysplasia have been found to alter the sugar construct of the ABO antigens.[75]

ABO isohemagglutinins in plasma are predominantly IgM with a small IgG portion, except for type-O blood where the IgG population is higher than IgM. It is unclear how the human body develops antibodies against the missing ABO antigens on RBCs. One possible, widely-accepted explanation suggests that bacteria and pollen particles along with other natural substances that have simple carbohydrates similar to the A and B antigens on their surfaces can stimulate the immune system to produce antibodies. The production of ABO antibodies reaches its peak in 5-10 years of age, then continues to decline as individuals get older. When it comes to transfusion of RBCs, type-A recipients can accept RBCs from type-A and -O donors. Type-B recipients can accept RBCs from type-B and -O donors. Type-AB recipients can accept RBCs from all types of RBC donors, making this group a universal recipient. While other blood types can accept type-O RBCs, type-O recipients can only accept RBCs from other type-O donors, making this group a universal donor (**Table 2-3**).

Table 2-3. ABO phenotypes and isohemagglutinins.

Genotype	Phenotype	Isohemagglutinins in plasma
A1A1, A1A2	A1	Anti-B
A2A2	A2	Anti-B
A1B	A1B	-
A2B	A2B	-
A1O	A1	Anti-B
A2O	A2	Anti-B
BB	B	Anti-A
BO	B	Anti-A
OO	O	Anti-A, anti-B

Remarks: A1 cells can agglutinate with anti-A and anti-A1 lectin (DBA lectin). A2 cells only agglutinate with anti-A but not anti-A1 lectin.[76] Individuals with A2B phenotype may naturally have anti-A1in plasma.[77,78]

Plasma transfusion is the reverse of RBC transfusion. Type-AB plasma can be delivered to recipients of all ABO blood types due to a lack of anti-A and anti-B isohemagglutinins. Type-O plasma can only be transfused to other type-O recipients due to the presence of anti-A and anti-B isohemagglutinins (**Table 2-4**). The presence of isohemagglutinins necessitates transfusion to be carefully performed because delivering unmatched whole blood or blood components to patients may ultimately lead to severe hemolytic reactions that can be life-threatening.

Table 2-4. Compatibility of red blood cell transfusion.

		Donor							
		A		B		O		AB	
		RBC	Plasma	RBC	Plasma	RBC	Plasma	RBC	Plasma
Recipient	A	✓	✓			✓			✓
	B			✓	✓	✓			✓
	O		✓		✓	✓	✓		✓
	AB	✓		✓		✓		✓	✓

2.2.2 The Rh Blood Group

The Rh system is the second in line after the ABO blood group for its immunogenicity and importance in transfusion medicine, yet far more sophisticated than the ABO system. It comprises more than 57 different subgroups. Within a pool of diverse Rh antigens, RhD is most commonly known, followed by RhCE. Normal RhD antigen expressed from different Rh genotypes occupies 110,000-202,000 sites on the RBC surface.[72] RhD negative individuals do not have natural antibodies against the RhD and other Rh antigens unless they are sensitized from a previous transfusion or pregnancy. RhD has immunogenicity of 50%, which entails that half of the transfusion recipients who are negative for RhD are likely to develop alloantibodies against it after the first transfusion.[72] In contrast to the ABO system, Rh antigens are multi-pass transmembrane proteins expressed on the surface of red blood cells (**Figure 2-1**). RhD and RhCE antigens consist

approximately of 400 residues and cross through the membrane of red blood cells 12 times. These two discrete antigen classes, however, are only 35 amino-acid different.

The expression of Rh antigens is regulated by two genes, namely the RHD gene, which encodes for an RhD antigen, and the RHCE gene, which encodes for RhCe, RhcE, RhCE and Rhce antigens. The absence of RHD gene results in an RhD negative phenotype. Mutations occurring in the Rh gene sequences may decrease the expression or cause partial expression of Rh antigens, resulting in weak D and partial D phenotypes. Multiple variations in RhD antigen expressions include (1) C in trans to RHD caused by the allele carrying RHD in a trans position to the allele carrying C (e.g. Dce or dCe phenotype), (2) weak D characterized by a fewer expression of RhD due to mutations that cause conformational changes, (3) partial D caused by a change in amino acid residues on one or more D epitopes (II-VII), (4) D_{el} that results in extremely low copies of RhD antigen, requiring sample incubation at 37^{o}C prior to detection and (5) D epitopes on RHCE.

2.2.3 The Kell Blood Group

Unlike the ABO and Rh systems, the Kell blood group was the first blood group to be discovered by the antibody screening of a female patient who developed antibody, which later was identified as anti-K (K1) against her newborn's RBCs.[72] This highlights both the immunogenicity of the K antigen and the clinical significance of alloantibodies developed through previous transfusions and pregnancy. With the surface occupation of 3,500 to 18,000 sites on RBCs,[79] the number of Kell antigens is not as high as ABO and Rh antigens. However, they are still highly immunogenic. Beside the K antigen, there are 31 other members in the Kell family, of which, k (K2), Kp^a and Kp^b are highly prevalent. Structurally, Kell antigens are on a single-pass, transmembrane glycoprotein made up of 731 amino acids expressed by the KEL gene and are observed in complex with a

440-amino acid, multi-pass membrane associated Kx protein in the XK system via a disulfide bridge.

2.2.4 Other Blood Group Systems

While ABO, Rh and Kell blood groups are the most critical in transfusion medicine, there are more than 300 other blood group antigens that may require clinical attention in certain scenarios based on their different immunogenicity profiles. Common blood group antigens beyond the previously discussed three blood groups are surface antigens on red blood cells that may serve specific cellular purposes, e.g. membrane transporters or receptors. The most commonly known are MNS (M, N, S, s), Duffy (Fy^a and Fy^b), Lewis (Le^a and Le^b), Kidd (Jk^a and Jk^b), P (P1) and Lutheran (Lu^a and Lu^b). Since alloantibodies against these antigens have been observed in the clinics, they can cause post-transfusion complications or hemolytic reactions. To give a brief example of what these antigens truly are, Duffy antigen is a 7-loop, multi-pass transmembrane glycoprotein that functions as a receptor for inflammatory cytokines. Interestingly, Duffy antigen is expressed in individuals who live in malaria pandemic area because it is also a site where malaria parasite, *Plasmodium vivax*, binds in order to invade RBCs. Kidd antigen, likewise, is a multi-pass transmembrane protein whose primary function is to transport urea in and out of RBCs and endothelial cells of the renal vasa recta in the kidneys.[80]

Table 2-5. Blood systems and genes associated with blood group phenotypes.[72]

Number	Name	Symbol	Gene name	Number of antigens
001	ABO	ABO	ABO (ABO)	4
002	MNS	MNS	MNS (GYPA, GPYB, GYPE)	46
003	P1PK	P1PK	P1PK (A4GALT)	2
004	Rh	RH	RH (RHD, RHCE)	52
005	Lutheran	LU	LU (LU)	20
006	Kell	KEL	KEL (KEL)	32
007	Lewis	LE	LE (FUT3)	6

Table 2-5 (Continued). Blood systems and genes associated with blood group phenotypes.[72]

Number	Name	Symbol	Gene name	Number of antigens
008	Duffy	FY	FY (DARC)	5
009	Kidd	JK	JK (SLC14A1)	3
010	Diego	DI	DI (SLC4A1)	22
011	Yt	YT	YT (ACHE)	2
012	Xg	XG	XG (XG), MIC2 (CD99)	2
013	Scianna	SC	SC (ERMAP)	7
014	Dombrock	DO	DO (ART4)	7
015	Colton	CO	CO (AQP1)	4
016	Landsteiner-Wiener	LW	LW (ICAM4)	3
017	Chido/Rodgers	CH/RG	CH/RG (C4A, C4B)	9
018	H	H	H (FUT1)	1
019	Kx	XK	XK (XK)	1
020	Gerbich	GE	GE (GYPC)	11
021	Cromer	CROM	CROM (CD55)	16
022	Knops	KN	KN (CR1)	9
023	Indian	IN	IN (CD44)	4
024	Ok	OK	OK (BSG)	3
025	Raph	RAPH	RAPH (CD151)	1
026	John Milton Hagen	JMH	JMH (SEMA7A)	6
027	I	I	IGNT (GCNT2)	1
028	Globoside	GLOB	GLOB (B3GALT3)	1
029	Gill	GIL	GIL (AQP3)	1
030	Rh-associated glycoprotein	RHAG	RHAG (RHAG)	2

2.3 Standard Blood Typing Procedures and Current Advances in Automation

Blood transfusion does not come without a risk. While infectious disease agents must be carefully screened for, the very first step in blood banking is to identify the blood type of a sample. The purpose of blood typing is to determine blood group antigens and antibodies present in the donor's or recipient's samples to ensure the compatibility of blood types prior to transfusion. In a standard typing procedure, ABO and Rh blood groups receive a priority in typing due to their highest immunogenicity. Modern typing techniques provide high accuracy of typing results which in turn contribute to a low number of transfusion-related fatalities compared to the total number of

transfusions delivered to patients. Despite this effort, the United States Food and Drug Administration (FDA) reported that hemolytic reactions accounted for 25% of the total fatalities through the fiscal year 2005-2008, following transfusion related acute lung injury (TRALI) that was responsible for 51% (114 cases) of all reported fatalities. Among the hemolytic transfusion cases, non-ABO and ABO incompatibilities account for 15% (34 cases) and 10% (22 cases), respectively. Other complications include transfusion associated circulatory overload (TACO), microbial infection, anaphylaxis and graft vs. host disease (GVHD).[81] Although the number of hemolytic reactions due to blood type mismatch is low (1:186,000 for RBC transfusion),[72] these mistakes were entirely preventable because most of them are clerical errors associated with sample handling.

The World Health Organization (WHO) has recommended a pre-transfusion testing of donors and recipients for ABO/RhD typing, antibody detection and antibody identification before serologic cross-matching. A cross-matching test between donor's RBCs and recipient's plasma, and vice versa , albeit crude, can sometimes be performed at the last step to guarantee the compatibility blood samples by checking for the undetected antibodies in patient's plasma that may react with donor's RBCs. The American Association of Blood Bank (AABB) also requires a donor's sample to be screened for unexpected antibodies reactive to antigens on RBCs for individuals with a history of transfusion or pregnancy. Conventional typing techniques can be performed either by forward (direct) and reverse (indirect) typing. A forward typing is generally done by adding antisera into red blood cell suspension in low-ionic strength saline. Some methods may require incubation or centrifugation before obtaining the results. A reverse typing, on the other hand, is done by adding standard reference cells of known A, B and O phenotypes into different titers of plasma (**Figure 2-3**). Agglutination of RBCs is the end result for both directions of typing that positively indicates the presence antigens (in case of forward typing) and antibodies (in case of reverse typing). The four conventional typing methods are summarized in **Table 2-6**.

Table 2-6. Conventional blood typing techniques performed in clinical laboratories.[72]

Method	Description
Slide	Slide method is the most convenient method to perform, but also is the least sensitive method compared to other conventional techniques. It cannot be used to determine weak phenotypes or used with samples whose level of isohemagglutinins is low.
Tube	Tube method is considered to be the gold standard for blood typing due to its high sensitivity. This technique is compatible with direct and indirect typing. In a direct typing, diluted red blood cells in saline solution are mixed with antisera in glass tubes, then centrifuged to allow weak antibodies to react with red blood cells. Cell pellets are resuspended and scored according to the level of agglutination on a scale of 1+ to 4+. Indirect typing is done in a similar fashion, except that plasma is used instead of red blood cells. Standard A1, A2, B and O red blood cells (reference cells) are added into a serial dilution of plasma. Agglutination of red blood cells is scored based on the same standard.
Microplate	Microplate (or solid-phase red cell adherence, SPRCA) method is an attempt to miniaturize the tube method. Typing can be done in a much smaller scale. This method offers a higher throughput while consuming less reagents. It can be used with an image analyzer to provide optical readouts of agglutination results. The unique advantage of this method is its compatibility with hemolyzed, lipemic (excess fat) and icteric (jaundice) samples that are often rejected by the tube method.
Column/ Gel centrifugation	Gel matrix (dextran-acrylamide or glass beads) will trap agglutinates, but permit non-agglutinated cells to elude during centrifugation. Gel centrifugation offers rapid results that do not require an extensive training to interpret the results. In addition, gel method eliminates the washing step to remove unbound antibody,[82] thus reducing an assay time. The procedures are more standardized with a known endpoint. Result patterns are more objective than other conventional methods. However, its main drawback comes from its incompatibility with samples that can clog the gel matrix due to an abnormal level of proteins such as patients with multiple myeloma. A coin stack of red blood cells (rouleaux) can produce false-positive results.

The main challenge of conventional typing methods is the turnaround time of results that may not best facilitate a rapid decision making required in time-sensitive scenarios, e.g. trauma. Per WHO guidelines,[71] physicians have to assess patient's need for transfusion and categorize it into three cases: (1) emergency, (2) definite blood needed and (3) possible need for blood. Bleeding in trauma or massive hemorrhage is the leading cause of hospital-related mortality.[83–86] In trauma, patients with 20-30% blood loss may be given multiple types of blood products for fluid resuscitation, depending case and the severity of exsanguination.

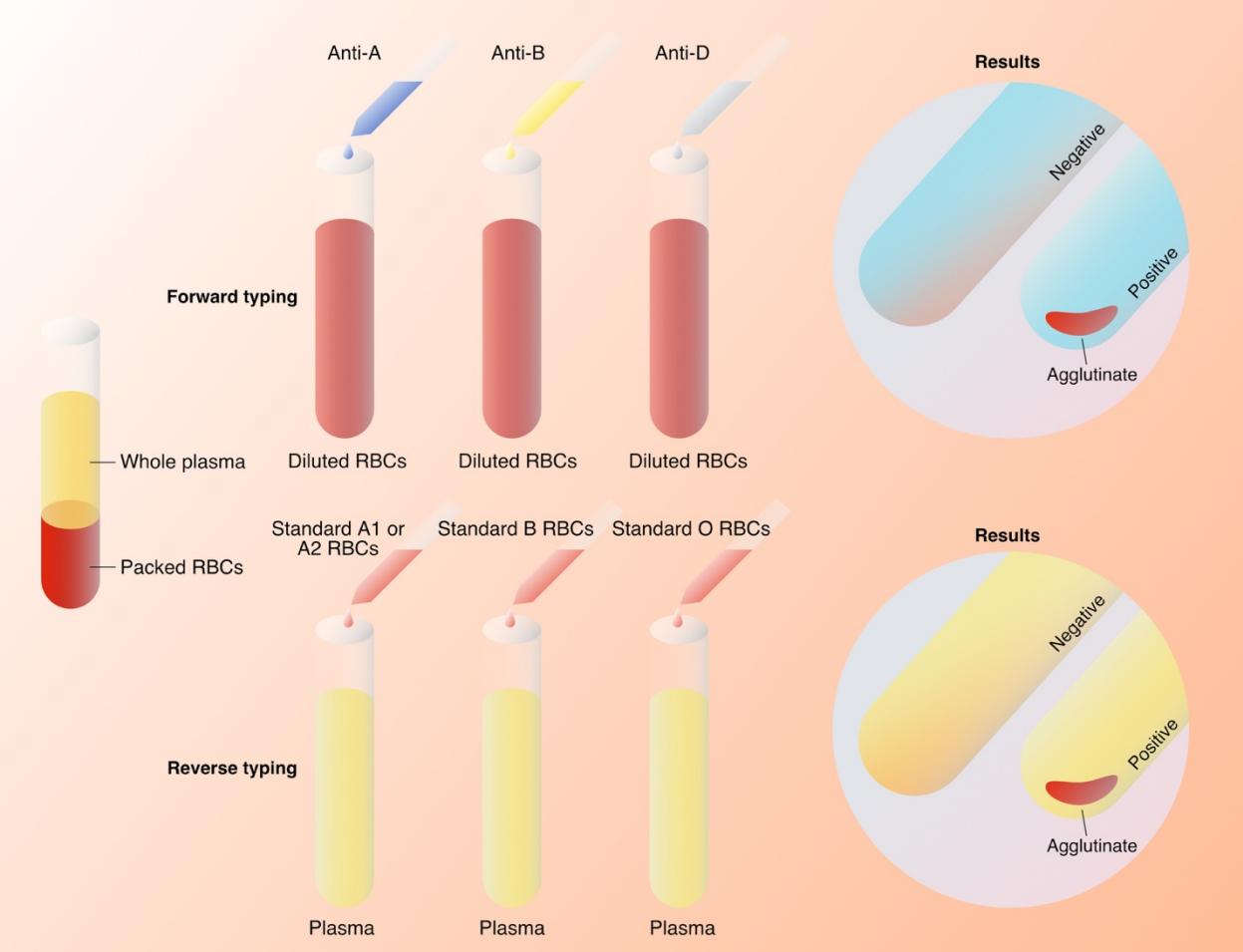

Figure 2-3. Schematic illustration of tube-based agglutination assays for forward and reverse typing. Forward (direct) typing is performed by adding antisera into red blood cell suspension in low ionic strength saline. Reverse (indirect) typing is performed by sequentially diluted plasma into different titers before mixing standard reference cells of type A1, A2, B and O. In both techniques, positive results are scored based on the level of agglutination observed micro- and macroscopically on a scale of 1+ to 4+. RBC or plasma sample that does not form hemagglutination is given a negative typing result with a score of 0.

The two common blood products that are often administered are packed red blood cells (pRBCs) and fresh frozen plasma (FFP) which has to be delivered for every given 4-5 packed red blood cells.[87] In theory, known patients' blood types are required in order for compatible blood products to be administered appropriately. This can be performed by a standard agglutination test at the site of transfusion. In practice, however, physicians are constrained by urgency and eventually are limited to using type-O pRBCs.[88] The current institutional protocol at the Harborview Medical Center (Seattle, WA) specifies type-O/RhD negative and type-O/RhD positive

red blood cells for resuscitation of trauma female and male patients, respectively. Although this seems sufficient, a recent retrospective study conducted in England and Wales has shown that only 2% of the patients with massive hemorrhage received transfusion in an optimal manner while also identifying that the administration of pRBCs is often delayed by 40 minutes,[85] a time that can be critically important to saving a patient's life. Moreover, the use of blood products that are not thoroughly screened for other blood group antigens has contributed to alloantibody production in patients.[89] The advent of a near-patient instrument for rapid blood typing can undoubtedly alleviate this problem by providing a more rapid time-to-result for thorough profiling of blood type, phenotypically and serologically. Most importantly it will also reduce the inventory burden of type-O red blood cells, allowing for a better matched blood product to be administered.

The existing gold standard methods require 15-20 minutes of assay time per sample, and thus might not be able to provide results to physicians in time-sensitive situations when several blood units maybe needed. (Of note, the assay is bottlenecked by multiple centrifugation steps.) Commercial automated blood typing instruments have been adopted by hospital and central blood collection laboratories to streamline the blood typing process, which reduces human handling and spares technician's time for post-typing analytic tasks. Most automated systems use solid-phase or gel-based techniques that can be performed in large volume with a definite end point of the assay. Computing algorithms have been integrated for data analysis to provide objective results. Automated systems have numerous advantages over the manual typing procedure. They reduce the cost-per-test and clerical errors, while obviating the requirement of skilled technicians to operate. The market for automated typing instruments has grown with the annual rate of 2%, and is expected to reach $645 million worldwide in 2018. The U.S. and E.U. sectors each share about 37-38% of the global market.[70] **Table 2-7** provides an overview of key players in blood typing automation.

Table 2-7. Commercial automated blood typing systems.

Manufacturer	Platform	Description	Test	Throughput	Turn-around time (TAT)
Immucor	NEO Blood Bank Analyzer	Fully automated systems aimed for hospital labs and blood donor centers. It is integrated with two CCD cameras for result interpretation.	ABO/RhD, weak D, antibody screening, IgG direct antibody test (DAT) and IgG cross-matching	Capacity for 224 samples with access for loading and unloading	30 min with real-time results
Immucor	Galileo ECHO Blood Bank Analyzer	Bench-top, fully-automated system aimed for small laboratories with built-in image analysis capability.	ABO/RhD, weak D, antibody screening, IgG direct antibody test (DAT) and IgG cross-matching	Capacity for 20 samples with access for loading and unloading	26 min with real-time results
Grifols	Erytra	Fully automated systems based on gel card technology aimed for hospital labs and blood donor centers.	ABO/RhD and Kell typing, antibody screening, antibody identification, direct antiglobulin technique, donor confirmation, cross-matching	Capacity for 400 gel cards and 96 samples (100 cards/h), 66 samples/h for ABO/Rh and 147 samples/h for antibody screening	Not reported
Grifols	Wadiana	Bench-top, fully-automated system based on gel card technology aimed for pre-transfusion testing.	ABO/RhD and Kell typing, antibody screening, antibody identification, direct antiglobulin technique, donor confirmation	Capacity for 48 samples	Not reported
Ortho Clinical Diagnostics	ORTHO VISION Analyzer	Fully automated systems based on gel card technology aimed for hospital labs and blood donor centers.	ABO/Rh typing, antibody screening, antibody identification, RH phenotype (Cc,Ee), cross-matching, DAT	Capacity for 42 samples, 120 gel cards	28 min[90]

Though automated blood analyzers can handle a large volume of workload, the price and maintenance of these high-end instruments are costly. Efforts to reduce the cost of blood typing while preserving the accuracy and throughput of an automated process have been reported as early as 1990 in portable point-of-care tests for blood typing.[91] The advent of affordable point-of-

care blood typing devices not only comes with a cost incentive over automated systems, but also presents a critical clinical benefit to hospitals. France and Slovakia enforce the law requiring patient's blood to be typed at the site of transfusion.[70] This legislation has pushed medical diagnostic manufacturers to launch more point-of-care blood typing platforms to the market, such as a card test kit consisting of dried anti-A and anti-B antisera for simultaneous typing of donor's and recipient's blood.[92] The ABORhCard from Micronics requires only a finger stick blood sample to perform ABO/RhD forward typing with 97.12% overall agreement in a clinical study of 1,700 volunteers.[93] This "last-minute" typing protocol is not implemented to replace the existing routine blood typing in centralized laboratories, but rather to affirm previous test results to ensure patient's safety. It has been shown that the bedside test could improve the sensitivity to 99.65% for ABO discrepancies.[94]

Aside from commercial products, numerous blood typing sensors based on paper,[95–100] surface plasmon resonance (SPR),[101–107] and optical waveguide,[108–110] have been shown in the literature (**Table 2-8**). Paper-based assays are very popular because of their simplicity, portability and fast turnaround time that appeals to the use in resource-limited settings. Noiphung, et al., developed a rapid dual paper-based test strip for simultaneous forward and reverse typing that provides results in ten minutes, yet with only 85-90% accuracy. [97] Another paper-based technique has further included non-ABO/RhD blood groups and demonstrated the detection of Kell, Kidd and P antigens with IgM capture antibodies.[98] Albeit simple, paper-based devices still suffer from insufficient sensitivity for serologic analyses. In response to the shortcomings of paper-based devices, microfluidics-based optical biosensors have been explored for blood typing applications. Microfluidic integration has opened a new avenue not only for novel approaches in blood typing to be explored, but also platform miniaturization to be engineered. Robb, et al., demonstrated successful ABO forward typing on the Biacore microarray platform based on the SPR principle.[104] On the reverse typing side, the authors also established an antibody screening assay on

microarray technology by printing membranes of RBCs and genetically modified cells presenting antigens on a solid surface.[111] Image analysis algorithm has also been used to evaluate agglutination results in a single-line microfluidic channel.[112] Ashiba, et al., have demonstrated the detection of RBC agglutination on a low-cost, sensitive optical waveguide mode sensor by observing dips in the reflectance spectra.[108] The sensitivity of this device is sufficient for determining microagglutination. The authors further integrated this technology with a high-throughput microfluidic system to perform multiple independent assays in parallel with real-time result readouts.[109,110]

Table 2-8. Selected point-of-care devices for blood typing.

Platform	Description	Method of analysis	Sample volume, TAT	Limitation	Ref
Paper	Separated test strips for forward and reverse typing. Forward typing was performed by agglutinating RBCs on antibody-functionalized filter paper. Reverse typing was performed by agglutinating reference cells with plasma samples on LF1 blood separation membrane.	Comparing the distance of agglutinated RBCs to non-agglutinated RBCs. Results were visually interpreted.	130 μL of whole blood, 8 min (reverse), 5 min (forward)	1) Insufficient sensitivity to detect microagglutination. 2) Only demonstrated on ABO system.	96
Paper	Approach 1 Blood sample and typing reagents were mixed before dispensed onto the filter paper. Approach 2 Filter paper was functionalized with typing reagents (IgM). Blood droplet was dispensed in the middle of the test strip and displacement was measured in relative to the control lane.	Measuring the ability of non-agglutinated and agglutinated samples to wick the filter paper test strip. Kinetic of wicking was analyzed by an image analyzer.	20 μL of whole blood, 10 min	1) Results were be difficult to interpret. 2) Complication with plasma separated on the test strip that might affect result interpretation. 3) Only demonstrated in forward typing.	100
Waveguide-mode sensor	Unfunctionalized waveguide sensor chip on prism. Agglutination took place in a sample chamber. Spectrum of reflectance was measured at different time points.	Measuring the absorbance changes of blood samples pre- and post-hemagglutination.	50 μL of whole blood, 5-10 min	1) The surface was not functionalized. False positive was possible in the case of rouleaux. 2) Multiple time points had to be taken because blood can sediment.	108

Table 2-8 (Continued). Selected point-of-care devices for blood typing.

Platform	Description	Method of analysis	Sample volume, TAT	Limitation	Ref
Microarray	Approach 1 Antibody or serum protein was functionalized on nitrocellulose-coated slides to capture RBCs labelled with a fluorescent tag. Approach 2 Synthetic blood group A antigen was used for anti-A detection and ranking on Biacore sensor chip.	1) Measuring fluorescence readout 2) Measuring Biacore response unit (RU)	70 μL of sample per probe, 4 samples/h	1) Long turnaround time. 2) Fluorescence readout requires a special equipment.	104

2.4 Blood Typing on Silicon Photonic Sensors

The development of several commercial automated, high-throughput blood analyzers, such as the ECHO platform (Immucor) or Erytra (Grifols), helps reduce handling errors and improve upon the throughput of typing assays. However, the main drawback of these instruments, aside from prohibiting cost, is a lack of portability that permits them to be used outside centralized laboratories. With their average turnaround-time of 20-30 minutes, the ability to rapidly type blood with precision is still an unmet need in transfusion medicine and urgent care. Silicon photonics has emerged as a promising diagnostic platform that provides real-time results for clinical assays. Miniaturization of these micro-fabricated biosensors in a microarray format can improve the multiplex and throughput when integrated with microfluidics. In addition to their low cost-per-device, various silicon photonic sensors have intrinsically high sensitivity that suits them for biomolecule detection in clinical assays.[113] In the Ratner lab, we are utilizing a commercial silicon photonic biosensing platform (Maverick M1; Genalyte, Inc., San Diego , CA) to develop biological and clinical assays. In the following chapters of this dissertation, the development of multiplexed forward and reverse blood typing assays for ABO/RhD blood groups will be discussed.

Chapter 3 : Developing an on-chip Forward Typing Assay

3.1 Abstract

The ability to rapidly perform blood typing for patients in trauma or emergency care is a technological unmet need in transfusion practice. Despite the existing high-throughput platforms to carry out such task, automated instruments in blood banking are not customized for a point-of-care use, and thus trauma physicians are limited by urgency to administering universal blood products, e.g. type-O erythrocytes, to patients. When the patient's blood type profile is not thoroughly characterized, this could provoke transfusion-associated complications as a result. To address this challenge, we developed forward typing assay of ABO, RhD and Kell antigens on silicon photonic microring resonator arrays capable of providing results in minutes of active assay time. Surface functionalization was accomplished by immobilizing biotinylated blood group-specific capture antibodies onto streptavidin coated sensor surface. Our successful establishment of a forward typing assay has laid a foundation for further developments of a reverse typing assay and multiplexed assays that will later be discussed in chapter 4 and chapter 5, respectively.

3.2 Introduction

Despite a growing market of point-of-care devices that cover nearly all major medical specialties, transfusion medicine is still an underserved area compared to others where point-of-care devices have already been used by providers and healthcare professionals. Technological advances in test automation and novel assay development in clinical laboratory have driven the innovation in blood banking instruments capable of performing various assays in serology and phenotypic characterization of red blood cells. Despite their advantages of short turnaround time (TAT) and standardization of test performance and result interpretation, high-end blood banking instruments, owing to their cost burden and sizes, are marketed to centralized laboratories in hospitals. To

address this clinical need for point-of-care devices in transfusion medicine, many research groups and commercial vendors have developed lateral flow driven paper-based or hand-held cassette devices with an intention to demonstrate their feasibility in clinical use,[96–98] and foster the adoption of simple, point-of-care blood typing devices in the clinics, specifically where transfusion occurs. However, these devices still have major drawbacks in qualitative result readouts, when not integrated with an external optical reader, and most importantly, a lack of multiplex that allows them to perform multiple assays in parallel. Given the number of quantitation assays that have to be performed in routine blood testing, multiplexing is a desired attribute of a blood typing device.

In response to the shortcomings of paper-based devices, microfluidics-based optical biosensors have been explored for blood typing applications. Microfluidic integration has opened a new avenue not only for novel approaches in blood typing to be explored, but also platform miniaturization to be engineered. Robb, et al., demonstrated successful ABO forward typing on the Biacore microarray platform based on the surface plasmon resonance (SPR) principle.[104] Since then, SPR has been utilized for detection of normal, weak and partial RhD phenotypes,[106,107] along with other antigens in the Rh system in a multiplexed fashion.[105]

Image analysis algorithm has further been integrated to evaluate the agglutination of RBCs in a single-line microfluidic channel in a standardized fashion.[112] As a result, Ashiba, et al., demonstrated the detection of RBC agglutination on a low-cost, sensitive optical waveguide mode sensor that could detect microagglutination.[108] The authors eventually integrated this technology with a microfluidic system to perform multiple separate assays in parallel with real-time result readouts.[109,110] Among these optical sensing technologies, silicon photonics has recently emerged as a promising diagnostic platform that can shorten the turnaround time of clinical assays by providing real-time results. Multiplexing capability of silicon photonic sensors is enabled through microfluidic integration and device miniaturization that leverages the well-established CMOS fabrications. In addition to their low cost-per-device, various silicon photonic sensors have

intrinsically high sensitivity for biomolecular detection in clinical assays.[113] The silicon photonic biosensing platform used in our research laboratory is the Maverick M1 system manufactured by Genalyte, Inc., (San Diego, CA). Over the past recent years, a number of studies have proven the suitability of the Maverick platform in diverse applications in molecular detection for nucleic acid,[41–43] cytokines,[44–46] viral particles,[33,47] and other disease antigens,[48–50] in both label-based and label-free strategies. Despite our early attempts in performing serologic and phenotypic typing analyses on the same system,[114] we only focused on the ABO blood group.

Herein, the grounding of method development and surface functionalization of silicon phonic microring resonator sensors is described for a forward typing application. ABO, RhD and Kell blood group antigens are molecular detection targets due to their high immunogenicity and clinical significance in red blood cell transfusions. The methods developed in this chapter are an immediate armamentarium for further developments of a reverse typing assay and a subsequent multiplexed assay in which we attempt to combine the forward and reverse typing on one sensor chip.

3.3 Materials and Methods

3.3.1 Materials

IMEC-3 microring resonator chips were purchased from Genalyte, Inc., (San Diego, CA). Lyophilized streptavidin from *Streptomyces avidinii* was purchased from Sigma Aldrich (St. Louis, MO). Proprietary printing solution (sci-SPOT protein D1, 2 mg/mL) was purchased from Scienion AG (Princeton, NJ).

Reagents for forward typing: standard typing mouse IgM anti-A (clone: BIRMA-1), mouse IgM anti-B (clone: LB-2), human IgM anti-RhD (clone: RUM-1), human IgM anti-RhD (clone: TH-28) and human IgM anti-Kell (K) (clone: AEK-4) were purchased from Merck Millipore (Billerica, MA).

Biotinylated IgG anti-glycophorin CD235a (GYPA) was purchased from Miltenyi Biotec (San Diego, CA). Biotinylated anti-mouse IgM, biotinylated anti-human IgM and mouse IgM isotype control were purchased from Thermo Fisher Scientific (Waltham, MA). Standard reference red blood cells (Panocells) of known RhD and Kell profiles were purchased from Immucor (Peachtree Corners, GA). Streptavidin-PE for flow cytometry analysis was purchased from Miltenyi Biotec (San Diego, CA)

3.3.2 Blood Sample Handling and Preparation for Analysis

Blood samples were processed immediately upon receipt. EDTA- or citrate-stored blood was centrifuged at 2,000×g for 10 minutes at 4^{o}C. Unless otherwise stated, this centrifugation setting was used throughout the red blood cell preparation protocol. Plasma was harvested from the top layer and stored separately. Care was taken not to disturb red blood cell pellets and the buffy coat layer consisting primarily of white blood cells. Plasma-equivalent volume of PBS was added to wash red blood cell pellets. Samples were then centrifuged, and the supernatant was removed. Whole plasma was used for reverse typing, while packed red blood cells were diluted 1:10 in PBS at room temperature (137 mM NaCl, 2.7 mM KCl, 8 mM Na_2HPO_4, 1.8 mM and KH_2PO_4, pH 7.4) prior to analysis. For storage, equal volume of Citrate Dextrose Phosphate Adenine-1 (CDPA-1) blood storage solution was added to resuspend red blood cell pellets. Specifically for the Kell antigen detection, agglutination test was performed on donors' samples using anti-K (clone: AEK-4) prior to the analysis due to old sample age. Samples with agglutination scores of 2+ were further tested on the sensors.

3.3.3 Forward Typing on Hand-Functionalized Sensor Chips

Preparation of ABO forward typing reagents:

To prepare an anti-A/biotinylated anti-mouse IgM mixture, 10 μL of anti-A capture IgM antibody was incubated with 2.7 μL biotinylated goat anti-mouse IgM at 4°C for 1 hour. For anti-B, 10 μL of anti-B primary antibody was incubated with 3.3 μL biotinylated goat anti-mouse IgM at 4°C for 1 hour. The total protein concentrations in the capture antibody stock solutions were 8.1 mg/mL for anti-A and 10.4 mg/mL for anti-B determined by NanoDrop 2000C spectrophotometer (Thermo Scientific, Waltham, MA). The ratio between the capture and anti-IgM antibodies was adjusted to be approximately 1:1 in molar ratio. After one hour of incubation, equal volume of sci-SPOT D1 buffer (12.7 μL for anti-A mixture and 13.3 μL for anti-B mixture) was added to each antibody mixture and incubated for another hour prior to reagent spotting. The final titers of capture antibodies are 1:403 and 1:1,540 for anti-A and anti-B, respectively. Reagents were incubated on ice for one hour prior to spotting on streptavidin-coated chips.

Preparing RhD/Kell forward typing reagents:

Anti-RhD and anti-K capture antibodies were functionalized in a different manner from anti-A and anti-B. Instead of statically incubating capture antibodies on the chips, anti-RhD and anti-K were flowed across the chip pre-functionalized with biotinylated anti-human IgM in the titer of 1:21 for both antibodies. Therefore, only biotinylated anti-human IgM, biotinylated anti-mouse IgM (negative control) and biotinylated anti-glycophorin A (GYPA) (positive control) were mixed with equal volume of sci-SPOT D1 buffer prior to chip functionalization.

Chip functionalization:

Protective polymer coating on the IMEC-3 chips were removed by soaking the chips in organic solvents in the following sequence: acetone for 2 minutes (twice), isopropyl alcohol for 2 minutes (twice), and finally ultrapure Milli-Q water for 2 minutes (twice). The chips were then blow dried with filtered house air. Functionalization with streptavidin was done immediately after the cleaning step. Chips were immersed in 0.1 mg/mL streptavidin solution in PBS for 3 hours at ambient temperature. Chips were rinsed with PBS thereafter to remove excess streptavidin. Streptavidin-coated chips can be used immediately for subsequent functionalization steps, or stored dry at 4^{o}C for future use. Due to a small footprint of the chip, only two 0.6-0.8 μL spots of reagents could be comfortably pipetted onto the chip without spot merging.

For ABO forward typing, anti-A mixture was spotted on either the left or right side of the chip, leaving the remaining side available for anti-B mixture (**Figure 3-1).** For RhD/Kell forward typing, biotinylated anti-human IgM was spotted on one side of the chip, leaving the remaining side available for either biotinylated anti-mouse IgM or biotinylated anti-GYPA to be spotted as a negative and a positive control, respectively (**Figure 3-2**). Each spot of reagent should generously cover three clusters of sensors in Channel 1 and three clusters of sensors in Channel 2 while keeping the middle region unfunctionalized. Reagents were incubated on streptavidin-coated chips for 1 hour in a humidified environment at ambient temperature. Reagent spots were wicked off by using Kimwipes (Kimtech). Chips were then rinsed vigorously with PBS, and immersed in 2 mg/mL BSA solution in PBS for 15 minutes for blocking at ambient temperature. Chips were rinsed again with PBS to remove excess BSA, and blow dried with filtered house air. Chips were stored at 4^{o}C for future use.

Forward typing assays:

Unless otherwise stated, the flowrate of every step is 20 μL/min. ABO forward typing is performed by flowing 1:10 diluted red blood cells in PBS directly over the chips functionalized with anti-A and anti-B for 5 minutes followed by a brief PBS rinse to remove unbound cells. RhD and Kell forward typing is similarly performed with an exception of the in-line functionalization of either anti-RhD cocktail consisting of RUM-1 (titer 1:21) and TH-28 (titer 1:41) or anti-K (AEK-4, titer 1:21) that precedes the cell step. The two steps are separated by a brief PBS rinse to remove excess anti-RhD or anti-K on the surface. Specifically for Kell detection, the assay requires a minimum of 5-minute pause in flow to allow cells to better interact with the capture antibodies immobilized on the sensor surface. Due to an instrumental limitation, the lowest flowrate could only be set to 1 μL/min to mimic a stop flow.

3.3.4 Establishment of Anti-RhD Functionalization Method

Prior to the finalization of anti-RhD and anti-Kell functionalization method discussed in section 3.3.3, three approaches were pursued first for anti-RhD (clone: RUM-1) functionalization of the sensors. In the first approach (simultaneous incubation), anti-RhD antibody was incubated with biotinylated anti-human IgM at different volumetric ratios (1:10, 1:5, 1:1, 1:0.5 anti-IgM : anti-RhD) for 15 minutes at 4^{o}C prior to spotting. In the second approach (sequential incubation), biotinylated anti-human IgM was directly spotted on streptavidin-coated chips on one side and incubated for 1 hour in a humidified environment at ambient temperature. The chips were rinsed with PBS, then anti-RhD was spotted over the previous anti-human IgM spot. Anti-RhD mixture prepared in the first approach was spotted on the remaining side of the chip for a direct comparison. Reagents were incubated for 1 hour in a humidified environment at ambient temperature. Reagents were wicked off by Kimwipes (Kimtech). Chips were rinsed with PBS, and blow dried with filtered house

air. Chips were tested with RBCs of known RhD positive and negative statuses. In the third approach (in-line functionalization), biotinylated anti-human IgM and biotinylated anti-mouse IgM (negative control) were spotted on the same chips. Different volumetric dilutions of anti-RhD in PBS (1:50, 1:100 and 1:250) (or 1:82, 1:41 and 1:16 in titers) were flowed across the chips at 20 μL/min for 5 minutes, followed by a brief PBS rinse. Then, 1:10 diluted packed RBC suspension in PBS was flowed, and cell-binding interactions were observed.

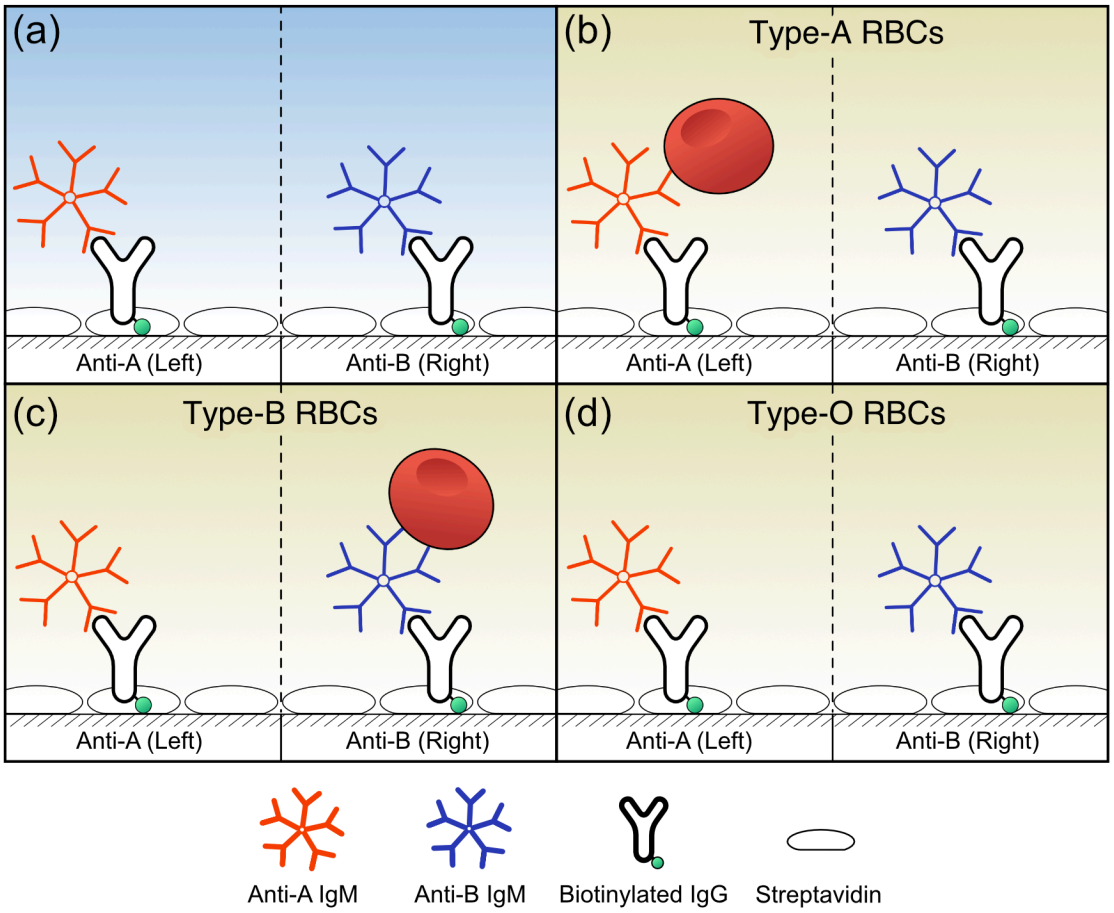

Figure 3-1. Schematic illustration of the surface functionalization strategy for ABO forward typing assay. Reagents are spotted by hand onto the left and right sides of microring resonator assays. Anti-A/biotinylated anti-mouse IgM mixture and anti-B/biotinylated anti-mouse IgM mixture were immobilized on streptavidin-coated sensor chip (**a**). After 1-hour incubation, the chips were rinsed with PBS to remove unbound antibodies before storage at 4°C. In this set of examples, chips are tested with type-A RBCs (Hct 10%) (**b**), type-B RBCs (Hct 10%) (**c**) and type-O RBCs (Hct 10%) (**d**) that are flowed across the sensor arrays at 20 μL/min. Illustration is not drawn to scale.

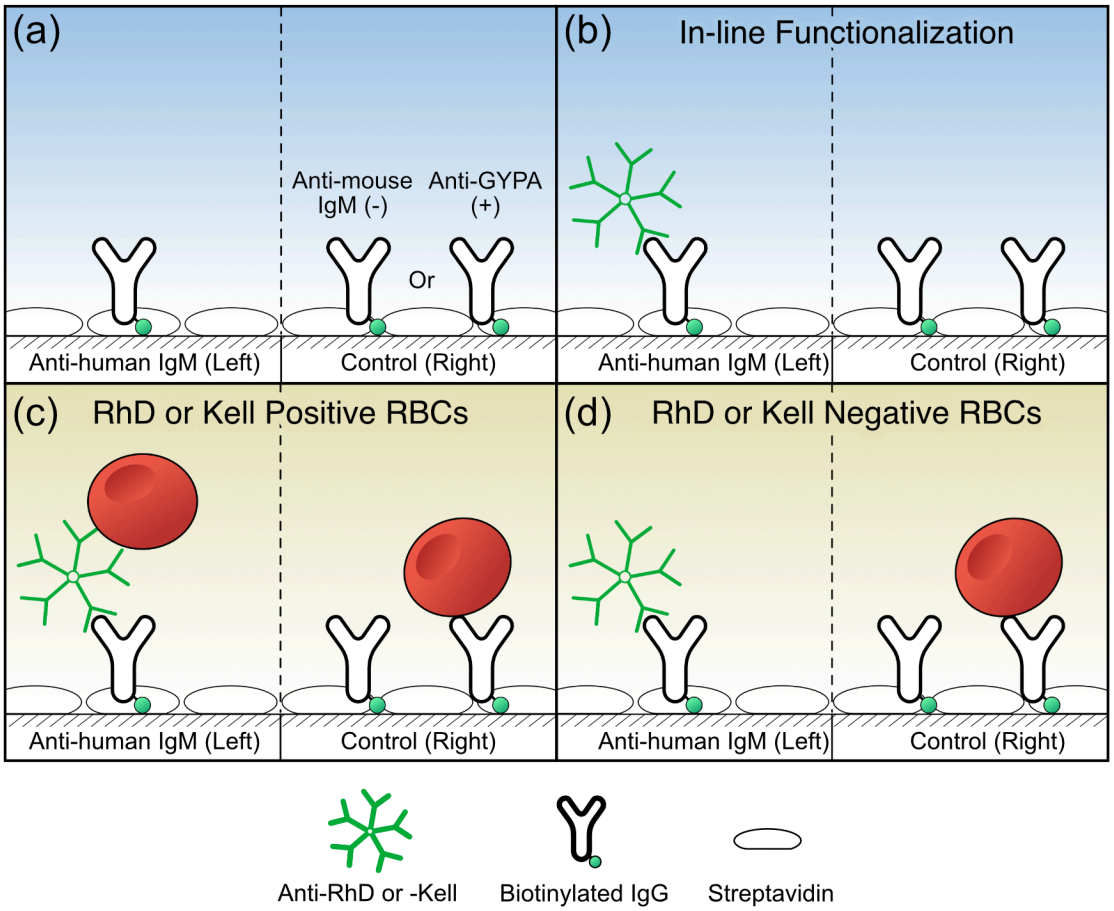

Figure 3-2. Schematic illustration of the surface functionalization strategy for RhD and Kell forward typing assays. Reagents are spotted by hand onto the left and right sides of microring resonator assays. Biotinylated anti-human IgM antibody and either one of biotinylated anti-mouse IgM (-) or biotinylated anti-GYPA (+) control were immobilized on streptavidin-coated sensor chip (**a**). After 1-hour incubation, the chips were rinsed with PBS to remove unbound antibodies before storage at 4°C. Anti-RhD (clones RUM-1 and TH-28) or anti-K (clone AEK-4) was flowed to immobilize on the pre-functionalized anti-human IgM (**b**). Owing to the same in-line functionalization strategy, RhD and Kell forward typing assays are always performed separately. In this set of examples, chips are tested with RhD or Kell positive RBCs (Hct 10-15%) (**c**) and RhD or Kell negative RBCs (Hct 10-15%) (**d**) that are flowed across the sensor arrays at 20 μL/min. Illustration is not drawn to scale.

3.3.5 Instrumentation and Analysis Software

The Maverick M1 system was purchased from Genalyte, Inc., (San Diego, CA). Detailed operating principle of the instrument is discussed elsewhere.[39] Briefly, the instrument consists of a high-power diode laser with a center wavelength of 1,550 nm and an optical scanner to track resonance wavelength shifts of individual microring resonators over time. The system is integrated with

automated microfluidics controlled by the software. Two samples can be tested simultaneously. Data are acquired in real-time and plotted in the analysis software for instantaneous visualization. All data were analyzed in MATLAB (MathWorks, Natick, MA). Processed sensorgrams show raw data from individual microring resonators and a plot of the average data with standard deviation of the mean at specific time points.

3.4 Results

3.4.1 Hand-Functionalized Chips for ABO Forward Typing

Despite the final goal toward printing all blood typing reagents on the sensor chips for multiplexing, various milestones in the assay development and validation of reagents were accomplished by a manual hand spotting of reagents onto the desired locations of the chip. The chip's miniature footprint (3.6 mm × 5.7 mm) only permit two spots of reagent to be dispensed on the left and right sides, each covering three active clusters in Channel 1 and three active clusters in Channel 2. Note that one spot of reagent actually covers six clusters of sensors in each channel, but only three nonadjacent clusters were interrogated. The four clusters in the middle part of the chip remained unfunctionalized, and were used as a buffer region to prevent contamination of reagents from both partitions. This allows four independent questions to be answered simultaneously when two different samples are tested. The volume of reagents required for spotting was typically in the range of 0.6-0.8 μL per spot to ensure a sufficient coverage.

Sensorgrams of positive forward typing results exhibited constantly fluctuating resonance wavelength shifts associated with cell binding to the sensors with respect to time. Proteins and other macromolecules, upon binding to the sensor surface, often cause a clear positive binding curve of the resonance wavelength shift following the Langmuir isotherms that can be observed homogeneously across sensor devices. However, signals in the forward typing are intrinsically noisy due to the stochastic binding of red blood cells, whose sizes are multiple orders of

magnitude larger than biomolecules, under the flow condition. Thus, the interpretation of forward typing results prioritizes the presence of cell binding-specific signal fluctuations over the magnitude of the wavelength shift. This cell binding characteristic and pattern of responses are demonstrated in the sensorgrams of forward typing of type-A, -B, -O and -AB RBCs where the average shift of sensor responses at each time point is shown as a solid line and the standard deviation of the mean is shown as a shaded area in the background (**Figure 3-3**). Since the specific cell capture signals are always fluctuating in the flow, the standard deviation of the mean of sensor responses is large, making the shaded area in the background spread out more than sensors without specific binding. When type-AB RBCs were tested, both anti-A and anti-B functionalized sensor probes show specific cell-binding signals based on the signal fluctuation whereas the unfunctionalized sensors were not responsive (**Figure 3-3d**). The shift observed from unfunctionalized sensors was likely caused by the refractive index change and nonspecific binding of biomolecules present in the cell suspension. These characteristic cell-binding signals were completely absent when type-O RBCs were tested (**Figure 3-3c**). A small, uniform spread in the standard deviation observed from the anti-A functionalized sensors was produced by steady shifts at slightly different degrees, and thus not indicative of cell binding. The matching forward typing results of type-A and -B RBCs to the samples' blood types also verify our hypothesis that fluctuating signals are associated with cell binding (**Figure 3-3a** and **b**).

3.4.2 Approaches in Anti-RhD Functionalization

Static incubation vs. in-line functionalization:

Among the four capture IgM antibodies used in the forward typing assay, human anti-RhD IgM (clones: RUM-1 and TH-28) and human anti-K IgM are particularly more tedious to functionalize on a solid substrate than anti-A and anti-B, which are mouse IgM antibodies. Anti-RhD (clone:

RUM-1) was selected as a surrogate for human IgM in the investigation of three different methods for antibody immobilization on the sensor for detecting RhD antigen on RBCs. These methods are (1) a static simultaneous mixing of anti-RhD with biotinylated anti-human IgM, (2) a static sequential spotting of biotinylated anti-human IgM followed by anti-RhD and (3) a flow-driven anti-RhD immobilization on the sensors pre-functionalized with biotinylated anti-human IgM.

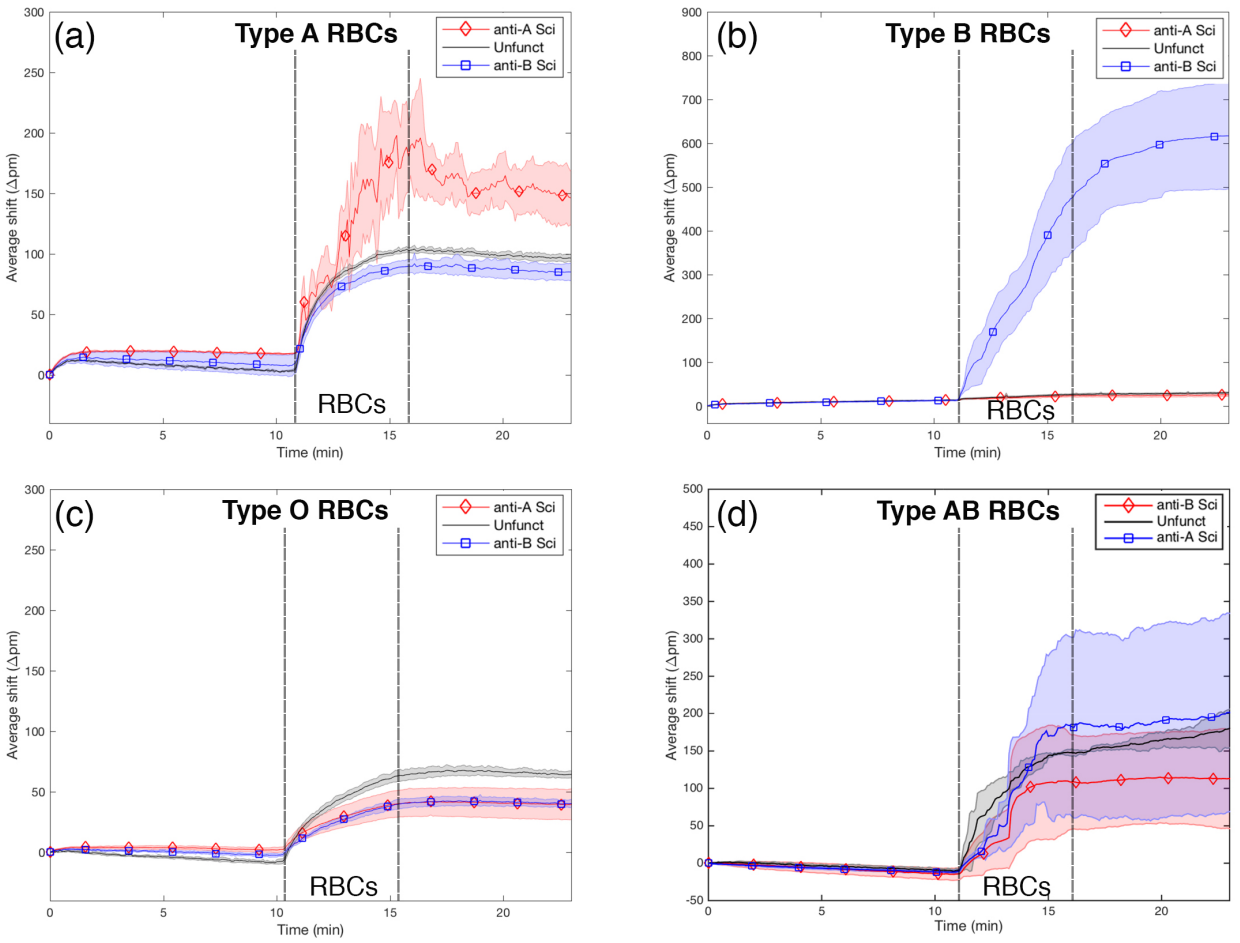

Figure 3-3. Sensorgrams of ABO forward typing on hand-functionalized chips. The wavelength shift on the y-axis is directly proportional to molecular binding that increases the local refractive index of the medium around the sensors. Standard deviation of the mean of individual sensor responses at a specific time point is represented by the shaded area in the background. Highlighted step is 1:10 diluted RBC suspension in PBS. Unlabeled steps are PBS rinses. Subplots (**a**-**d**) show typing results of type-A, -B, -O and -AB, respectively, when they were flowed across the sensor arrays at 20 μL/min. Specific forward typing signals are characterized by their noise-like fluctuations as RBCs interacted with the sensors under the flow condition. Shifts of unfunctionalized region observed in some samples were likely generated by nonspecific binding of proteins (**a**, **c** and **d**).

In both static incubation techniques, the volumetric ratios of biotinylated anti-human IgM to anti-RhD primary antibody vary from 1:0.5, 1:1, 1:5 and 1:10. These volumetric ratios were pre-validated first by flow cytometry to determine the most effective ratio between the primary and secondary antibodies that could further be adopted for hand-functionalization of the sensor chip. A 1:100 diluted red blood cells in PBS was incubated with different mixtures of the two antibodies for 15 minutes at 4^{o}C before the final centrifugation step to remove excess antibodies. In the second method, a 1:100 diluted RBC suspension in PBS was initially incubated with anti-RhD for 15 minutes at 4^{o}C first, then centrifuged to remove excess antibodies. After the supernatant was removed, biotinylated anti-human IgM was added to the RBC suspension following the volumetric ratios used in the first method. Cells were further incubated for 15 minutes at 4^{o}C and centrifuged to remove excess antibodies in the supernatant. In both methods, cell pellets were finally resuspended in PBS, and subsequently stained with streptavidin-PE. Excess fluorophores were removed by centrifugation. Cells were ultimately resuspended in PBS prior to flow cytometry analysis. Based on the fluorescence intensity, using volumetric ratios of 1:1 and 1:0.5 (biotinylated anti-human IgM : anti-RhD) was shown to capture RhD positive RBCs more efficiently than the other two ratio groups that contained higher portions of anti-RhD in the simultaneous incubation method (**Figure 3-4b**). The sequential incubation of anti-RhD and anti-human IgM method, however, showed nearly identical fluorescence intensity across all ratio groups (**Figure 3-4d**).

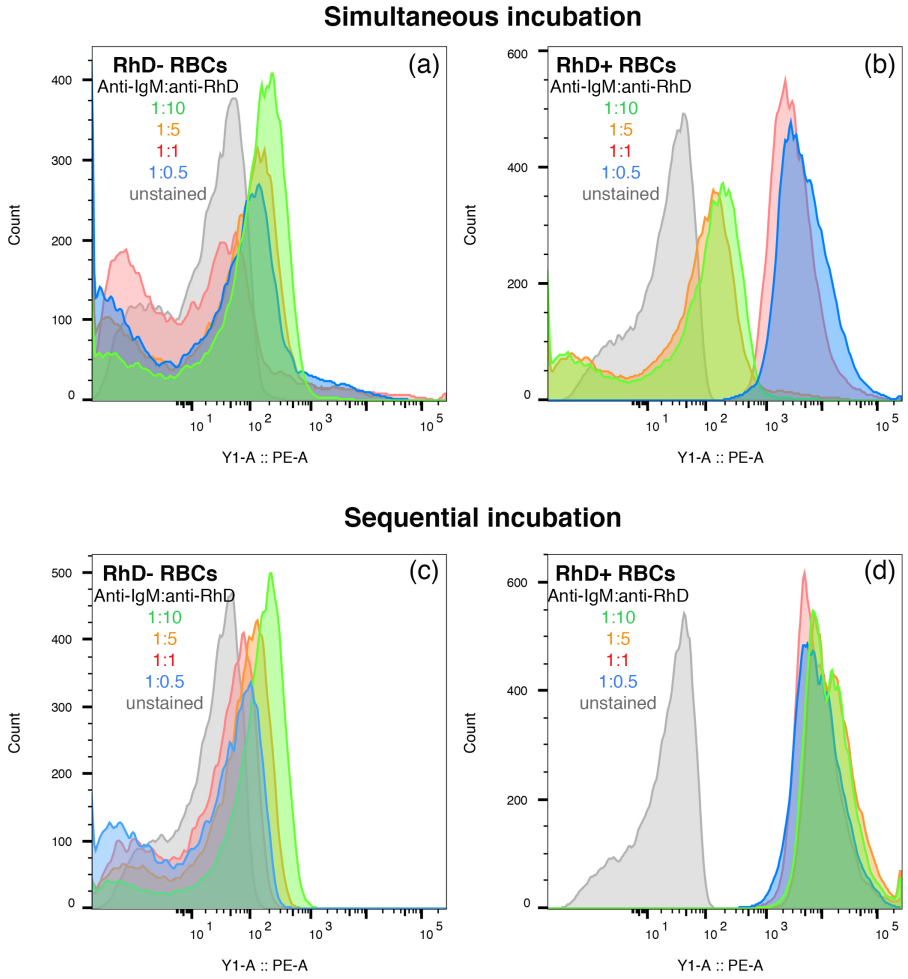

Figure 3-4. Fluorescence intensity histograms of RhD+ and RhD- RBCs stained with biotinylated anti-human IgM and anti-RhD (clone: RUM-1). The volumetric ratios of anti-human IgM to anti-RhD antibodies vary from 1:10, 1:5, 1:1 and 1:0.5. In the first group (simultaneous incubation), both antibodies were mixed well prior to incubating with RBCs. In the second group (sequential incubation), anti-RhD was incubated with RBCs first before incubating further with anti-human IgM after excess anti-RhD was removed. Successful RhD capture observed from the 1:1 and 1:0.5 volumetric ratio groups in the simultaneous incubation implies that excess anti-RhD in the cocktail of the 1:10 and 1:5 ratio groups may rapidly occupy the RBC surface and prevent anti-RhD/anti-human IgM complex from binding to RBCs (**b**). All ratios tested in the sequential incubation group yielded similarly successful results (**d**).

Following the flow cytometry analysis, we then attempted to replicate these results on the sensor chips. Chips were spotted either with 1:10 or 1:0.5 antibody mixture (biotinylated anti-human IgM : anti-RhD) on one side of the chip, and with biotinylated anti-human IgM alone on the

other side for sequential incubation of anti-RhD. The 1:10 ratio group was chosen as a negative control due to its inability to capture RhD positive RBCs in flow cytometry, whereas the 1:0.5 ratio was selected for its positive RhD capture result. Anti-RhD was spotted over the sensors previously functionalized with biotinylated anti-human IgM. Biotinylated anti-mouse IgM was spotted in the middle to serve as another negative control (denoted "IgG" in **Figure 3-5a** to **d**). The chips were then tested with RhD positive and negative RBCs for RhD antigen detection. The overall results indicated that methods developed for flow cytometry still could not be directly translated to surface functionalization of the sensor chip. Nevertheless, the sequential incubation of anti-RhD onto biotinylated anti-human IgM could slightly capture RhD positive RBCs better than using a 1:0.5 antibody mixture based on a larger average shift and a higher degree of cell-binding noises in the signals (**Figure 3-5b**). The 1:0.5 antibody mixture, despite its success in detecting RhD antigen in flow cytometry, did not show much improvement on the ability to capture RhD positive RBCs than the 1:10 ratio group (negative control) once immobilized on a solid substrate (**Figure 3-5b** and **d**). In addition, negative shifts during the final PBS rinse suggest that both static incubation techniques of anti-RhD functionalization could not capture RBCs with enough affinity to withstand the PBS rinse (**Figure 3-5a** to **d**).

The low cell-capture responses observed from both static incubation techniques had called for the in-line anti-RhD functionalization to be investigated as an alternative method. Streptavidin-coated chips were spotted with biotinylated anti-human IgM and biotinylated anti-mouse IgM (negative control) on alternating sides of the chip. Anti-RhD (clone: RUM-1) was flowed at 20 μL/min to functionalize the biotinylated anti-human IgM previously immobilized on the sensors. First, PBS was flowed to establish the initial baseline. Diluted anti-RhD (unknown titer) in PBS was flowed across both channels for 10 minutes, followed by a brief PBS rinse to remove excess antibodies. RhD positive and negative RBC suspensions were subsequently flowed in separate channels simultaneously for 5 minutes. Cells were washed off by the final PBS

rinse. Although the non-specific binding of constituents in the anti-RhD dilution was observed on the unfunctionalized region and biotinylated anti-mouse IgM spot, only sensors pre-functionalized with biotinylated anti-human IgM could capture anti-RhD and subsequently respond specifically to RhD positive RBCs. The differential shift produced by RhD positive and RhD negative samples on the anti-human IgM spots is approximately 180 pm (**Figure 3-5e** and **f**). These preliminary results of an in-line functionalization of anti-RhD are encouraging, yet this approach still has a challenge that needs to be overcome in regard to what appears like a slight positive cell capture signal when RhD negative RBCs were tested (**Figure 3-5e**). Albeit minor, this ambiguity may confound the interpretation of test results further downstream, therefore the process of in-line anti-RhD functionalization was optimized in order to avoid the incidence of false positives produced by the sensors.

Effective titer of anti-RhD for RhD antigen detection:

The first step in determining the effective titer of anti-RhD for an in-line functionalization started with observing the binding of anti-RhD suspension to the sensors functionalized with anti-human IgM, and investigating how well it could resist fouling from a type-O plasma. The sensor chip was spotted with biotinylated anti-human IgM and biotinylated anti-mouse IgM (negative control). Different volumetric dilutions of anti-RhD in PBS (1:500, 1:100 and 1:50 or **1:8**, **1:41** and **1:82 in titers**, respectively) were flowed separately across the chips (**Figure 3-6**). Distinct binding of anti-RhD suspension was observed from 1:100 and 1:50 volumetric dilutions of anti-RhD (**Figure 3-6c** and **d**), while the 1:500 volumetric dilution did not produce a significant binding curve on the anti-human IgM spot that could differentiate itself from the nonspecific binding to anti-mouse IgM spot (**Figure 3-6b**), suggesting that the antibody was too diluted and the response was overwhelmed by fouling of other protein constituents present in the anti-RhD solution.

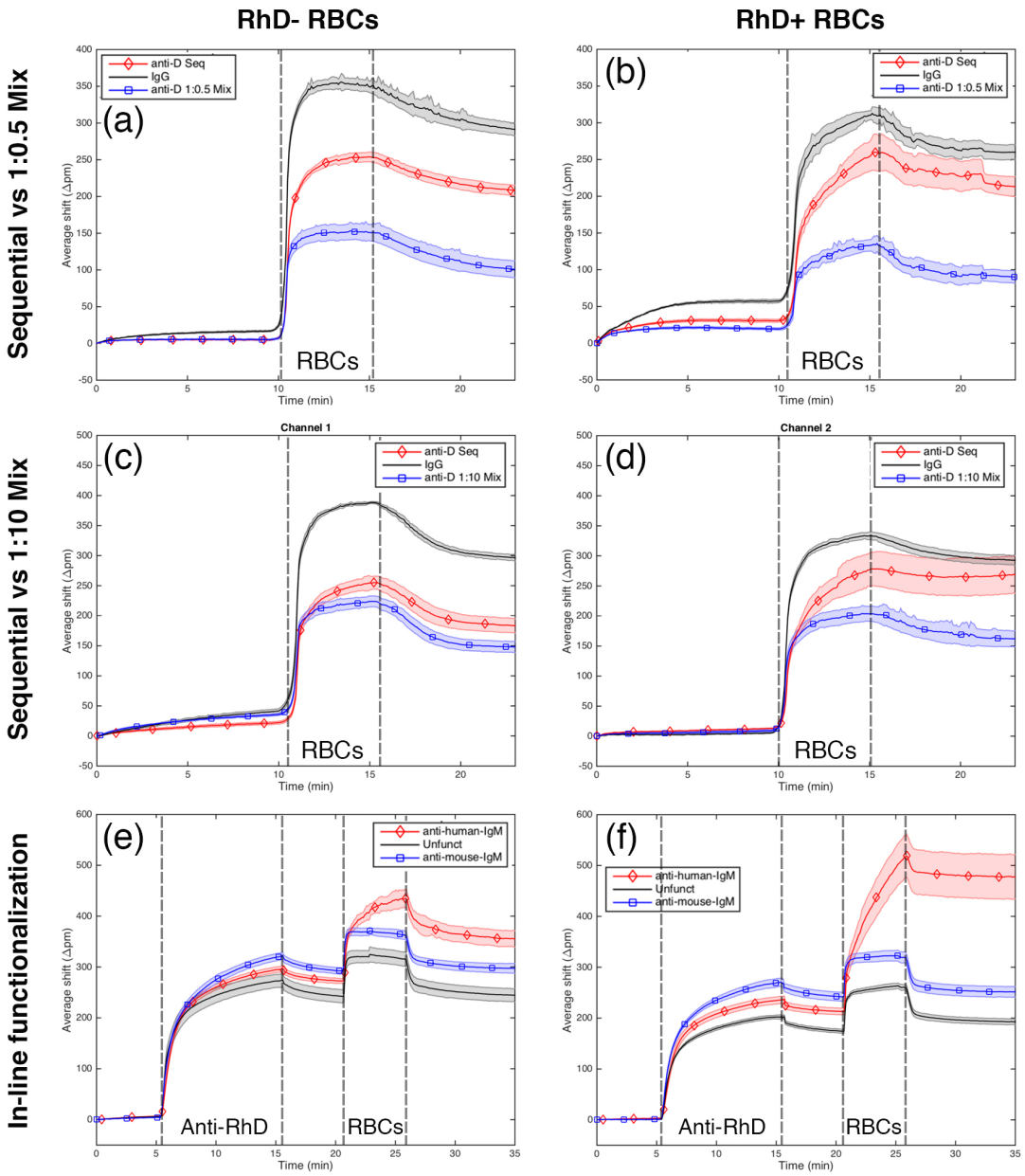

Figure 3-5. Sensorgrams of forward typing results of preliminary approaches in anti-RhD functionalization. Highlighted steps are anti-RhD (for **e** and **f**) and 1:10 diluted RBC suspension in PBS. Unlabeled steps are PBS rinses. The wavelength shift on the y-axis is directly proportional to molecular binding that increases the local refractive index of the medium around the sensors. Standard deviation of the mean of individual sensor responses at a specific time point is represented by the shaded area in the background. Sequential spotting of anti-RhD following biotinylated anti-human IgM and simultaneous spotting of the anti-RhD and biotinylated anti-human IgM cocktail were compared on the same chips (**a-d**). For in-line functionalization, anti-RhD was flowed across the sensor chip pre-functionalized with biotinylated anti-human IgM and biotinylated anti-mouse IgM (negative control) (**e-f**). No significant cell-binding interactions were observed when anti-RhD was immobilized by both static incubation techniques. Among the three approaches, the in-line functionalization of anti-RhD showed the highest potential of being further optimized to detect RhD antigen on RBCs.

After a brief PBS rinse, undiluted type-O plasma was flowed for 5 minutes followed by a PBS rinse. The degree of fouling caused by a nonspecific binding of plasma proteins was determined by subtracting the absolute shift of final PBS rinse with the baseline shift of PBS step prior to plasma exposure. We observed the reduction of fouling level as the titer of anti-RhD increased. The initial fouling of plasma was approximately 390 pm when no anti-RhD was immobilized. While the final shift of PBS baseline remains at comparable levels across all dilution groups, the degree of plasma fouling was attenuated by anti-RhD functionalization, going from 385 pm (1:500) to 230 pm (1:100) and finally to 202 pm (1:50) (**Figure 3-6b** to **d**). This means that anti-RhD immobilized on the chip had occupied sites that would have otherwise been available for nonspecific binding of plasma proteins. However, we also acknowledge that this "blocking" could be attributed by both the bound anti-RhD and constituents of anti-RhD suspension that had already fouled the sensor surface during in-line functionalization. Although this experiment could provide an approximation of how much anti-RhD was immobilized on the sensors, the ability to capture RhD positive RBCs has yet to be empirically determined.

Immobilized anti-RhD was then tested for its ability to capture RBCs by using 1:10 diluted type-O/RhD positive RBC suspension in PBS. Based on the previous fouling experiment, sensor chips were functionalized with three different volumetric dilutions of anti-RhD (clone: RUM-1) antibody (1:250, 1:100 and 1:50 or **1:16**, **1:41** and **1:82 in titers**, respectively) (**Figure 3-7**). Cell-binding specific signals were clearly observed in the 1:100 and 1:50 dilution groups, which have previously been shown to bind specifically on the anti-human IgM functionalized spots (**Figure 3-7d** and **f**).

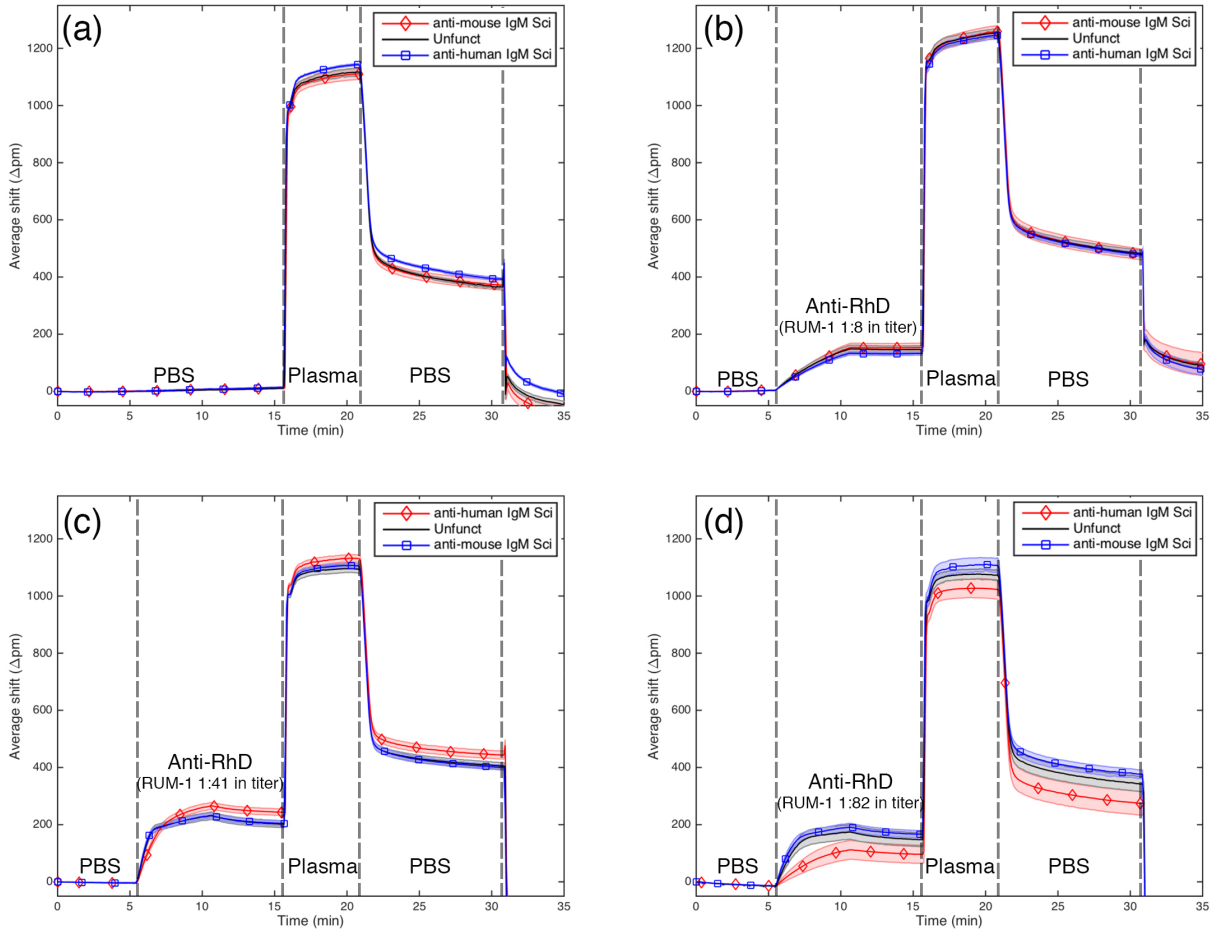

Figure 3-6. Sensorgrams of the surface blocking effect of in-line anti-RhD functionalization. The wavelength shift on the y-axis is directly proportional to molecular binding that increases the local refractive index of the medium around the sensors. Standard deviation of the mean of individual sensor responses at a specific time point is represented by the shaded area in the background. Undiluted type-O plasma was used to foul the sensor as PBS rinse simply could not remove non-specific binding of plasma proteins from the surface (**a**). Different titers of anti-RhD (clone: RUM-1) were flowed across the chip pre-functionalized with biotinylated anti-human IgM and biotinylated anti-mouse IgM (negative control) (**b** to **d**). Distinct binding curves of anti-RhD binding are observed when the titer is higher than 1:41 (**c** and **d**). Reduction in protein fouling based on surface blocking of immobilized anti-RhD progresses as the potency of titer increases, indicating a successful immobilization of anti-RhD by this approach.

Immobilization of a 1:250 volumetric dilution of anti-RhD produced very low signals of cell interactions (**Figure 3-7b**). Such signals are too ambiguous to be used in the prediction of the sample's blood type. On the contrary, shifts observed from the 1:100 and 1:50 volumetric dilution groups are more than 150 pm and 240 pm higher than shifts of the RhD negative control,

respectively. For the purpose of minimizing reagent consumption, the 1:100 dilution of anti-RhD was selected, for its ability to demonstrate successful RhD antigen capture, to the next experiment where a cocktail comprising two clones of anti-RhD antibody (human IgM) was tested for RBC capture.

Improving the specificity of RhD antigen detection by TH-28 anti-RhD antibody:

Owing to the conformational complexity of the RhD antigen, two clones of anti-RhD antibody are often mixed together and used as a cocktail of standard typing reagents. Here, a combination of RUM-1 and TH-28 clones of anti-RhD were used for capturing RhD positive RBCs. RUM-1 recognizes 18 out of 19 epitopes of RhD antigen. TH-28 recognizes 16 out of 19 epitopes, and is often used for the typing of a weak D phenotype. Chips were functionalized with anti-A and biotinylated anti-human IgM on alternating sides. A 1:100 volumetric dilution of either RUM-1 (**1:41 in titer**) or TH-28 (**1:82 in titer**) or a cocktail of both clones in PBS was flowed across the chip to functionalize the anti-human IgM spot with anti-RhD for 5 minutes at 20 μL/min followed by a brief PBS rinse to remove excess antibodies (**Figure 3-8**). A 1:10 diluted type-O/RhD positive or type-A/RhD negative RBC suspension in PBS was subsequently flowed after a PBS rinse. The chip was finally rinsed with PBS for 10 minutes to remove unbound red blood cells. Both RUM-1 and TH-28 were successfully immobilized on the chip under the flow condition and able to capture type-O/RhD positive RBCs (**Figure 3-8b** and **d**). However, raw data of individual sensors showed that cells were interacting more with RUM-1 functionalized sensors based on the signal fluctuations. Signals produced by the TH-28 functionalized sensors may appear high in the average shift, yet the degree of noise associated with cell binding was not as prominent compared to the signals observed from RUM-1.

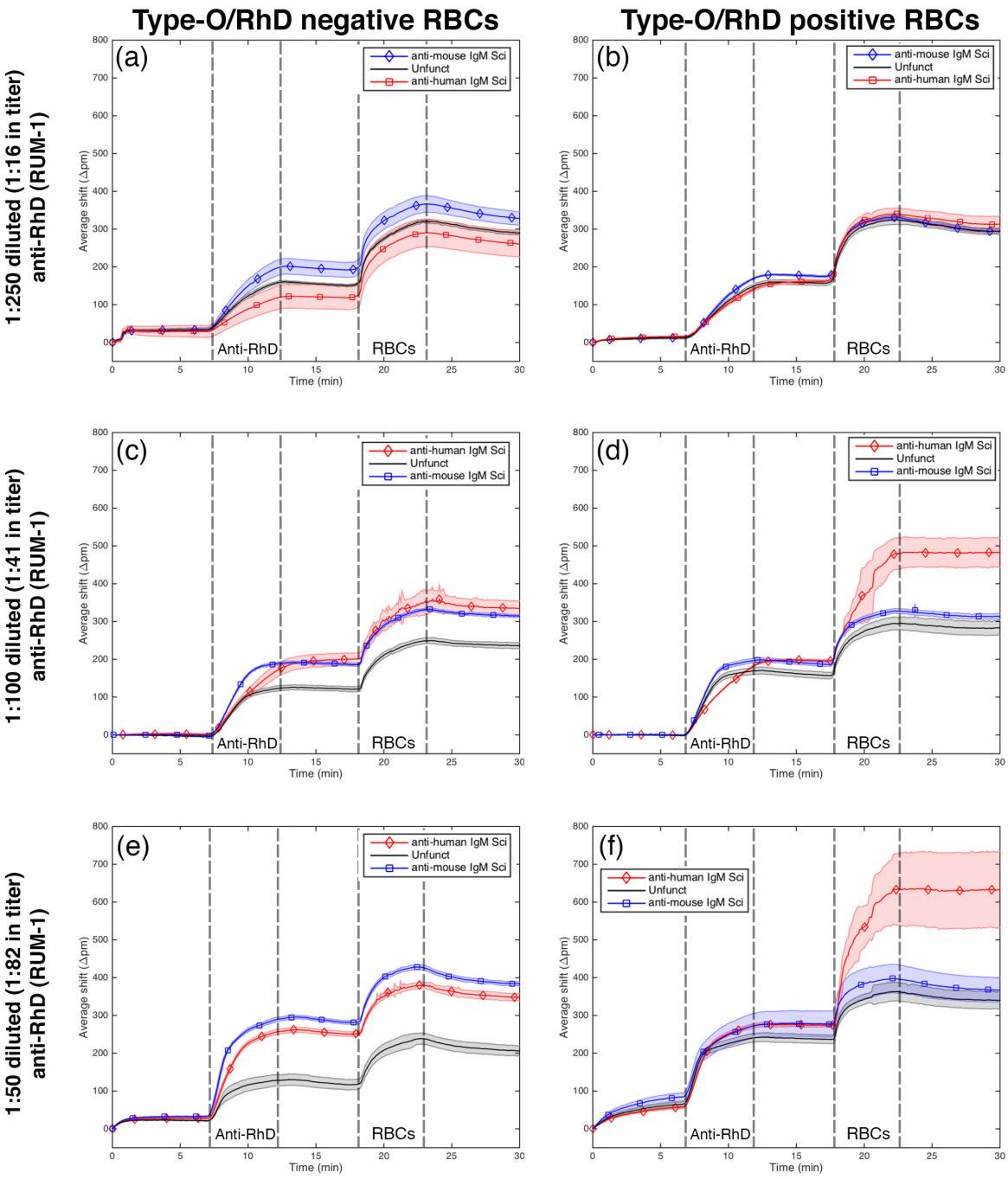

Figure 3-7. Sensorgrams of RhD forward typing results by in-line functionalization of anti-RhD (clone: RUM-1). Highlighted steps are anti-RhD and 1:10 diluted RBCs in PBS. Unlabeled steps are PBS rinses. The wavelength shift on the y-axis is directly proportional to molecular binding that increases the local refractive index of the medium around the sensors. Standard deviation of the mean of individual sensor responses at a specific time point is represented by the shaded area in the background. Different titers of anti-RhD were flowed across the chip pre-functionalized with biotinylated anti-human IgM and biotinylated anti-mouse IgM (control). The observed cell-binding interaction is directly proportional to the potency of anti-RhD titer (**b**, **d** and **f**). A small degree of false-positive noises produced by clone RUM-1 can be seen when type-O/RhD negative RBCs were tested (**c** and **e**).

Combining RUM-1 and TH-28 into a single cocktail of 1:100 diluted antibody (**1:21** and **1:41 in titer** for RUM-1 and TH-28, respectively) has also successfully captured RhD antigen on type-O/RhD positive RBCs, albeit with a slightly lower absolute shift compared to RUM-1 alone (**Figure 3-8f**). Raw data of individual sensors suggested that cell-binding signals could still persist even during the final PBS rinse step. This observation also applies to when TH-28 alone was immobilized on the sensors. When a type-A/RhD negative RBC suspension in PBS was tested, anti-A spots on all chips could elicit strong responses with no significant differences among them. Although we expected no signals to be produced by an anti-human IgM spot when tested with a type-A/RhD negative sample, high-frequency signal fluctuations were observed only when RBCs were flowed after RUM-1 alone was used to functionalize the sensors (**Figure 3-8a**).

These false-positive noises, however, were attenuated when TH-28 was functionalized in conjunction with RUM-1 (**Figure 3-8e**), and almost completely absent when it was used alone (**Figure 3-8c**). It is important to note that this pattern of false signals only persisted through the duration of RBC exposure on the sensors, and would eventually fade when PBS was introduced in the final rinse. Using only RUM-1 comes with a drawback that makes the assay prone to producing this type of temporary false positives when tested with RhD negative RBCs. A cocktail of RUM-1 and TH-28 clones is thus preferred over a single clone based on the evidences shown previously. This combination of anti-RhD antibody has been shown to be active even at a lower volumetric dilution of 1:200 (**1:10** and **1:20 in titer** for RUM-1 and TH-28, respectively) in PBS when tested with other samples of different RhD statuses (**Figure 3-9**). To finalize the anti-RhD functionalization protocol, the 1:100 volumetric dilution of RUM-1 and TH-28 cocktail (**1:21** and **1:41 in titer** for RUM-1 and TH-28, respectively) was chosen for future analysis.

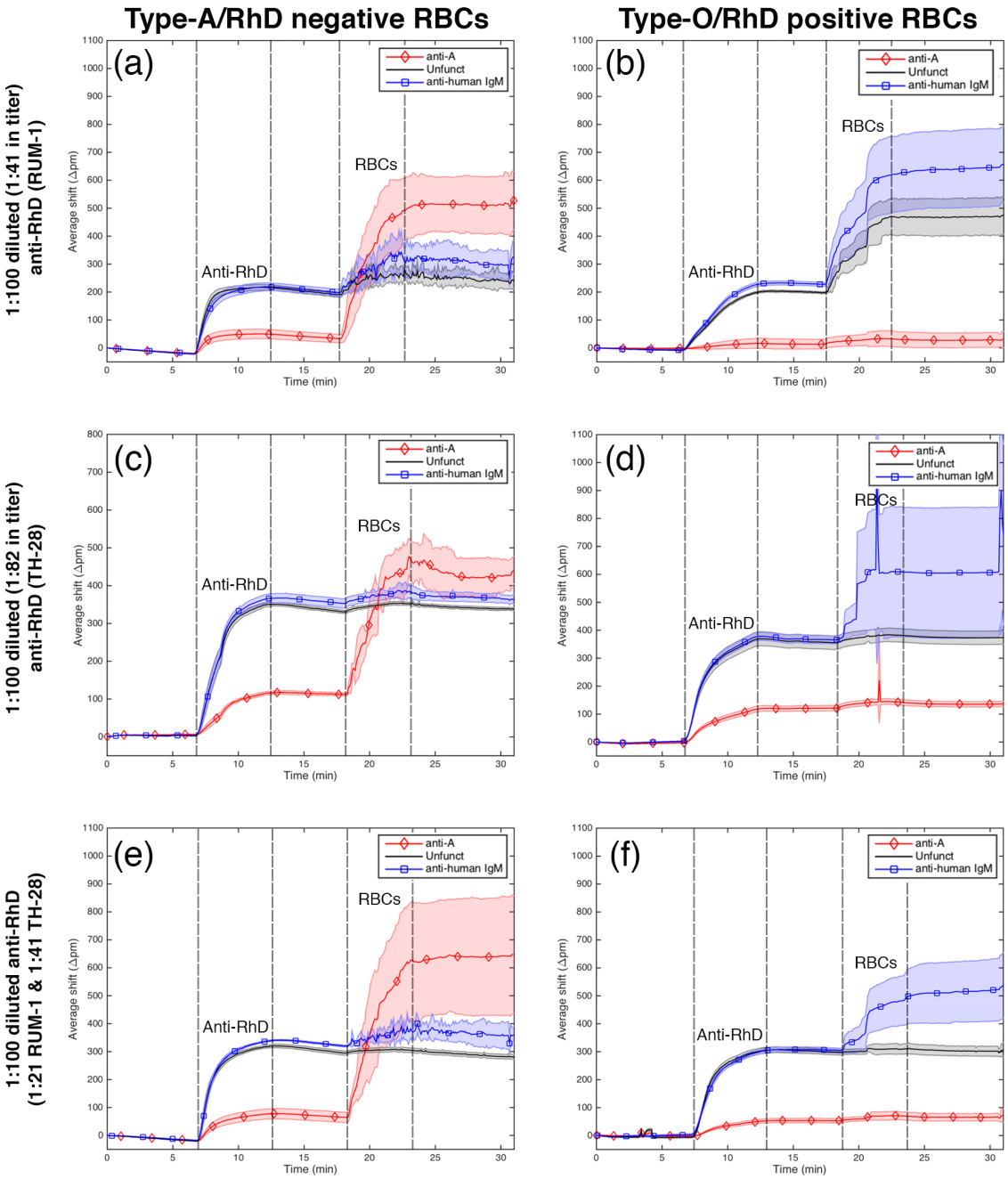

Figure 3-8. Sensorgrams of RhD forward typing results by in-line functionalization of anti-RhD cocktail (clone: RUM-1 and TH-28). Highlighted steps are anti-RhD and 1:10 diluted RBCs in PBS. Unlabeled steps are PBS rinses. The wavelength shift on the y-axis is directly proportional to molecular binding on the sensors. Standard deviation of the mean of individual sensor responses at a specific time point is represented by the shaded area in the background. Different titers of either RUM-1 or TH-28 or a cocktail of both were flowed across chips pre-functionalized with anti-A and biotinylated anti-human IgM. Sensor chips were tested with type-A/RhD negative and type-O/RhD positive RBCs. Clone RUM-1, when immobilized alone or in cocktail, is prone to producing false-positive noises (**a** and **e**) while such signals are absent when TH-28 was used (**c**). Combining both clones of anti-RhD helps reduce the non-specific noises (**e**), and still retains their ability to interact with RhD positive RBCs (**f**).

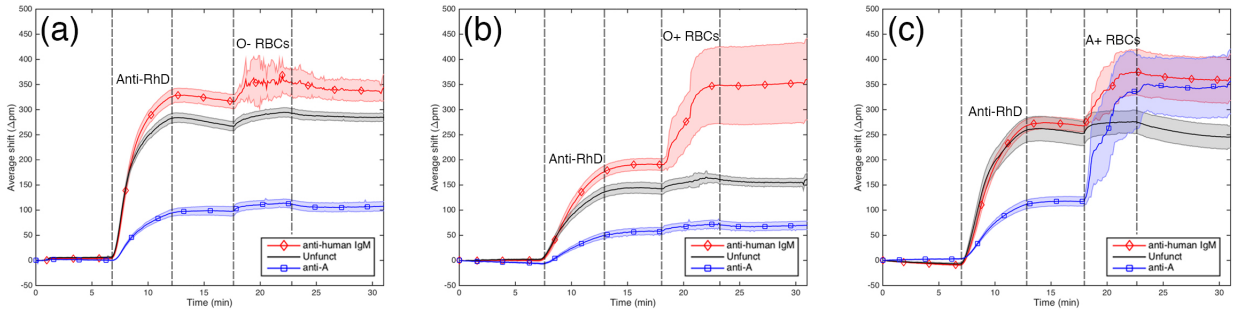

Figure 3-9. Sensorgrams of RhD forward typing results by in-line functionalization of anti-RhD cocktail (clone: RUM-1 and TH-28). The titers of RUM-1 and TH-28 are 1:10 and 1:21, respectively. Highlighted steps are anti-RhD and 1:10 diluted RBCs in PBS. Unlabeled steps are PBS rinses. The wavelength shift on the y-axis is directly proportional to molecular binding on the sensors. Standard deviation of the mean of individual sensor responses at a specific time point is represented by the shaded area in the background. Half the potencies of RUM-1 and TH-28 titers shown in Figure 3-8 was flowed across chips pre-functionalized with anti-A and biotinylated anti-human IgM. Chips were tested with type-O/RhD positive, type-O/RhD negative and type-A/RhD positive RBCs. At this titer level, anti-RhD cocktail is still capable of capturing RhD positive RBCs (**b** and **c**) while still generating non-specific noises in the signal when RhD negative RBCs were tested (**a**).

3.4.3 Detection of Kell Antigen

The in-line functionalization of human IgM capture antibody (anti-RhD) developed in section 3.4.2 was adopted for the functionalization of anti-K (clone: AEK-4) to detect the Kell (K or K1) antigens expressed on Kell positive RBCs. Although the in-line functionalization of the capture antibody is the same as anti-RhD cocktail, namely, 1:50 volumetric dilution of anti-Kell in PBS (**1:21 in titer**) was flowed on sensors functionalized with biotinylated anti-human IgM for 5 minutes at 20 μL/min, the difference lies during the flow of RBC suspension. Instead of continuously flowing RBCs for 5 minutes, Kell antigen detection requires a 5-minute pause (1 μL/min) of flow after the cells were flowed across the sensors for 5 minutes. Unbound cells were removed by the final PBS rinse. We first demonstrated the Kell antigen detection on commercial reagent red blood cells (Panocell, Immucor; Peachtree Corners, GA) as a proof of concept (**Figure 3-10**). Sensor chips were hand-functionalized with biotinylated anti-human IgM on one side along with either biotinylated anti-

GYPA (positive control) or biotinylated anti-mouse IgM (negative control) on the remaining side of the chip for control.

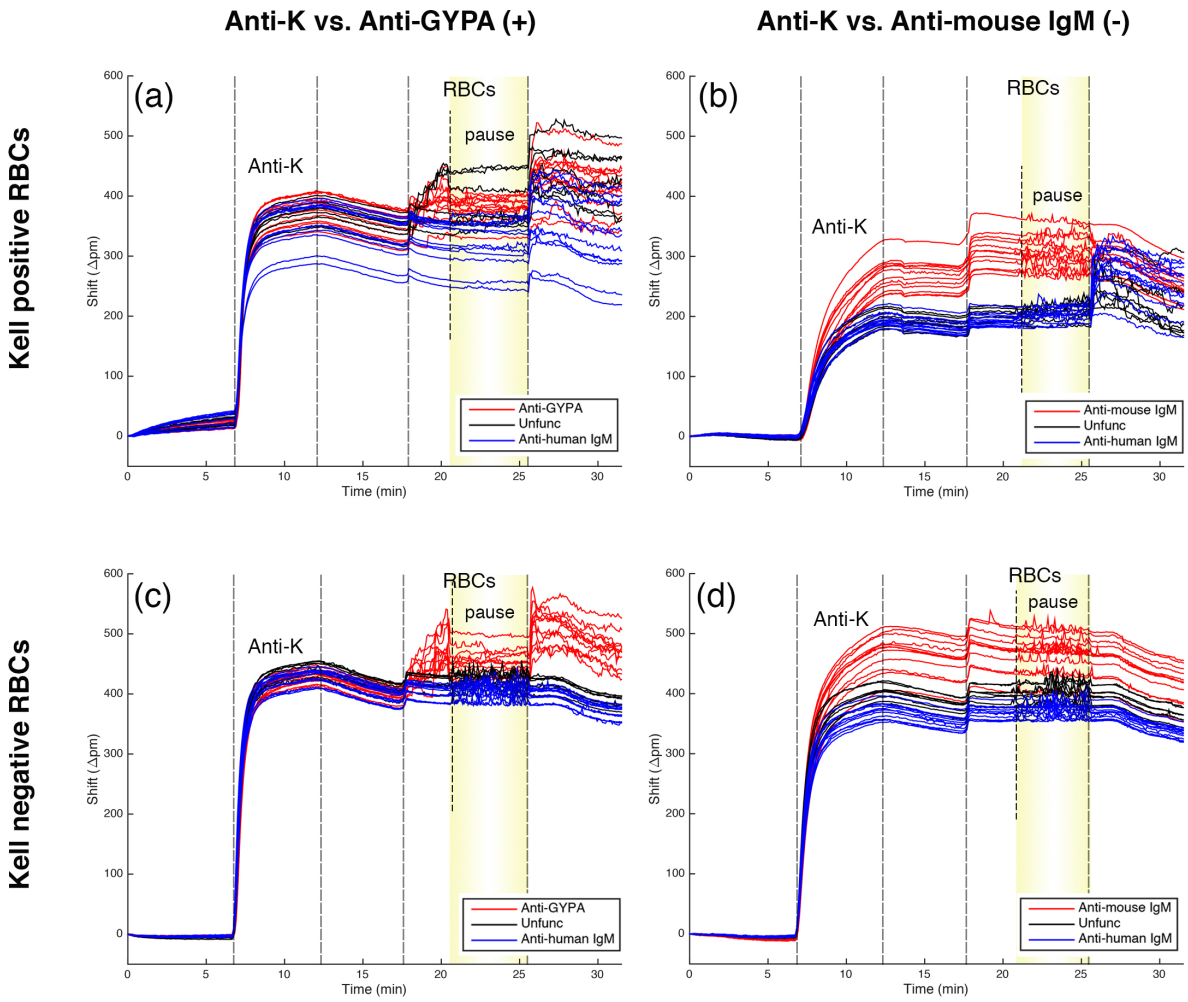

Figure 3-10. Sensorgrams of Kell forward typing results of reagent red blood cells by in-line functionalization of anti-K. Sensor chips were pre-functionalized with biotinylated anti-human IgM and either of anti-GYPA (+) (**a** and **c**) or biotinylated anti-mouse IgM (-) (**b** and **d**). Highlighted steps are anti-K (AEK-4, 1:21 in titer) and 1:10 diluted RBCs in PBS. Unlabeled steps are PBS rinses. Unprocessed data are shown to clearly display a weaker strength of cell-binding signals of Kell antigen compared to those of RhD and ABO antigens. In contrast to other forward typing assays, a 5-minute flow pause (1 μL/min) was incorporated to help detect the Kell antigen after the flow resumed (**a** and **b**). Note that the normal appearance of GYPA signals strongly suggests that the absence of specific cell binding signals of anti-K prior to a flow pause is not an artifact of using reagent cells, but rather associated with the Kell antigen. Kell negative reagent RBCs showed nonspecific noises during the flow pause, but no cell-binding signals were observed once the flow resumed (**c** and **d**).

Nonspecific binding of anti-K to anti-mouse IgM spot was consistently observed in all sensorgrams, however, the specific detection of Kell positive RBCs was not impeded. Interestingly, a transient, high-frequency noise previously described in the RhD antigen detection was observed during the flow pause on both anti-mouse IgM and anti-human IgM spots (**Figure 3-10c** and **d**). This noise would completely dissipate once the flow was resumed. For Kell-positive RBCs, The resumption of flow has triggered sudden wavelength shifts that reflect specific cell-binding signals of RBCs to anti-K functionalized sensors (**Figure 3-10a** and **b**). Anti-GYPA used a positive control for RBCs has a different pattern of response as Kell positive and negative RBCs could readily interact to the anti-GYPA spot during the initial flow before a pause. Cell-binding signals of anti-GYPA might attenuate to baseline during the flow pause, but would still reemerge once the flow was resumed (**Figure 3-10a** and **c**). The method developed for analyzing reagent cells here was successfully translated to the detection of Kell positive RBCs from donors' samples that exhibited similar behaviors of cell-sensor interactions to reagent cells (**Figure 3-11**).

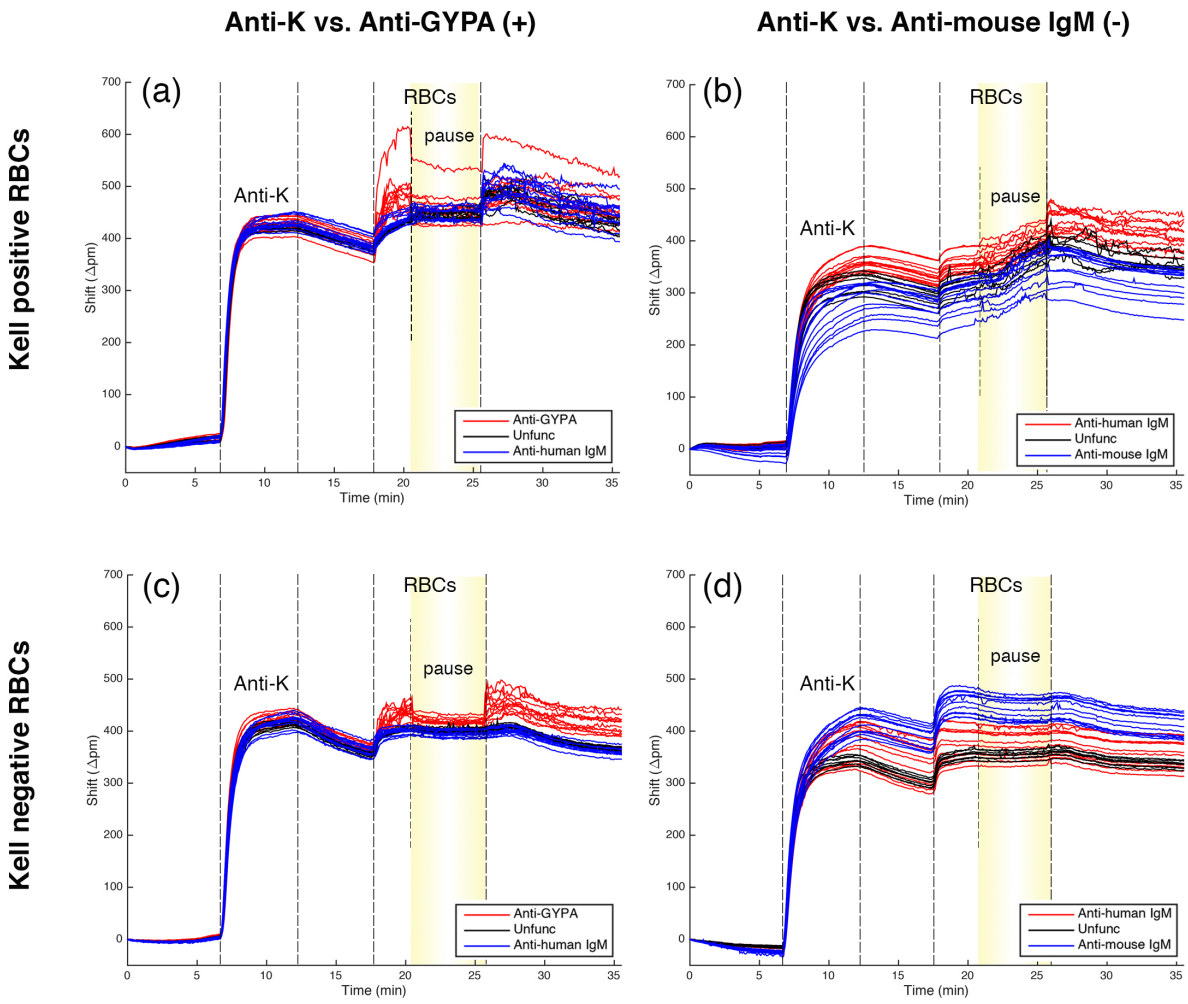

Figure 3-11. Sensorgrams of Kell forward typing results of donors' red blood cells by in-line functionalization of anti-K. Sensor chips were pre-functionalized with biotinylated anti-human IgM and either of anti-GYPA (+) (**a** and **c**) or biotinylated anti-mouse IgM (-) (**b** and **d**). Highlighted steps are anti-K (AEK-4, 1:21 in titer) and 1:10 diluted RBCs in PBS. Unlabeled steps are PBS rinses. Unprocessed data are shown to clearly display a weaker strength of cell-binding signals of Kell antigen compared to those of RhD and ABO antigens. To be consistent with the method developed for reagent RBCs (**Figure 3-10**), a 5-minute flow pause (1 μL/min) was incorporated to help detect the Kell antigen after the flow resumed (**a** and **b**). The overall signals of donors' RBCs are weaker than what observed from reagent RBCs, and this could be explained by the age of RBCs that were stored in regular anticoagulants for approximately one month after draw. Kell negative RBCs showed no cell-binding responses both during the flow pause and once the flow resumed (**c** and **d**).

3.5 Discussion

3.5.1 ABO Forward Typing on Red Blood Cells

We pioneered the surface functionalization method for ABO antigen detection of RBCs on the microring resonator chips with the limitation of using a standard forward typing IgM anti-A and anti-B antibodies. Immobilization of capture antibodies to the silicon oxide substrate was simply accomplished by the well-studied biotin-streptavidin affinity. A lack of biotin tag on typing IgM reagents was circumvented by using commercial biotinylated anti-mouse IgM that could be incubated with the capture antibodies prior to surface functionalization by a hand spotting technique. The most valuable aspect of developing the strategies for ABO forward typing of RBCs lies in a new type of cell-binding signals to the microring sensors that, to our knowledge, has neither been demonstrated nor described elsewhere in the literature.

In contrast to a regular binding characteristic of biomolecules, such as proteins, onto the sensor surface that often follows the Langmuir adsorption, specific interactions of RBCs with the microring resonators generate noise-like fluctuating signals that have been observed repeatedly on our system. This hallmark of specific cell binding has set the benchmark for the interpretation of forward typing data later on in the detection of membrane-associated RhD and Kell antigens whose structures are much more sophisticated than carbohydrate antigens in the ABO family.

3.5.2 Detection of RhD and Kell Antigens

In the process of surface functionalization of the sensor chips, whether hand-spotting or printing, it is favorable for all reagents to be spotted in a single effort. However, the immobilization of human IgM antibodies is not simply a one-step process like mouse IgM capture antibodies used in ABO typing. We learned from the flow cytometry analysis that incubating anti-RhD with biotinylated anti-human IgM (simultaneous incubation) prior to cell incubation yielded a poorer fluorescence intensity than conjugating RBCs first with anti-RhD, followed by biotinylated anti-human IgM

(sequential incubation). This discrepancy suggests that anti-human IgM may indirectly inhibit the binding of anti-RhD to RBCs possibly through induced conformational change of IgM or a significant steric hindrance that affects the binding affinity of anti-RhD to RBCs even if the anti-human IgM (isotype: IgG) was raised to target only the μ-chain of IgM. In fact, conformational change of IgM has only been reported upon antigen binding,[115,116] Using electron microscopy, Feinstein, et al., described a staple-like form of IgM from various species when it was in complex with a single flagellum where a single IgM molecule gave up its pentameric planarity, forming a dome shape to increase the binding avidity. Interestingly, this form has also been observed when IgM binds to red blood cells.[116] It is possible that the occupation of μ-chains by anti-human IgM may put a structural constraint that prevents anti-RhD from efficiently binding to RBCs.

Discoveries from these early studies of conformational changes of IgM perfectly explain the success of the sequential incubation in flow cytometry where anti-RhD was allowed to interact with RBCs in its most favorable conformation first. The subsequent binding of anti-human IgM to the μ-chains of anti-RhD could then be made without interfering with the anti-RhD/RBC complex that has already been formed. We later confirmed this finding in agglutination results by which anti-human IgM was found to interfere with the agglutination of RBCs by anti-RhD. Regardless, chips functionalized with anti-RhD through both static strategies did not exhibit the ability to capture RhD positive RBCs under the flow condition without producing ambiguous results. Despite a success in flow cytometry, functionalizing sensors sequentially with antibodies still did not improve the sensor responses much from the previous simultaneous incubation technique. This perhaps can be explained by the order of reagents spotted on the chip that was reverse from the cell staining procedure for flow cytometry. The chip was spotted first with biotinylated anti-human IgM to establish the first layer of antibody on streptavidin coated chips. Anti-RhD was spotted thereafter to form the second layer over the anti-human IgM functionalized sensors. This

order reversal forced anti-RhD to first bind to anti-human IgM before it could actually interact with RBCs, thus repeating the flaw of method development encountered in the simultaneous antibody incubation. Unfortunately, flowing RBCs pre-incubated with anti-RhD across anti-human IgM functionalized sensor probes was not an option because RhD positive RBCs would agglutinate instantly upon incubation with the anti-RhD capture antibody, and would not interact well with the sensors due to their aggregated sizes.

We then finally investigated the in-line functionalization of anti-RhD under the flow condition on the chip that was pre-functionalized with biotinylated anti-human IgM and biotinylated anti-mouse IgM (negative control). Initial results show that in-line functionalization could significantly improve cell binding from the previous two techniques. To optimize this process, the most effective volumetric dilution of anti-RhD in PBS was found to be 1:100 (clone: RUM-1, **1:41 in titer**). Although the overall signal observed from type-O/RhD positive RBCs is stronger than what observed from type-O/RhD negative RBCs, a minor degree of transient noises produced by type-O/RhD negative RBCs during the flow suggests that clone RUM-1 should not be used alone in order to avoid nonspecific cell-sensor interactions and preserve the specificity of a typing assay. At least two clones of anti-RhD antibodies, e.g. RUM-1 and MS-26, are normally used for clinical typing due to the structural complexity of antigens in the Rh family. Anti-RhD (clone: TH-28) was investigated for on-chip forward typing in conjunction with RUM-1. Both clones are well-characterized and have binding affinity towards the same epitopes on the RhD antigen, with an exception that TH-28 recognizes two epitopes less than RUM-1. Empirically, TH-28 is not as sensitive to RhD positive RBCs as RUM-1, but it is also less prone to producing a transient false positive noise on RhD negative samples. Thus, combining the two clones together can help reduce false positive signals by making the anti-RhD cocktail more specific. The method developed for anti-RhD functionalization was directly translated to the functionalization of anti-K capture antibody.

Due to various differences between antigens in the RhD and Kell systems, such as expression levels, structures, and how they associate in the lipid bilayer of cell membrane, etc., the detection of Kell antigen on RBCs was performed differently from RhD as it requires a brief pause in the flow (1 μL/min) to allow cells to incubate with the capture antibodies on the sensors. Though the transient noises were observed during the flow pause on both anti-mouse IgM and anti-human IgM spots, it is not likely an artifact contributed solely by a low flow profile because such signals were not observed on the anti-GYPA spot. This type of transient, nonspecific signals has been observed in the detection of RhD antigen despite the continuous flow of cells at 20 μL/min. These false-positive noises might be associated with weak cross-reactivity of the capture antibodies with other similar antigenic determinants on RBCs that can be simply overcome by PBS rinse.

3.6 Conclusions and Future Directions

The forward typing of ABO, RhD and Kell antigens on hand-functionalized sensors is successfully demonstrated in this chapter. Early results from ABO forward typing not only show specific outcomes of red blood cell typing, but also provide a foundation of how forward typing data are recognized and interpreted. Although the surface immobilization technique for anti-ABO capture antibodies could not be applied to anti-RhD and anti-K, we developed an alternative in-line functionalization method at which capture antibodies were immobilized under the flow condition, and as a result were able to capture RhD and Kell positive RBCs. Insights gained from developing a forward typing assay on hand-functionalized sensors described in this chapter have contributed immensely to the success of our efforts in assay multiplexing that will be discussed in Chapter 5.

The static incubation of the human IgM capture antibodies, e.g. anti-RhD and anti-K, with other biotinylated anti-human IgM reagents prior to surface functionalization is currently being

reinvestigated. The implication of this effort will allow all capture antibodies to be spotted in a single attempt of surface functionalization of the sensors. Using a biotinylated anti-human IgM nanobody whose molecular weight is only 12-15 kDa or 10 folds lower than typical IgG is shown not to inhibit the agglutination test, and is still compatible with the in-line functionalization strategy of human IgM. This encouraging finding has highlighted the use of small or engineered antibody alternatives for the future optimization of antibody immobilization process.

3.7 Acknowledgements

I would like to thank Dr. Jill Johnsen, Sophie Schmidt, Sarah Galdzicka and Sarah Ruuska from Bloodworks Northwest for their efforts in sample acquisition, distribution and management. This work could not be completed without collaborative efforts of Kerry Lannert, Dr. Jing Shang and Dr. Adam Munday. This proof-of-concept work is supported by Life Sciences Discovery Fund (LSDF), National Science Foundation (NSF) and Coulter Foundation. I also would like to personally thank the Royal Thai Government for the financial supports throughout my doctoral study.

Chapter 4 : Developing an On-Chip Reverse Typing Assay

4.1 Abstract

In the context of transfusion, serology tests that identify blood group specific isohemagglutinins and alloantibodies in plasma are equally important to the forward typing in which red blood cells are phenotypically characterized for blood group antigens. Despite the ability of high-end automated blood banking instruments to perform basic antibody screening assays, they are not customized for a point-of-care use that translocates blood typing from centralized laboratories to the site of transfusion in urgent care. With the development of multiplexed biosensing technology that provides results in real-time, the time-to-result of serologic assays can be shortened. In this chapter, the method development of the ABO reverse typing assay is described through surface immobilization of synthetic blood group A and B trisaccharides functionalized on the polyacrylamide scaffold. We demonstrated a specific detection of anti-A and anti-B antibodies from both mouse antisera and human plasma samples. This success, together with the previously established on-chip forward typing assay, has paved the way for the following development of multiplexed sensor arrays for simultaneous forward and reverse blood typing on a single chip.

4.2 Introduction

The current clinical blood typing assays are not limited to the phenotypic profiling of red blood cells performed in forward typing. In certain scenarios, knowledge of the patient's and donor's plasma antibody profiles is critically important for the safe transfusion of both packed RBCs (pRBCs) and fresh frozen plasma (FFP). In the case of pRBCs transfusion, plasma is required for every 4-5 units of pRBCs delivered to the patient who suffers from severe bleeding for fluid resuscitation.[87] In addition, pathogen-deactivated fresh frozen plasma has been therapeutically

used to improve clotting factor deficiency,[117] among its other applications in various medical procedures, such as high-risk cardiovascular surgery[118] and the treatment of coagulopathy in kidney disease.[119,120] To reduce the risk of adverse effects[121] associated with blood type incompatibility, reverse typing has to be performed along with forward typing of RBCs to semi-quantitatively identify the species of naturally occurring antibodies and alloantibodies reactive to blood group antigens. Beyond anti-A, anti-A1,[122] anti-B isohemagglutinins in the ABO family, plasma may contain unexpected alloantibodies against non-ABO blood groups that are produced in patients who may become sensitized by previous transfusions and pregnancy. Although the level of alloantibodies are found to decay over time,[123] a longer circulation of these antibodies in women[124] calls for a rigorous screening of these antibodies in patient before transfusion takes place. Thus, the efforts in performing forward and reverse typing are equally important in order to mitigate the risk of delivering incompatible RBCs to the patient's plasma, and vice versa.

Previously, the method development for translating forward blood typing assay onto the silicon photonic microring resonator chips was described. In this chapter, we attempted to reutilize the same approach in developing the on-chip reverse typing test for ABO antibodies, specifically, anti-A and anti-B isohemagglutinins in plasma samples. Together with the success from forward typing assay, our reverse typing on hand-functionalized sensor chips will be further multiplexed to allow the two typing assays to be performed in parallel on the same sensor chip.

4.3 Materials and Methods

4.3.1 Materials

IMEC-3 microring resonator chips were purchased from Genalyte, Inc., (San Diego, CA). Lyophilized streptavidin from *Streptomyces avidinii* was purchased from Sigma Aldrich (St. Louis, MO). Bovine serum albumin (BSA) was purchased from Sigma Aldrich (St. Louis, MO) to prepare

a 2 mg/mL blocking solution in PBS. Proprietary printing solution (sci-SPOT protein D1, 2 mg/mL) was obtained from Scienion AG (Princeton, NJ).

Reagents for reverse typing: biotinylated polyacrylamide (PAA), biotinylated polyacrylamide functionalized with blood group A trisaccharides (PAA-A) and biotinylated polyacrylamide functionalized with blood group B trisaccharides (PAA-B) were purchased from GlycoTech (Gaithersburg, MD). Standard typing anti-A and anti-B antisera were purchased from Immucor (Peachtree Corners, GA). Anti-human IgG/A/M were purchased from Thermo Fisher Scientific (Waltham, MA).

4.3.2 Blood Sample Handling and Preparation for Analysis

Blood samples were processed immediately upon receipt. EDTA- or citrate-stored blood was centrifuged at 2,000×g for 10 minutes at 4^{o}C. Unless otherwise stated, this centrifugation setting was used throughout the red blood cell preparation protocol. Plasma was harvested from the top layer and stored separately. Care was taken not to disturb red blood cell pellets and the buffy coat layer consisting primarily of white blood cells. Plasma-equivalent volume of PBS was added to wash red blood cell pellets. Samples were then centrifuged, and the supernatant was removed. Whole plasma was used for reverse typing, while packed red blood cells were diluted 1:10 in PBS at room temperature (137 mM NaCl, 2.7 mM KCl, 8 mM Na_2HPO_4, 1.8 mM and KH_2PO_4, pH 7.4) prior to analysis. For storage, equal volume of Citrate Dextrose Phosphate Adenine-1 (CDPA-1) blood storage solution was added to resuspend red blood cell pellets. Red blood cells were stored at 4^{o}C until use.

4.3.3 Reverse Typing on Hand-Functionalized Sensor Chips

Preparing reverse typing reagent for chip functionalization:

Biotinylated polyacrylamide (PAA) and biotinylated multivalent blood group antigen functionalized PAA-A and PAA-B were mixed with an equal volume of 2x sci-SPOT D1 printing solution to prepare a 1 mg/mL aliquot of each variation of PAA reagent. Reagents were incubated on ice for one hour prior to spotting on streptavidin-coated chips.

Chip functionalization:

Protective polymer coating on the IMEC-3 chips were removed by soaking the chips in organic solvents in the following sequence: acetone for 2 minutes (twice), isopropyl alcohol for 2 minutes (twice), and finally ultrapure Milli-Q water for 2 minutes (twice). The chips were then blow dried with filtered house air. Functionalization with streptavidin was done immediately after the cleaning step. Chips were immersed in 0.1 mg/mL streptavidin solution in PBS for 3 hours at ambient temperature. Chips were rinsed with PBS thereafter to remove excess streptavidin. Streptavidin-coated chips can be used immediately for subsequent functionalization steps, or stored dry at 4^{o}C for future use. Due to a small footprint of the chip, only two 0.6-0.8 μL spots of reagents could be comfortably pipetted onto the chip without spot merging. For reverse typing, biotinylated PAA-A was spotted on either the left or right side of the chip, leaving the remaining side available for biotinylated PAA-B or biotinylated PAA (negative control) (**Figure 4-1a**). Each spot of reagent should generously cover three clusters of sensors in Channel 1 and three clusters of sensors in Channel 2 while leaving the middle region unfunctionalized. Reagents were incubated on streptavidin-coated chips for 1 hour in a humidified environment at ambient temperature. Reagent spots were wicked off by using Kimwipes (Kimtech). Chips were then rinsed vigorously with PBS, and immersed in 2 mg/mL BSA solution in PBS for 15 minutes for blocking at ambient

temperature. Chips were rinsed again with PBS to remove excess BSA, and blow dried with filtered house air. Chips were stored at 4^{o}C for future use.

Reverse typing assays:

Unless otherwise stated, the flowrate of every step is 20 μL/min. ABO reverse typing was performed by flowing undiluted human plasma directly over the chips functionalized with PAA-A and PAA-B for 5 minutes followed by a brief PBS rinse to remove unbound antibodies and plasma proteins (**Figure 4-1b**, **d** and **f**). Anti-human IgG/A/M (40 μg/mL) was flowed across the sensor chips to amplify the signals for 5 minutes (**Figure 4-1c**, **e** and **g**). During the capture reagent validation with anti-A and anti-B mouse antisera (Immucor; Peachtree Corners, GA), anti-mouse IgM (40 μg/mL) was used instead as the secondary antibody. Excess antibodies were removed by a brief PBS rinse.

4.3.4 Instrumentation and Analysis Software

The Maverick M1 system was purchased from Genalyte, Inc., (San Diego, CA). Briefly, the instrument consists of a high-power diode laser with a central wavelength of 1,550 nm and an optical scanner to track resonant wavelength shifts of individual microring resonators over time. The system is integrated with automated microfluidics controlled by the software. Two samples can be tested in parallel. Real-time data are plotted in the analysis software for instantaneous visualization. All data are finally plotted and analyzed in MATLAB (MathWorks, Natick, MA) using a script developed in house. Processed sensorgrams show raw data from individual microring resonators and an average plot with standard deviation of the mean with respect to time.

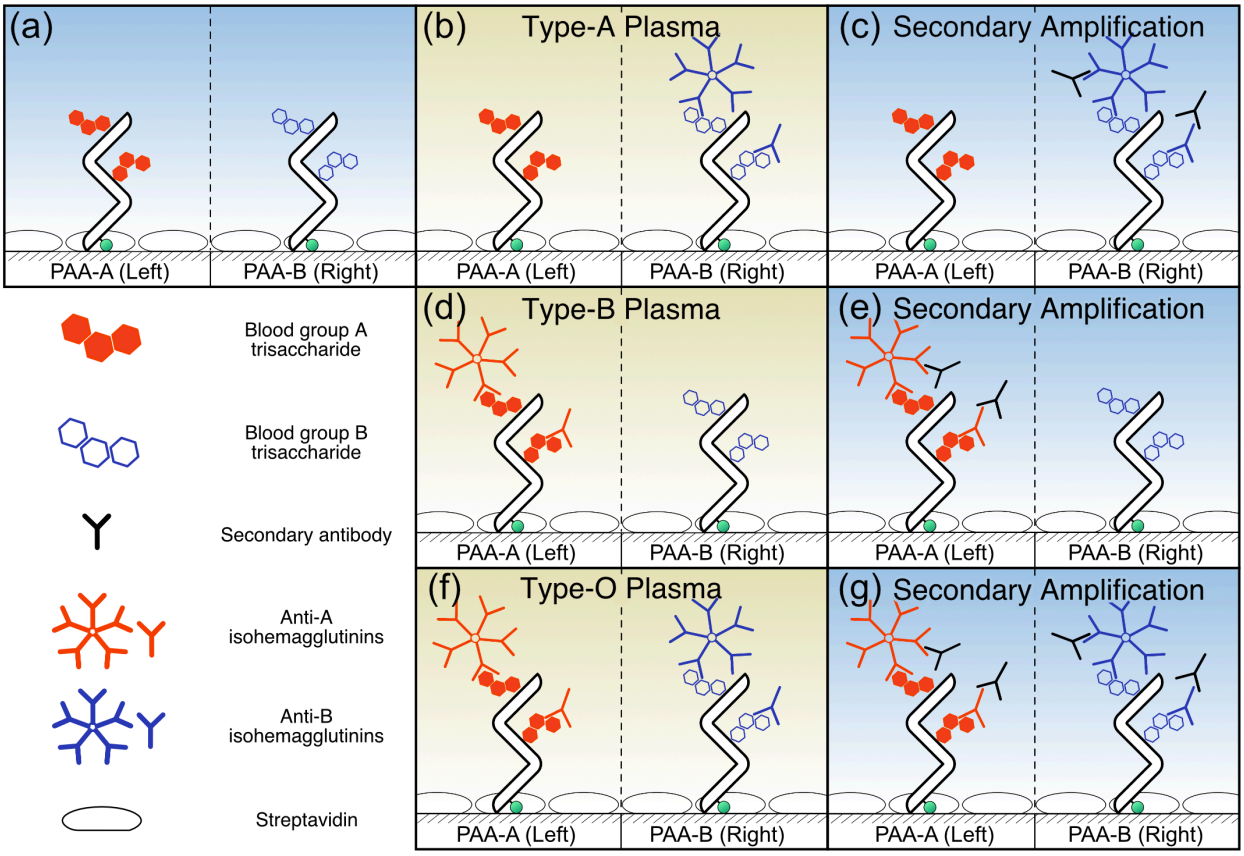

Figure 4-1. Schematic illustration demonstrating the reverse typing performed on the silicon photonic microring resonator chip. Biotinylated PAA-A and biotinylated PAA-B were immobilized on streptavidin-coated chip (**a**). In this example, type-A (**b**), type-B (**d**) and type-O (**f**) plasma samples are flowed across the sensors to allow blood group specific isohemagglutinins to bind to functionalized sensors. Following the initial plasma binding, secondary antibody is flowed to amplify the binding signals (**c**, **e** and **g**). Illustration is not drawn to scale.

4.4 Results

To take an additional step closer towards developing multiplexed sensor chips for blood typing, reverse typing was investigated on hand-functionalized chip following the same approach pursued for forward typing discussed in chapter 3. Biotinylated PAA-A and PAA-B in sci-SPOT D1 printing buffer were immobilized onto streptavidin-coated sensor chips. The volume of reagents required for spotting was typically in the range of 0.6-0.8 μL per spot. The chips were rinsed with PBS and blocked in 2 mg/mL BSA following a 1-hr incubation of the polymers. The chips were rinsed with PBS to remove excess BSA and stored at 4°C until use. Results were visualized on a sensorgram

plot where resonance wavelength shift in picometer is plotted with respect to time. The positive shift on the y-axis is directly proportional to the molecular binding on the sensor surface that increases the effective refractive index of the local medium. In reverse typing, the increasing resonance wavelength shift indicates specific binding of antibodies, along with nonspecific binding of other plasma constituents, to the sensors. Fouling by a complex medium, such as human plasma, necessitates the use of secondary antibody to amplify the specific binding signals.

Prior to the a reverse typing of human plasma samples, sensor chips functionalized with PAA-A and PAA-B were first validated with standard typing mouse anti-A and anti-B antisera (**Figure 4-2**). This step serves as an initial demonstration for the capturability of mouse antibodies (IgM) raised against human ABO blood group antigens by the synthetic blood group constructs that were functionalized on PAA. A 1:10 diluted anti-A or anti-B in PBS (unreported titers) was flowed across the sensors, followed by anti-mouse IgM as a secondary antibody. Distinct specific binding curves of anti-A (**Figure 4-2a**) and anti-B (**Figure 4-2b**) to PAA-A (red) and PAA-B (blue) functionalized sensors, respectively, were observed with the average shifts of approximately 400 pm for both typing antisera. Despite our effort in surface passivation by BSA, fouling by other stabilizing components of antisera was also observed from anti-A and anti-B indicated by a post-PBS rinse baseline of unfunctionalized sensors (black) that could not recede to the original baseline prior to antibody exposure. With the secondary amplification, the differential shift of anti-A was enhanced to 600 pm, which is nearly 2-fold higher than that of anti-B. Regardless of the degree of secondary amplification, both PAA-A and PAA-B have exhibited here a specific recognition by their corresponding antibodies.

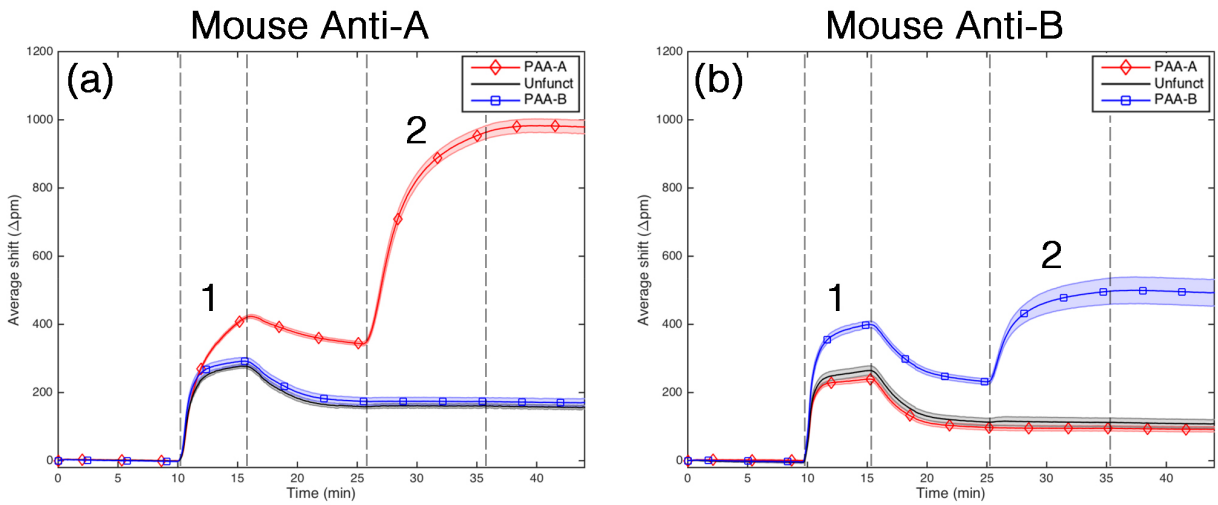

Figure 4-2. Sensorgrams of reverse typing of mouse anti-A and anti-B antisera (IgM) for initial reagent validation. The wavelength shift on the y-axis is directly proportional to molecular binding that increases the local refractive index of the medium around the sensors. Standard deviation of the mean of individual sensor responses at a specific time point is represented by the shaded area in the background. Highlighted steps are (1) 1:10 diluted antisera in PBS and (2) anti-mouse IgM secondary antibody. Unlabeled steps are PBS rinse. PAA-A and PAA-B functionalized sensors were validated with anti-A (**a**) and anti-B (**b**). Specific binding of both antisera to their corresponding multivalent synthetic blood group antigens during the initial binding (step 1) and secondary amplification (step 2).

With the promising preliminary results from mouse antisera, reverse typing was then translated to human plasma. Undiluted plasma samples generally produced a rapid rise in the shift when it was flowed across the sensors due to its bulk refractive index that is significantly greater than that of PBS (n_{PBS} = 1.336 at 20°C). Like other clinical samples, plasma is composed of a myriad of proteins and other constituents that can foul the sensor surface. The observed level of fouling was higher than 40% of the maximum shift of plasma in nearly all plasma samples tested on the sensor chips (**Figure 4-3**). Although the specific reactions of PAA-A and PAA-B to a type-O plasma sample were apparent during the initial binding (**Figure 4-3c**), it is still ambiguous in all other samples whether the initial binding was observed. Thus, the anti-human IgG/A/M secondary antibody was used to improve the sensitivity, specifically by binding to the isohemagglutinins bound to the blood group trisaccharides on PAA.

As expected, a type-AB plasma did not show any specific responses to the multivalent polymers both during the initial plasma binding and the following signal amplification steps (**Figure 4-3d**). This observation was reverse from when a type-O plasma was tested in which two strong specific binding isotherms of anti-human IgG/A/M on PAA-A and PAA-B were observed with the differential shifts of 564 pm and 407 pm for PAA-A and PAA-B, respectively (**Figure 4-3c**). Specific signals produced from type-A and -B plasma samples were not as high as the observed signals produced by a type-O plasma in this donor pool, yet still clearly distinguishable from the baseline fouling. The secondary amplification differential shifts of a type-A plasma to PAA-B and PAA-A are 328 pm and 69 pm, respectively (**Figure 4-3a**). Since the shift of PAA-A was comparable to the response observed on unfunctionalized sensors, the secondary shift of PAA-A was not suggestive of the presence of anti-A in the sample. Type-B plasma initially showed a weak reaction to PAA-A during plasma binding, but a clearer response of 238 pm was later observed during the secondary amplification, while the PAA-B response remained at the baseline. Despite surface passivation by BSA blocking, nonspecific binding was still observed on unfunctionalized sensors during secondary amplification in some plasma samples. This suggests the presence of naturally existing antibodies in those plasma samples that may adsorb to the sensor surface.

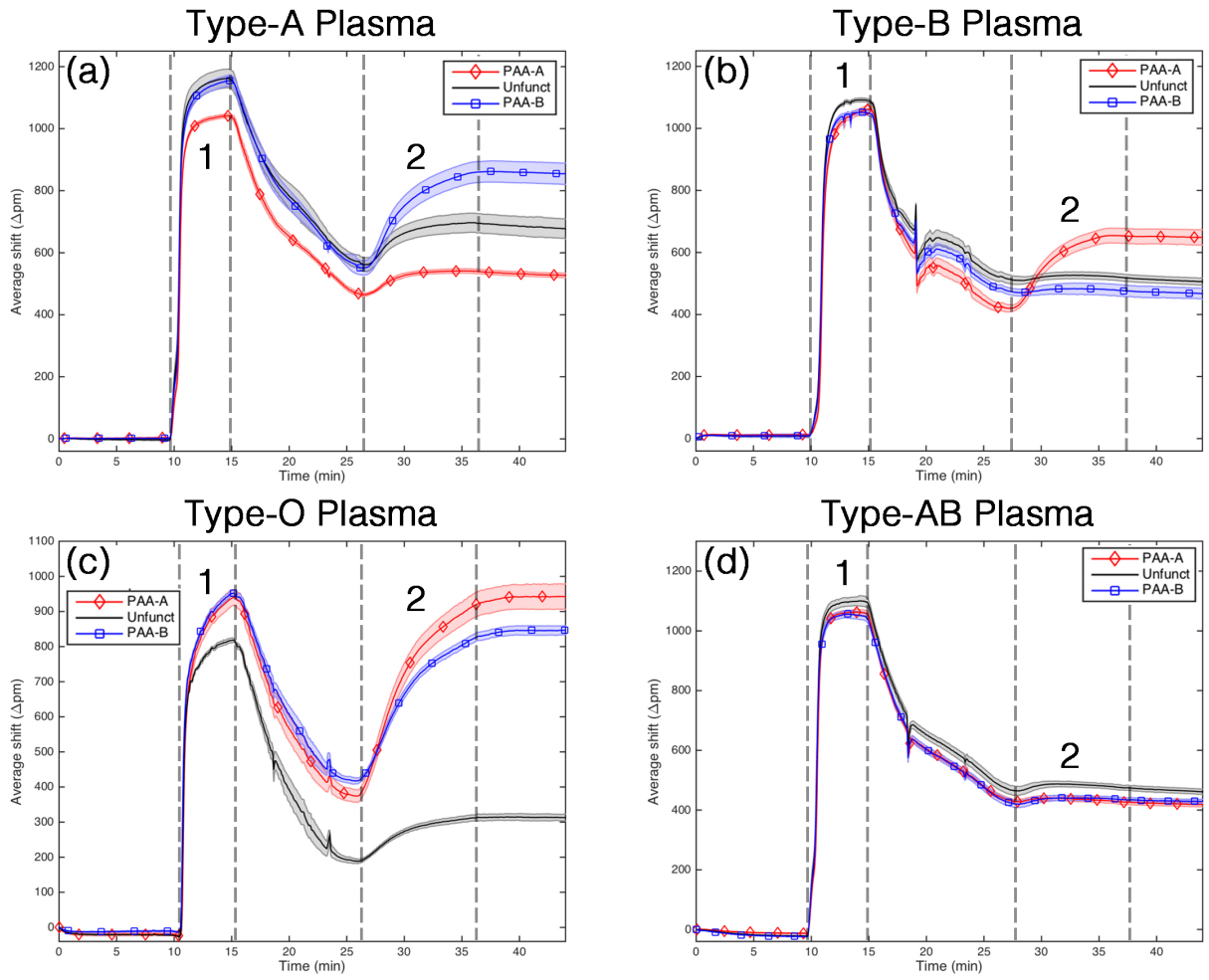

Figure 4-3. Sensorgrams of reverse typing of undiluted human plasma on hand-functionalized chips. All sensorgrams show the average wavelength shift of the sensors with respect to time. Standard deviation of the mean of individual sensor responses is represented by the shaded area in the background. Highlighted steps are (1) undiluted human plasma and (2) anti-human IgG/A/M secondary antibody. Unlabeled steps are PBS rinse. Type-A (**a**), type-B (**b**), type-O (**c**) and type-AB (**d**) plasma samples were tested for their specific reactivity to the multivalent blood group antigens immobilized on the sensors. Anti-human IgG/A/M used as the secondary antibody helped amplifying specific binding signals of blood group antibodies on PAA-A and PAA-B functionalized sensors.

4.5 Discussion

We successfully detected anti-A and anti-B in mouse antisera and human plasma samples varying in ABO profiles. Although the reverse typing results from both sources of antibodies are specific, the differences in patterns of response highlight how mouse IgM and a repertoire of ABO blood group isohemagglutinins in human plasma may recognize the multivalent trisaccharides on

the PAA backbone differently. As commercial reagents, mouse antisera were purified and tested with a panel of RBCs to ensure the specificity of antibodies to the target ABO antigens. Both antisera used for reagent validation showed specific responses during the initial binding and the secondary amplification with anti-mouse IgM. A lower secondary response of PAA-B to anti-B (**Figure 4-2b**) than the secondary response of PAA-A to anti-A (**Figure 4-2a**) reflects two possible underlying causes. First, it is possible that mouse anti-B IgM, being raised against a naturally occurring B antigen, did not recognize the synthetic type-B trisaccharides well, resulting in the observed lower interaction. However, this still does not explain why anti-A was more reactive to type-A trisaccharides when the only difference between the two synthetic blood group trisaccharides lies in the terminal N-acetylgalactosamine (GalNAc) and galactose (Gal) for the A and B antigen, respectively. Thus, it is more likely that the titer of anti-B in the commercial reagent was lower than anti-A reagent. Regardless of the degree of sensor responses, both PAA-A and PAA-B exhibited the ability to be specifically recognized by the standard typing antisera commonly used in clinics.

The challenge of using undiluted plasma samples for on-chip reverse typing is associated with their complex constituents that can foul the sensor surface via possibly multiple molecular interactions.[125] Plasma also contains a wider repertoire of naturally occurring isohemagglutinins that vary in isotypes and titers. Although the anti-fouling effect of zwitterionic polymer coating was previously demonstrated,[51] its required surface chemistry prevented this anti-fouling polymer from being exploited in our reverse typing application which is currently based upon the biotin-streptavidin affinity. As a result, significant fouling was observed in all plasma samples. Anti-human IgG/A/M was used as the secondary antibody to amplify the specific binding of blood group antibodies that may exist in multiple isotypes. In the ABO blood group, IgM predominates the pool of anti-A and anti-B antibodies in non-O plasma, while isohemagglutinins identified in type-O plasma are largely of IgG isotype. Interestingly, the secondary responses of PAA-A and PAA-B

produced by a type-O plasma was significantly higher than what observed when type-A and type-B plasma samples were tested. This high response correlates with the titer results of a type-O plasma (anti-A1 titer: 64, anti-B titer: 32) determined by reverse agglutination test of A1 and B RBCs. Although the titer of a type-A plasma is unknown, it might be similar in value to the titer of a type-B plasma (anti-A1 titer: 4, anti-B titer: 0). Based on our experiences of performing reverse typing on the sensor chips with multiple plasma samples from different individuals, some plasma samples did not always produce correlating responses on the sensors when compared to their titers. This stark contrast underlies the complexity of how isohemagglutinins interact with structurally diversified carbohydrate blood group antigens in the ABO and related blood group systems[126] in a way that simplified blood group trisaccharides cannot recapitulate.

4.6 Conclusion and Future Directions

We demonstrated the performance of reverse blood typing on silicon photonic microring resonators. With immobilized multivalent blood group antigen trisaccharides, our sensors were functionalized for capturing blood group specific antibodies present in the test samples. Validation with mouse antisera and human plasma showed specific sensor responses during the initial plasma binding in high-titer samples and secondary amplification in all samples. This initial proof of concept in translating the reverse typing assay onto silicon photonics will later be incorporated with the forward typing in our attempt to develop multiplexed blood typing assays on a single chip.

The screening for unexpected antibodies for non-ABO blood groups, namely alloantibodies against RhD and Kell antigens, is clinically performed in addition to the reverse typing. However, the task of representing intact RhD and Kell antigens whose structures are more complex than carbohydrate antigens in the ABO family comes with a challenge associated with the fact that these antigens are membrane-bound. Our early attempt in chemically fixing RBC ghosts to preserve the structures of RhD antigen showed no convincing evidence of specific anti-

RhD capture on the sensors functionalized with these RBC ghosts. Another on-going effort has been made on recombinantly expressing an extracellular-domain structure of the Kell antigen in bacterial vectors. Preliminary results on western blots showed that the expressed product is Kell-antigen sized and specifically recognize by anti-K. Despite a lack of success in using this recombinant antigen to detect anti-K on the sensors, we still believe that we are only a few steps away toward the ability to express functional Kell antigen that can be immobilized on the solid substrate without compromising its structural integrity.

4.7 Acknowledgements

I would like to thank Dr. Jill Johnsen, Sophie Schmidt, Sarah Galdzicka and Sarah Ruuska from Bloodworks Northwest for their efforts in sample acquisition, distribution and management. This work could not be completed without collaborative efforts of Kerry Lannert, Dr. Jing Shang and Dr. Adam Munday. This proof-of-concept work is supported by Life Sciences Discovery Fund (LSDF), National Science Foundation (NSF) and Coulter Foundation. I also would like to personally thank the Royal Thai Government for the financial supports throughout my doctoral study.

Chapter 5 Simultaneous Serologic and Phenotypic Analyses of Blood on Multiplexed Microring Resonator Arrays

5.1 Abstract

Blood transfusion in trauma and urgent care, when time permits, requires a blood typing to ensure the compatibility of the given blood products to the patient's blood type. With a lack of current technology to support a rapid bedside typing, many institutions adopt a widely used protocol that places an inventory burden on type-O red blood cells. Our previous success in the development of forward and reverse blood typing assays on silicon photonic microring resonators further has ushered in a new advancement on multiplexed assay that incorporates both serologic (reverse) and red blood cells (forward) typing to be performed in parallel on a single chip, requiring only a small amount of blood sample per test. Reagents were spotted directly onto individual sensor probes by piezoelectric printing technology. Sensor chips were validated with standard typing antisera and human blood samples prior to a large-scale test involved 220 clinically-obtained donors' blood samples. Overall, the performance of our sensor chips is close to the gold standard agglutination test based on the accuracy of the first 100 chips. To our knowledge, this is the first proof-of-concept demonstration of using multiplexed silicon photonic microring resonators in a clinical blood typing application. This initial achievement will serve as a technological basis for the future development of blood typing assays and test platform catered to near-patient testing.

5.2 Introduction

In the previous two chapters, the groundwork for developing forward and reverse typing assays on silicon photonic sensors has been established and elaborated in details. Despite their abilities to perform blood typing accurately, these assays lack a key attribute of multiplexing that would

enable their transition into the use in clinics and near-patient settings. Multiplexing is the ability of a sensor to perform multiple assays in parallel. In other words, multiplexing allows multiple clinical questions of interest, such as blood group associated antigen and antibody profiles in a patient's blood sample, to be answered in a single attempt. The development of multiplexed sensors for blood typing has a direct implication and immediate practicality in trauma or massive hemorrhage where bleeding is the leading cause of hospital-related mortality.[83–86] In trauma, patients with 20-30% blood loss may be given multiple types of blood products for fluid resuscitation, depending the cases and the severity of exsanguination. Two common blood products that are often administered are packed red blood cells (pRBCs) and fresh frozen plasma (FFP), which has to be delivered for every 4-5 units of pRBCs given.[87]

In theory, known patients' blood types are required in order for compatible blood products to be administered appropriately. This can be performed by standard agglutination test at the site of transfusion. In practice, however, physicians are constrained by urgency and eventually are limited to using type-O red blood cells.[88] The current institutional protocol at the Harborview Medical Center (Seattle, WA) specifies type-O/RhD negative and type-O/RhD positive red blood cells for fluid resuscitation of female and male trauma patients, respectively. Although this seems sufficient, a recent retrospective study conducted in England and Wales has shown that only 2% of the patients with massive hemorrhage received transfusion in an optimal manner while also identifying that the administration of pRBCs is often delayed by 40 minutes[85], a time that can be critically important to saving patient's life. The advent of near-patient instrument for rapid blood typing could undoubtedly alleviate this issue by providing a more rapid time-to-result for blood typing and, most importantly, reducing the inventory burden of type-O red blood cells. In this chapter, the process of combining both forward and reverse typing assays onto a single silicon photonic chip for simultaneous serologic and red blood cells analyses will be discussed along with the first proof-of-concept demonstration of blood typing on multiplexed sensors.

5.3 Materials and Methods

5.3.1 Materials

IMEC-3 microring resonator chips were purchased from Genalyte, Inc., (San Diego, CA). Lyophilized streptavidin from *Streptomyces avidinii* was purchased from Sigma Aldrich (St. Louis, MO). Proprietary printing solution (2x sci-SPOT protein D1) was purchased from Scienion AG (Princeton, NJ). Fresh stocks of 125 mM glycine (pH 3.0) and 0.1 M acetate (pH 4.5) in Milli-Q water were prepared prior to use or shipment.

Reagents for forward typing: standard typing mouse IgM anti-A (clone: BIRMA-1), mouse IgM anti-B (clone: LB-2), human IgM anti-RhD (clone: RUM-1) and human IgM anti-RhD (clone: TH-28) were purchased from Merck Millipore (Billerica, MA). Biotinylated IgG anti-glycophorin CD235a (GYPA) and PE-streptavidin were purchased from Miltenyi Biotec (San Diego, CA). Biotinylated anti-mouse IgM, biotinylated anti-human IgM and mouse IgM isotype control were purchased from Thermo Fisher Scientific (Waltham, MA).

Reagents for reverse typing: biotinylated polyacrylamide (PAA), biotinylated polyacrylamide functionalized with multivalent blood group A trisaccharides (PAA-A) and biotinylated polyacrylamide functionalized with multivalent blood group B trisaccharides (PAA-B) were purchased from GlycoTech (Gaithersburg, MD). Standard typing anti-A and anti-B antisera (IgM) were purchased from Immucor (Norcross, GA). Biotinylated anti-human IgM and anti-human IgG/A/M were purchased from Thermo Fisher Scientific (Waltham, MA).

Blood sample collection and handling: blood samples were obtained from consented donors at Bloodworks Northwest (Seattle, WA) based on the protocol approved by the IRB of University of Washington. During a large-scale proof of concept of blood typing, five whole blood samples were drawn one day prior to delivery. Daily samples were divided into two batches and typed in parallel by the multiplexed sensor chips and tube-based agglutination test on the day of receipt. All blood samples were stored in either K_2EDTA or citrate upon collection.

5.3.2 Blood Sample Handling and Preparation for Analysis

Blood samples were processed immediately upon receipt. EDTA-stored blood was centrifuged at 2,000×g for 10 minutes at 4°C. Unless otherwise stated, this centrifugation setting was used throughout the red blood cell preparation protocol. Plasma was harvested from the top layer. Care was taken not to disturb red blood cell pellets and the buffy coat layer consisting primarily of white blood cells. Plasma-equivalent volume of PBS was added to wash red blood cell pellets. Samples were then centrifuged, and the supernatant was removed. Whole plasma was used for reverse typing, while packed red blood cells were further diluted 1:10 in PBS at room temperature (137 mM NaCl, 2.7 mM KCl, 8 mM Na_2HPO_4, 1.8 mM and KH_2PO_4, pH 7.4) prior to analysis. For sample storage, equal volume of Citrate Dextrose Phosphate Adenine-1 (CDPA-1) blood storage solution was added to resuspend red blood cell pellets. Samples were centrifuged and stored at 4°C until use.

5.3.3 Buffer Optimization of Forward Typing on Printed Chips

The effect of printing buffers on the activity of IgM capture antibodies was primarily investigated on the printed chips. Sensor probes were functionalized with anti-A/biotinylated anti-mouse IgM mixture printed in four different buffers: sci-SPOT D1, glycine (pH 3.0), acetate (pH 4.5) and 1:2

diluted acetate buffers. Streptavidin-coated chips prepared according to the standard protocol described in Chapter 3 and 4 were aligned on a 10×10 grid in a Gel-Pak chip container (Hayward, CA) and stored at 4°C in a resealable plastic pouch containing a packet of desiccant. Chips and reagents were shipped in BloodworksNW's FDA-approved container overnight to the printing facility. Temperature inside the box was maintained at 2-5°C by cooling materials. Anti-A/anti-mouse IgM mixture in its manufacturer's stock solution was shipped in a separate container from printing buffers. The anti-A mixture was then reconstituted in these printing buffers immediately before printing following a guideline listed in **Table 5-1**. There are 16 probes available per each channel of the chip, but only 8 nonadjacent probes were functionalized to avoid contamination. A print map is shown in **Figure 5-1a**. Printed chips were tested with type-A and -O RBCs.

5.3.4 Instrumentation and Analysis Software

The Maverick M1 system was purchased from Genalyte, Inc., (San Diego, CA). Detailed operating principle of the instrument is discussed elsewhere.[39] Briefly, the instrument consists of a high-power diode laser with a center wavelength of 1,550 nm and an optical scanner to track resonance wavelength shifts of individual microring resonators over time. The system is integrated with automated microfluidics controlled by the software. Two samples can be tested simultaneously. Data are acquired in real-time and plotted in the analysis software for instantaneous visualization. All data were analyzed in MATLAB (MathWorks, Natick, MA). Processed sensorgrams show raw data from individual microring resonators and a plot of the average data with standard deviation of the mean at specific time points.

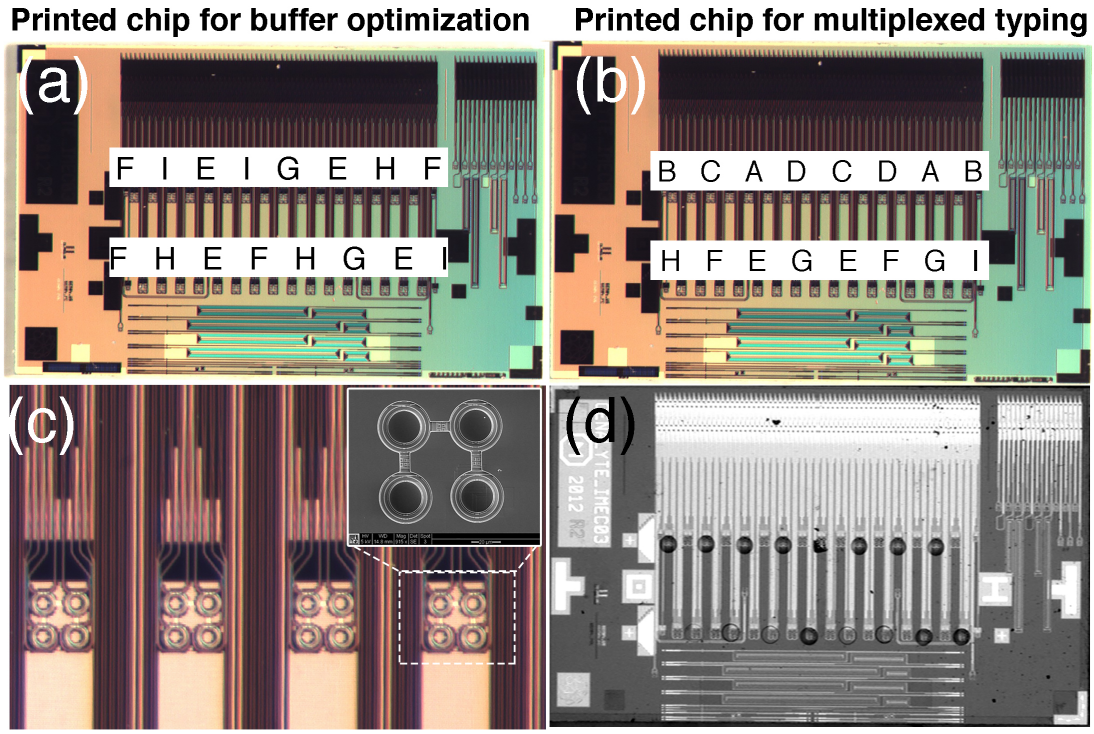

Reagents for the buffer optimization
E: Anti-A in sci-SPOT D1; **F**: Anti-A in acetate buffer (pH 4.5); **G**: Anti-GYPA in sci-SPOT D1;
H: Anti-A in glycine buffer (pH 3.0); **I**: 1:2 diluted anti-A in acetate buffer
Reagents for the multiplxed chip
A: PAA-A; **B**: PAA; **C**: Anti-human IgM; **D**: PAA-B; **E**: Anti-A + anti-IgM; **F**: Anti-B + anti-IgM;
G: Anti-human IgM (for anti-RhD functionalization); **H**: Murine IgM isotype + anti-IgM; **I**: Anti-GYPA

Figure 5-1. Reagent print maps for multiplexed sensor chips. Print maps for print buffer optimization (**a**) and large-scale print for reverse and forward typing (**b**). Reagents were printed directly on every other individual sensor probe consisting of four sensors (**c**). Printed spots are visible under the microscope (**d**). Unfunctionalized sensors were not interrogated. Reverse and forward typing assays are performed separately in Channel 1 (top sensor array) and Channel 2 (bottom sensor array), respectively.

Table 5-1. Reagents and required volumes of their corresponding printing buffers.

Spot	Reagent	Volume of reagent (μL)	Printing buffer, volume (μL)	Final titer
E	Anti-A/anti-mouse IgM	19.7/5.3	Sci-SPOT, 25	1:403
F	Anti-A/anti-mouse IgM	19.7/5.3	Acetate, 25	1: 403
G	Anti-glycophorin A	25	sci-SPOT D1, 25	-
H	Anti-A/anti-mouse IgM	19.7/5.3	Glycine, 25	1: 403
I	Anti-A/anti-mouse IgM	19.7/5.3	Acetate, 50	1: 403

5.3.5 Large-Scale Printed Chips for Simultaneous Forward and Reverse Typing

Prior to a large-scale print, 10 chips were sent to the printing facility at Scienion AG (Princeton, NJ) to optimize the printing conditions. Chips and reagents were shipped in the condition specified

in section 5.3.3. A technician at the printing facility was instructed to dilute individual reagents in designated printing buffers following the guideline listed in **Table 5-2** and **Figure 5-1b**. Following the test print, a total number of 400 chips were sent to the printing facility in two different batches for a large-scale print. Standard operating procedure for chip handling during the shipping process can be found in Appendix A. In Channel 1, reverse typing reagents were dispensed onto individual sensor probes consisting of four microring resonators using a droplet volume of approximately 475 pL (~100 μm in diameter). All four reverse typing reagents (PAA, PAA-A, PAA-B and anti-human IgM) were printed on both the left and right partitions of the chip with differing orders (**Figure 5-1b**). In Channel 2, forward typing reagents were dispensed onto sensor probes with anti-A mixture, anti-B mixture and anti-human IgM printed on both partitions of the chip. Anti-glycophorin A (GYPA) and mouse IgM isotype controls were printed on the two outermost sensor probes.

Table 5-2. Reagents and required volumes of the printing buffers for a large-scale print.

Spot	Reagent	Volume of reagent (μL)	Printing buffer, volume (μL)	Final titer
A	PAA-A (2 mg/mL)	25	sci-SPOT D1, 25	-
B	PAA (2 mg/mL)	25	sci-SPOT D1, 25	-
C	Anti-human IgM (1 mg/mL)	25	sci-SPOT D1, 25	-
D	PAA-B (2 mg/mL)	25	sci-SPOT D1, 25	-
E	Anti-A/anti-murine IgM	19.7/5.3	Glycine, 25	1:403
F	Anti-B/anti-murine IgM	18.8/6.2	Glycine, 25	1:1540
G	Anti-human IgM (1 mg/mL)	25	sci-SPOT D1, 25	-
H	Isotype/anti-murine IgM	19.2/5.8	Glycine, 25	-
I	Anti-glycophorin A	25	sci-SPOT D1, 25	-

Remarks: Printed chips were sent back inside the same container under the same condition specified in section 5.3.3. A 125 mM, pH-3 glycine buffer was used to print anti-A (spot E) and anti-B (spot F) antibodies. Proprietary 2x sci-SPOT D1 buffer obtained from Scienion AG was used to print all other reagents. Images of individual chips were taken for visual evaluation of the spot quality. (Please see Appendix B for a standard operating procedure for chip handling.) Chips whose both channels were printed perfectly (i.e. spot coverage over sensor probes was full), were used for a blind test. Chips whose only one channel was printed perfectly were used for validation and training purposes.

5.3.6 Blood Typing of Blind Samples on Printed Chips

A large-scale demonstration of performing blood typing using clinically-obtained, blind blood samples on our multiplexed sensors began after the printed chips from a large-scale print were

fully validated with commercial antisera and human blood samples. This proof-of-concept demonstration spanned the duration of 5 months with a brief pause for 15 days due to a logistics issue of sample distribution. The total of 220 samples with a nearly even distribution of ABO/RhD profiles were used specifically for the blind blood typing. These samples were previously typed by BloodworksNW's automated instrument upon collection. Information of donors and their blood types was curated by the Blood Bank Computer Systems (BBCS; Auburn, WA). Five samples were distributed daily from BloodworksNW's central campus (Seattle, WA) to BloodworksNW Research Institute (Seattle, WA) and the University of Washington for tube-based agglutination test and on-chip typing, respectively. Tube test provides agglutination scores of red blood cells in antisera and DBA lectin for forward typing, and those of reference A1, A2, B cells in plasma for reverse typing. Typing data from multiplexed chips provide qualitative information regarding which blood group associated antigens and antibodies are present in the sample.

Once all samples were typed, three independent observers were trained to interpret and analyze the typing data from the printed chips through a MATLAB-based analysis tool. Training datasets were garnered from the initial test print and a large-scale print in which the ABO/RhD profiles of the samples were revealed specifically for the training purpose. The three observers then separately analyzed the data from 220 blood samples. They were instructed to provide a prediction of the sample blood type based on the forward and reverse typing results individually and an overall prediction of the sample's ABO/RhD profile. The order of the samples was randomized uniquely for each observer. When the forward and reverse typing results conflict with each other, observers were advised to prioritize forward typing data over reverse typing due to a higher fidelity of the forward typing assay. Once the analysis was complete, overall predictions of blood types from each observer were compared. Samples whose predictions were discordant among the observers were flagged and harmonized by another independent observer who was experienced with data interpretation. BBCS blood types of the samples were revealed thereafter

to match the finalized predictions of the samples' blood types. Unmatched samples were further analyzed to identify the types of error associated with ABO and RhD detection. The analysis workflow is summarized in **Figure 5-2**.

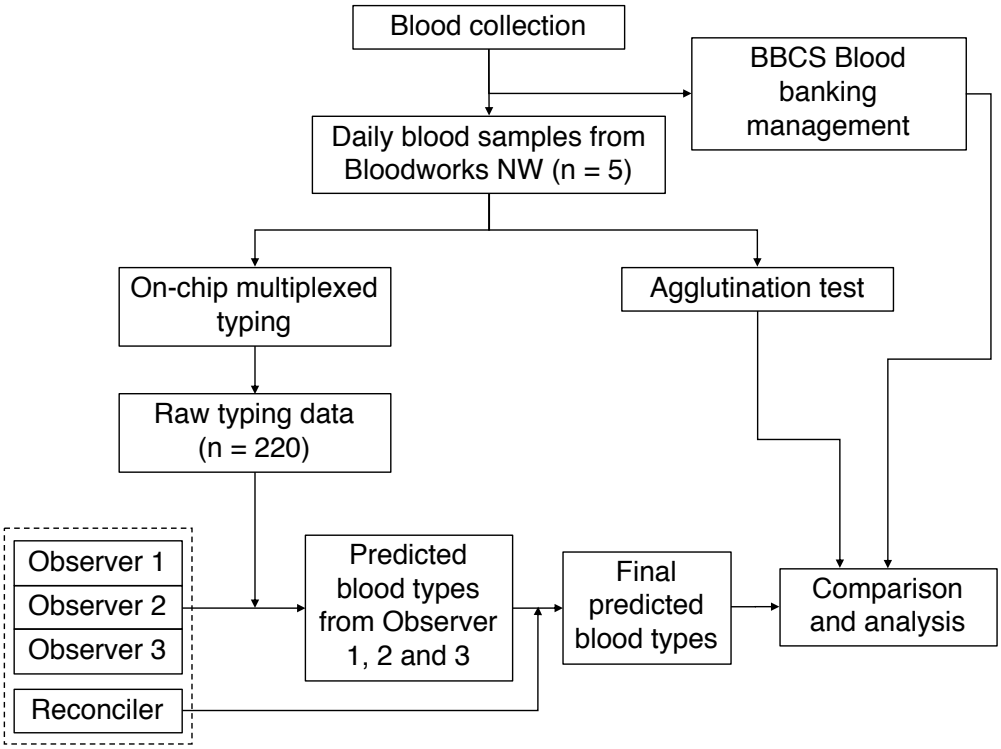

Figure 5-2. Schematic of the workflow of blood typing analysis in a large-scale proof of concept.

Analysis of Forward-Reverse typing discrepancies:

Results from forward and reverse typing were both presented to the observers in order for them to predict the sample ABO/RhD status. Conflicts of test results between the forward and reverse typing have been observed on multiple occasions during the analysis of 220 blood samples. When such incidence occurs, observers were instructed to prioritize forward typing results. The first 100 chips in analysis (by the order of use) were analyzed for discrepancies between the forward and reverse typing results. Reverse typing results from the tube test and on-chip typing were used to predict the samples' ABO blood types. Predicted ABO blood types from both methods were

compared to the samples' BBCS blood types. Unmatched samples were flagged for further analysis which identifies false positives and false positives based on the observed responses of PAA, PAA-A, PAA-B and anti-human IgM. Antibody titers of the samples determined by tube test were also taken into consideration to help distinguish false responses on the sensors. The analysis workflow is summarized in **Figure 5-3**.

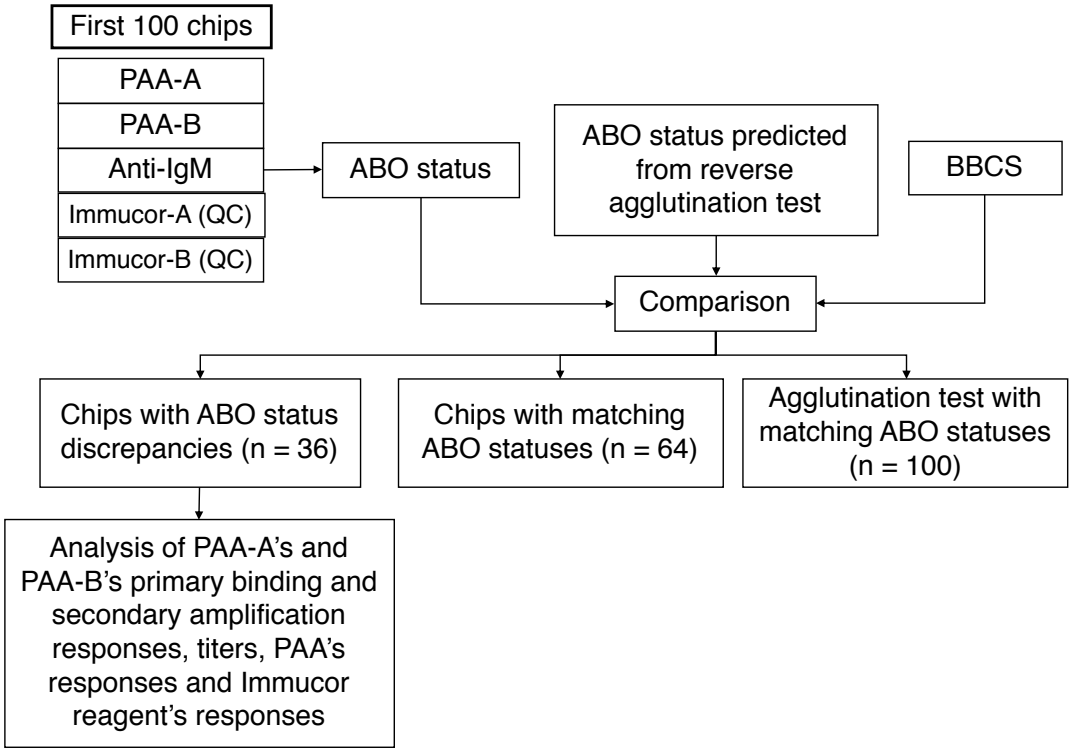

Figure 5-3. Schematic of the analysis workflow of forward and reverse typing discrepancies.

5.4 Results

5.4.1. Forward Typing Buffer Optimization on Printed Chips

We have so far been limited to using sci-SPOT D1 buffer on hand functionalized chips for forward typing. Here, the effect of acidic glycine (pH 3) and acetate (pH 4.5) buffers on the activity of IgM capture antibodies used in ABO forward typing was examined on printed chips before proceeding to a large-scale print. Anti-A was selected in this analysis due to its higher activities than anti-B

capture antibody observed on our test platform. To our surprise, the activity of anti-A/anti-mouse IgM mixture printed in the glycine buffer (blue) on capturing type-A RBCs was consistently higher than the activities observed from anti-A mixture printed in sci-SPOT D1 (green) and acetate buffers (red) (**Figure 5-4**). Despite these encouraging results, another critical concern regarding the use of acidic printing buffer is the stability of IgM capture antibodies in storage after printing. A time course investigation of hand-functionalized chips spotted with anti-A mixture in sci-SPOT D1 or pH-3 glycine buffer shows that anti-A in both buffers was still active after 32 weeks post-functionalization (**Figure 5-5**). Therefore, we decided to proceed with using a pH-3 glycine buffer for the printing of anti-A and anti-B IgM capture antibodies while all other IgG and polymer reagents were printed in sci-SPOT D1 buffer.

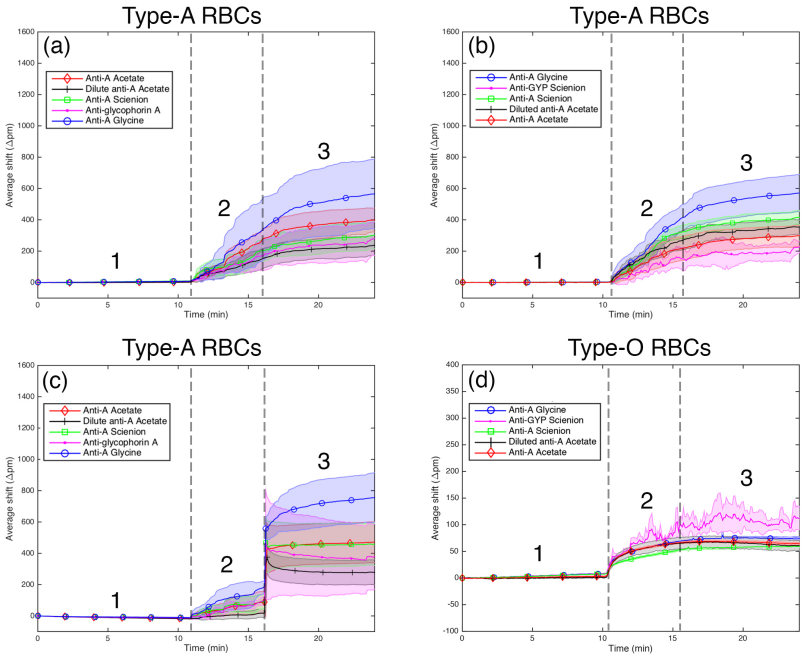

Figure 5-4. Sensorgrams of forward typing results on sensor chips printed with anti-A in acidic buffers to examine the effect of pH on IgM activity. Highlighted steps are (1) PBS, (2) 1:10 diluted RBC suspension in PBS and (3) PBS. The wavelength shift on the y-axis is directly proportional to the molecular binding on the sensors. Standard deviation of the mean of individual sensor responses at a specific time point is represented by the shaded area in the background. Glycine (pH 3.0) and acetate (pH 4.5) buffers were used as a printing buffer to compare with the sci-SPOT D1 printing solution. Anti-glycophorin A (GYPA) was used as a positive control. Subplots **(a-c)** show that anti-A printed in a glycine buffer consistently has higher activities than its counterparts in other printing buffers.

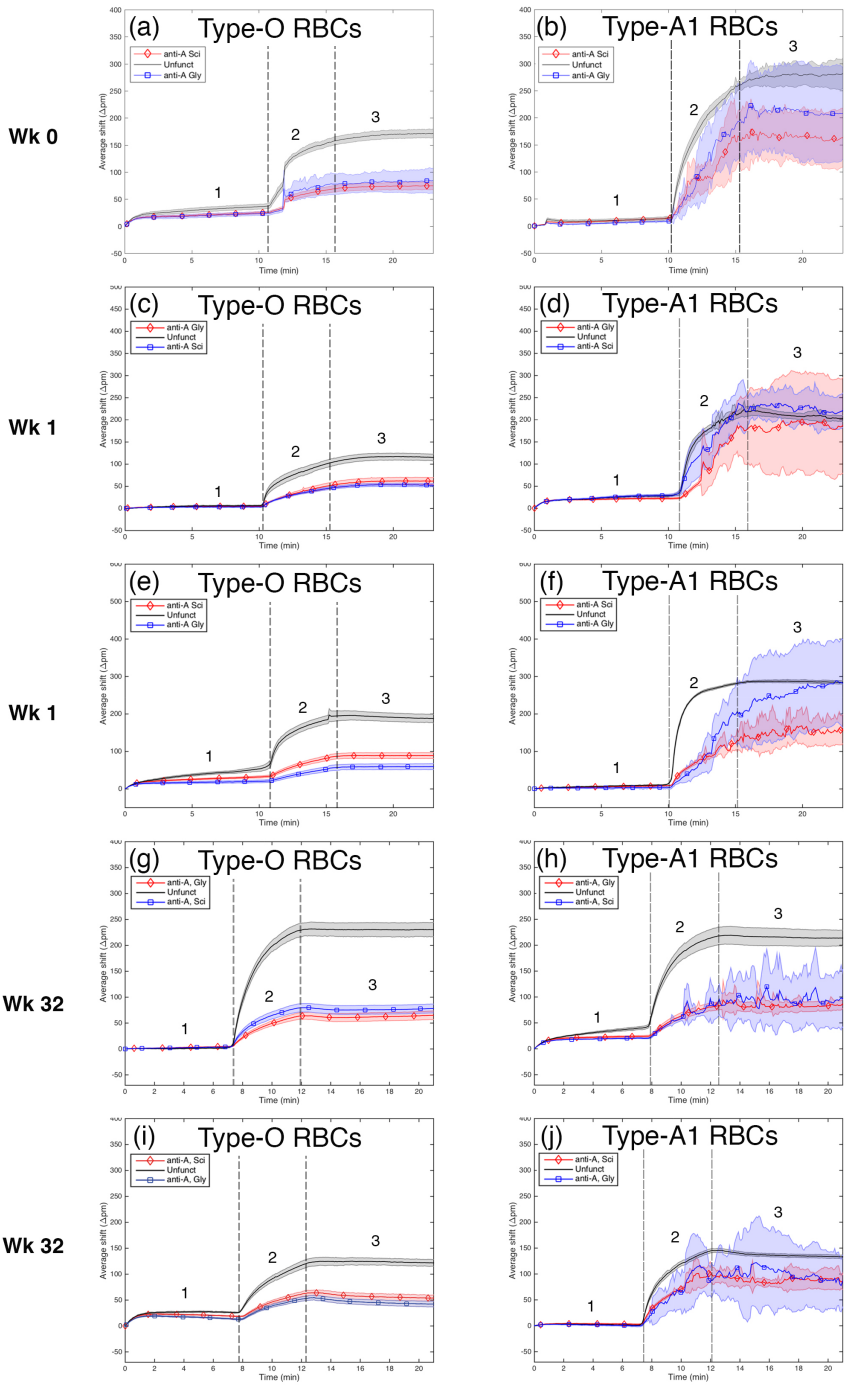

Figure 5-5. Time-course study of the activity of immobilized anti-A in glycine and sci-SPOT D1 buffers. Sensorgrams of forward typing results of hand-functionalized chips after week 1 **(c-f)** and week 32 **(g-j)** of storage at 4°C. Highlighted steps are (1) PBS, (2) 1:10 diluted RBC suspension in PBS and (3) PBS. The wavelength shift on the y-axis is directly proportional to the molecular binding on the sensors. Standard deviation of the mean of individual sensor responses at a specific time point is represented by the shaded area in the background. Initially, anti-A printed in glycine shows a higher response than anti-A printed in the sci-SPOT D1 buffer at week 0. The differences between the two anti-A spots continued to decline as the storage time of the chips increased. The absolute shifts were comparable after 32 weeks.

5.4.2 Initial Validation of Large-Scale Printed Chips for Forward and Reverse Typing

Validation of printed reverse typing reagents by Immucor antisera:

A set of test printed chips prepared prior to a large scale print was used to validate the activity of reverse typing reagents spotted in Channel 1 with standard Immucor anti-A and anti-B antisera (**Figure 5-6**). The orders of printed reagents are different on the two sides of the chip: (left) PAA, anti-human IgM, PAA-A, PAA-B, and (right) anti-human IgM, PAA-B, PAA-A and PAA (**Figure 5-1b**). Unless otherwise stated, the flow rate of every step was 20 μL/min. The initial baseline was established by a brief PBS rinse, followed by 1:10 diluted anti-A for 10 minutes. Excess anti-A was removed by a brief PBS rinse, then followed by 1:10 diluted anti-B in PBS. Excess reagent was removed by a final PBS rinse. Specific binding curves were uniformly observed on all sensor probes functionalized with PAA-A and PAA-B. This demonstrates a detectable antigenicity of the immobilized blood group A and B trisaccharides on PAA that can react well to the standard typing antisera used in clinical laboratories. Responses from PAA spots (negative controls) were not indicative of specific binding, and likely generated by a nonspecific binding of stabilizing proteins present in the reagents. Anti-human IgM that serves as a positive control for IgM antibodies in human plasma also did not respond to the antisera.

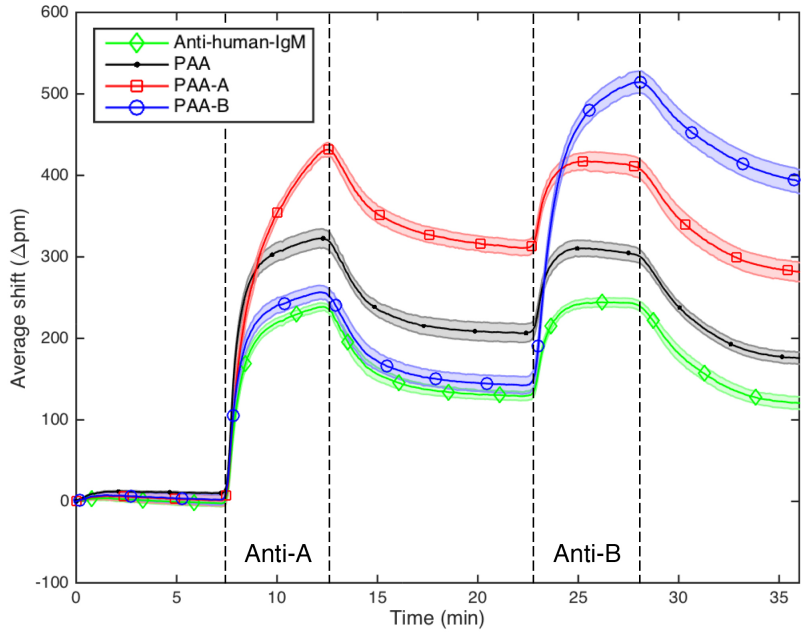

Figure 5-6. Validation of reverse typing reagents on the printed chips with Immucor antisera. Highlighted steps are 1:10 diluted anti-A in PBS and 1:10 diluted anti-B in PBS. Unlabeled steps are PBS rinses. The wavelength shift on the y-axis is directly proportional to the molecular binding on the sensors. Standard deviation of the mean of individual sensor responses at a specific time point is represented by the shaded area in the background. PAA-A and PAA-B responded to the anti-A and anti-B typing reagents in a specific manner.

Reverse typing on printed chips:

Test printed chips were then verified with undiluted plasma to ensure that the immobilized reverse typing reagents on the chips were suitable for testing human samples. Reverse typing was performed in Channel 1 using a 120-μL undiluted plasma harvested from EDTA- or citrate-stored blood samples. Unless otherwise stated, all reagents were flowed at 20 μL/min. PBS was initially flowed across the chip to establish the baseline, followed by whole plasma for 5 minutes. After a 10-minute PBS rinse, 40 μg/mL anti-human IgG/A/M in PBS was introduced to amplify the signals for 5 minutes. Excess, unbound reagent was removed by a final PBS rinse. For in-line validation of PAA-A and PAA-B, 1:10 diluted Immucor anti-A and anti-B antisera in PBS were flowed in sequence, separated by a brief PBS rinse in between. The order of these two antisera can be

switched. A schematic illustration of reverse typing on the multiplexed chip is shown in **Figure 5-7**.

Reverse typing results of type-AB, -O, -B and -A plasma samples are specific and indicative of their ABO profiles based on the initial binding of undiluted plasma to functionalized sensor probes and the subsequent secondary amplification by anti-human IgG/A/M (**Figure 5-8**). However, it is important to acknowledge that every plasma sample has a unique profile of antibody repertoire, titers and protein constituents—all of which could influence the pattern and degree of responses of the sensors. The interpretation of reverse typing results is done by comparing the secondary amplification shifts of PAA-A and PAA-B to PAA (negative control). Although some plasma samples may show a specific binding response right when they were initially flowed on the sensors, only the secondary amplification responses were taken into consideration for the interpretation of reverse typing results. In this pool of donors' samples, the degree of nonspecific background shift produced by a type-AB plasma was quite high based on the average shift of PAA (negative control), which is roughly tantamount to the secondary amplification shifts of PAA-A and PAA-B (**Figure 5-8d**). The observed shifts were likely not associated with the specific binding of blood group isohemagglutinins in type-AB plasma that lacks both anti-A and anti-B antibodies. A final in-line validation step with Immucor reagents showed that both PAA-A and PAA-B could still respond to antisera with a low degree (data not shown).

When a type-O plasma was tested on the chip, PAA-A and PAA-B probes showed secondary amplification responses nearly as high as the anti-human IgM (positive control) while the shift of PAA was negligible (**Figure 5-8c**). This suggests that natural anti-A and anti-B isohemagglutinins present in a type-O plasma could recognize and interact well with multivalent blood group trisaccharides functionalized polymers. Reverse typing of type-B and -A plasma samples was also successful as the specific initial plasma binding and secondary amplification responses on PAA-A and PAA-B were observed, respectively (**Figure 5-8a** and **b**). Note that the

activity of immobilized anti-human IgM was low on both chips. This is attributed to the fact that reagents used for that batch of the test print were sent to the printing facility two months before they were printed. Chips used for testing type-AB and -O plasma samples were printed with freshly prepared reagents that were shipped in a well-controlled condition.

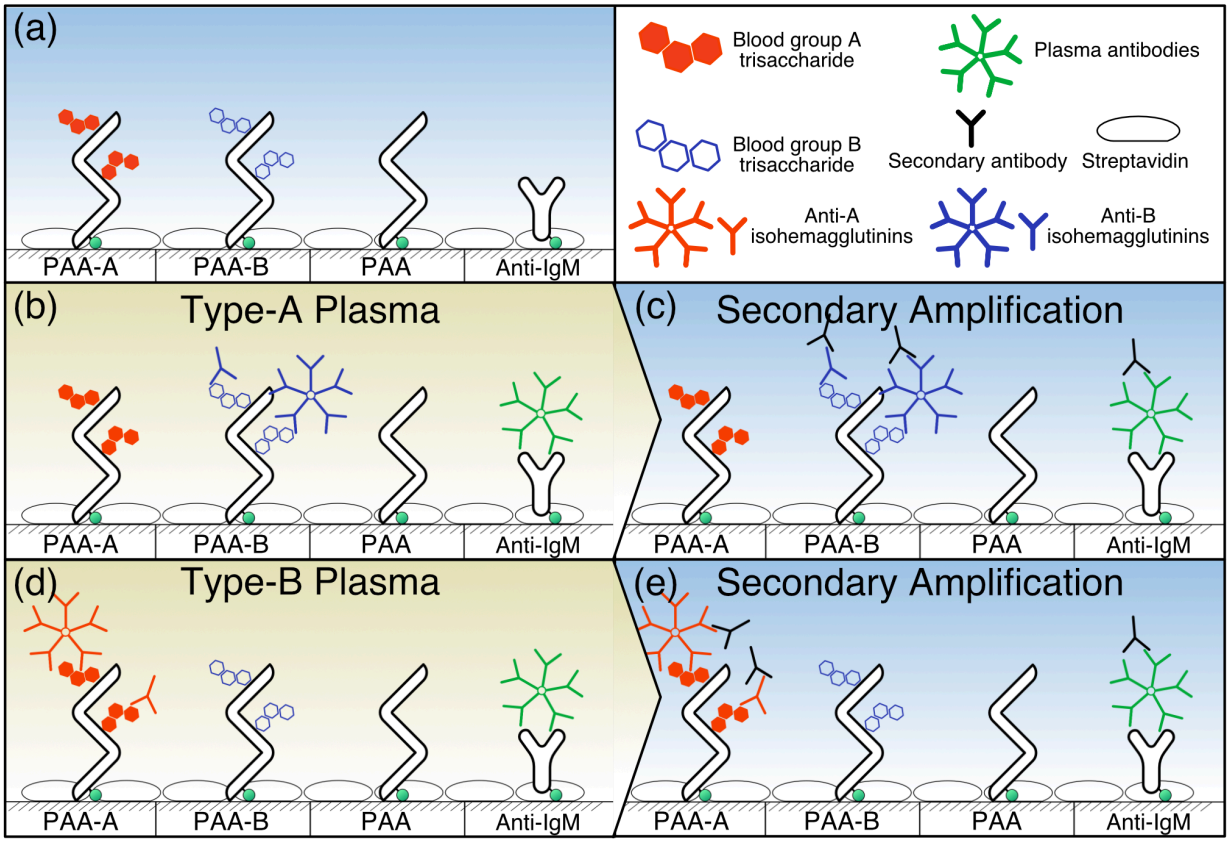

Figure 5-7. Schematic illustration of reverse typing performed on the multiplexed chip. PAA-A, PAA-B, PAA (negative control) and anti-human IgM (positive control) are printed directly onto individual clusters of four sensors. ABO isohemagglutinins are captured by multivalent blood group antigen functionalized polymers (**b** and **d**). Anti-human IgG/A/M secondary antibody was used to amplify the signals (**c** and **e**). Illustration is not drawn to scale.

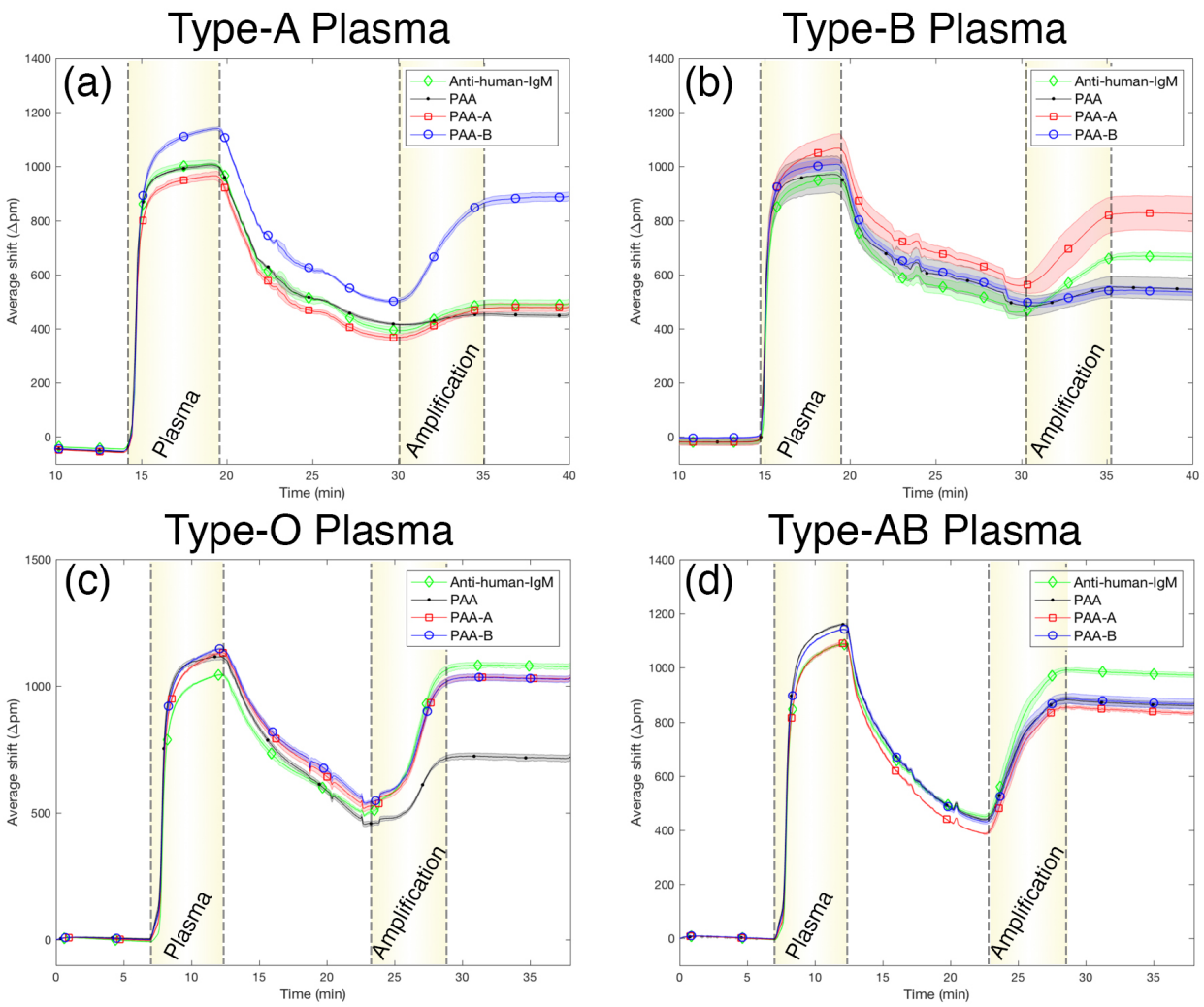

Figure 5-8. Sensorgrams of reverse typing results on multiplexed chips of type-A plasma (**a**), type-B plasma (**b**), type-O plasma (**c**) and type-AB plasma (**d**). Highlighted steps are undiluted plasma and the secondary amplification by anti-human IgG/A/M. The final validation step by Immucor antisera is omitted from these sensorgrams. Unlabeled steps are PBS rinses. All sensorgrams show the average wavelength shift of the sensors with respect to time. Standard deviation of the mean of individual sensor responses is represented by the shaded area in the background. Anti-human IgM (positive control, green) shows positive shifts after the secondary amplification in every sample. PAA-A (red) and PAA-B (blue) responded to type B, A and O plasma samples in a specific manner during both plasma introduction and secondary amplification steps. The observed secondary amplification shifts of PAA-A and PAA-B probes are also high for type-AB plasma; however, the equivalent degree of response of PAA suggests that the binding is nonspecific.

Forward typing on test printed chips:

Similarly to reverse typing, test printed chips were validated for their ability to perform forward typing using 1:10 diluted packed RBCs in PBS. Forward typing reagents were printed in Channel 2 of the chip in the following order: (left) isotype control, anti-B, anti-A, anti-human IgM, and (right) anti-A, anti-B, anti-human-IgM, anti-glycophorin A (GYPA). Four different blood samples with different ABO/RhD profiles were used. Initial baseline was first established by flowing PBS, then anti-RhD cocktail (clone: RUM-1, titer = 1:21 and TH-28, titer = 1:41) was flowed to functionalize the two anti-human IgM sensor probes. **Figure 5-9** provides a schematic illustration of the forward typing assay. In contrast to the molecular binding observed at the sensor's interface that typically follows the Langmuir adsorption isotherm, specific forward typing results are characterized by constant noise-like signal fluctuations that take place when RBCs are flowed across the sensors. Based on this characteristic, the forward typing results of four RBC samples used for validation were unambiguous (**Figure 5-10**). Anti-GYPA (magenta) appeared to show a specific response to anti-RhD cocktail (**Figure 5-10a** to **d**) when it was flowed to immobilize onto the anti-human IgM (green) probes. Other reagents showed no significant interactions with anti-RhD and remained at the baseline. After a brief PBS rinse, diluted RBC suspension in PBS was flowed.

All samples showed accurate forward typing results that are predictive of their blood types. Responses observed from anti-A functionalized probes (red) to type-AB/RhD negative (**Figure 5-10d**) and type-A/RhD negative (**Figure 5-10a**) RBC samples were evidently high (300-900 pm). It has been shown on hand-functionalized chips that anti-A tended to produce stronger signals upon interacting with RBCs in a specific manner than anti-B. Although anti-B functionalized probes (blue) could show specific interactions with type-B RBCs, its activity was significantly lower than anti-A based on the absolute shifts of cell binding (**Figure 5-10b** and **d**). Nevertheless, cell-binding associated signal fluctuations were still visible and prioritized in interpreting forward typing data. Anti-B functionalized probes responded to type-B/RhD positive RBCs with a low shift (143

pm), yet raw data from individual sensors were shown to be specific to cell binding (**Figure 5-10b**). Comparing the response of anti-B to a quiet signal of anti-A functionalized probes remaining at the baseline allows for a correct prediction of the ABO profile that matches the blood type of this sample. When type-O/RhD positive RBCs were flowed, no signals were observed from either anti-A or anti-B (**Figure 5-10c**).

Interpretation of the RhD status, though is still based on the presence of signal fluctuations, is not as straightforward as ABO, and has to take an overall response of anti-GYPA probes into account. The criterion used for resolving the RhD status of RBCs is to compare signals of anti-GYPA (magenta) with anti-human IgM (now functionalized with anti-RhD, green). If the absolute shift of anti-human IgM is higher than that of anti-GYPA, the sample is likely RhD positive. When the shifts of both probes are comparable or when the shift of anti-human IgM is lower, the sample is likely RhD negative. Occasionally, false positive high-frequency signals produced by RhD negative samples could be observed. However, these false positive signals are transient in nature and often disappear after a PBS rinse.

In this pool of samples, both type-O/RhD positive and type-B/RhD positive samples used for validation showed different patterns of response that could still be scored as positive because their anti-human IgM shifts were higher than the anti-GYPA responses (**Figure 5-10b** and **c**). The type-O/RhD positive sample produced a much narrower fluctuation of RhD signals than what observed from the type-B/RhD positive sample, although both share similar absolute shifts of approximately 300 pm during the initial cell exposure step. Also present here in the sensorgram of type-O/RhD positive sample is a new phenomenon in direct typing concerned with cell binding observed during a long final PBS rinse, specifically right when the flow was temporarily halted for the reagent wells to switch. A stark increase in the shifts (520-590 pm) was observed on anti-GYPA and anti-human IgM probes (**Figure 5-10c**). This discretized leap in the signals has been

observed exclusively on the printed chips during the rinsing step, and is not limited to these two reagents. Its appearance usually reinforces a positive cell capture on the sensors.

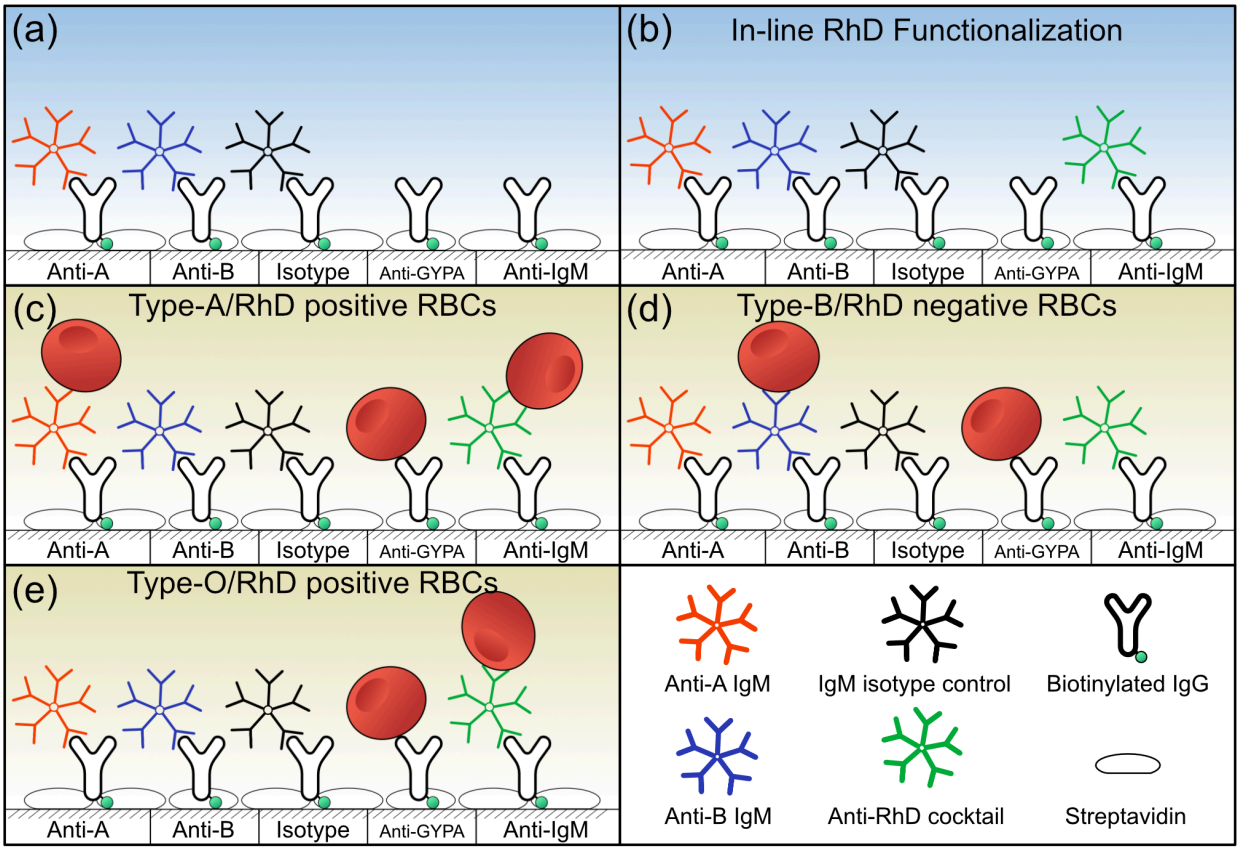

Figure 5-9. Schematic illustration of the forward typing performed on the multiplexed chip. Capture antibodies are printed directly onto individual clusters of four sensors. These reagents include anti-A, anti-B, mouse IgM isotype control (negative control), anti-human IgM (for in-line anti-RhD functionalization) and anti-glycophorin A (GYPA; positive control) (**a**). Anti-RhD cocktail (clones: RUM-1 and TH-28) is immobilized in-line under the flow condition (**b**). Subplots **c** to **e** are examples of a specific capture of RBCs of different ABO/RhD profiles.

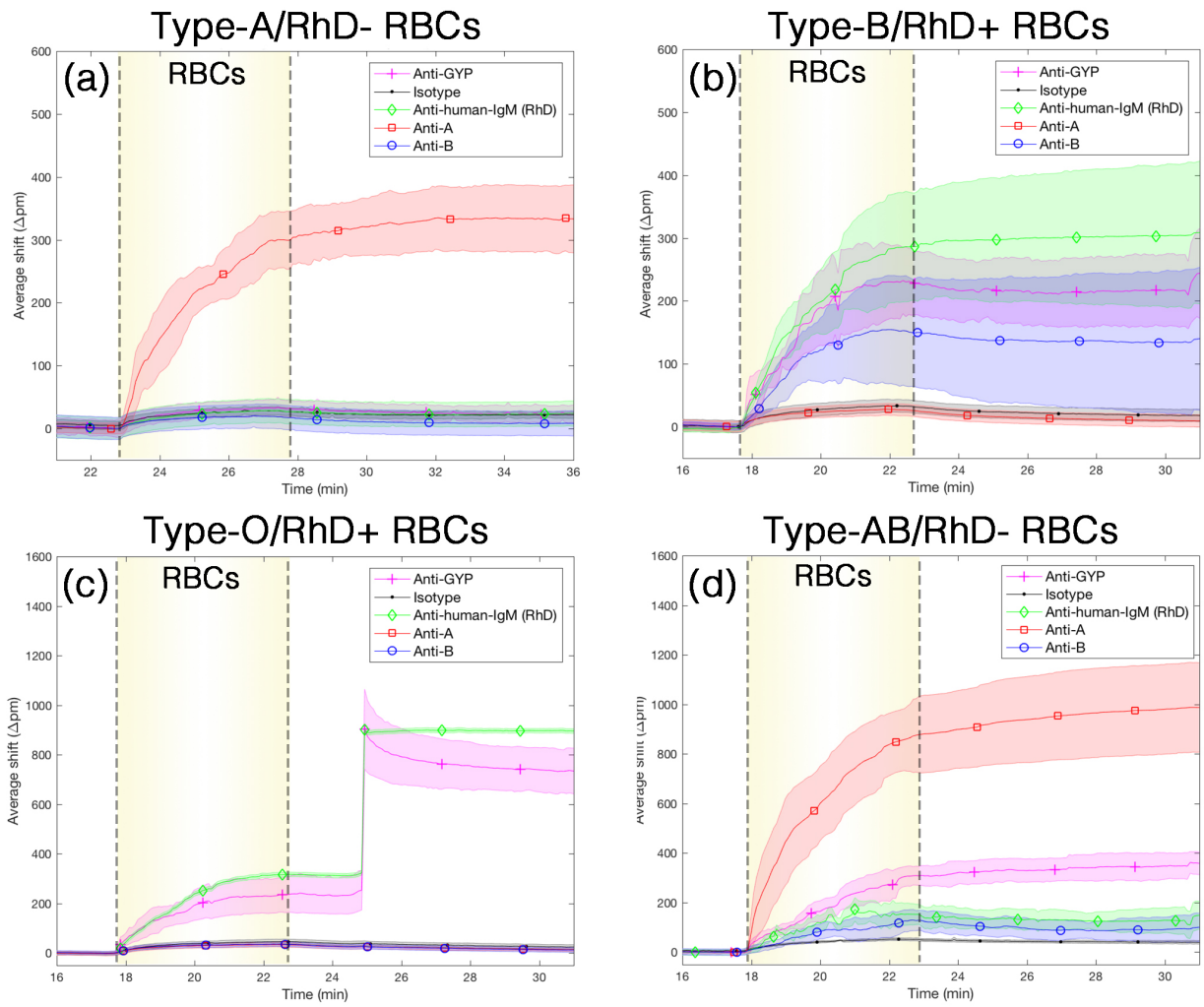

Figure 5-10. Forward typing results on the multiplexed chips with type-A/RhD negative (**a**), type-B/RhD positive (**b**), type-O/RhD positive (**c**) and type-AB/RhD negative (**d**) RBCs. Highlighted step is 1:10 diluted RBCs in PBS. Anti-RhD functionalization step is omitted from the sensorgrams. Unlabeled steps are PBS rinses. Anti-A generally shows higher activities than anti-B, but both antibodies are still capable of generating cell-binding signals when RBCs interact with the sensors. Interpretation of RhD status takes the shift of anti-glycophorin A (GYPA) into account. A higher overall shift of anti-human IgM (functionalized with anti-RhD) in relative to anti-GYPA indicates a positive RhD status of the sample.

5.4.3 Proof-of-Concept Demonstration of Blood Typing on Multiplexed Sensor Chips

On-chip typing:

We successfully performed serologic and phenotypic characterization of blood samples on our silicon photonic biosensing platform with an overall accuracy of predicting ABO/RhD profiles and ABO status alone of approximately 83% and 91%, respectively (**Table 5-3**). Upon further

chronological breakdown of the chips into two sets, the first 100 chips in the study, with an overall percent accuracy of 91% (98% for ABO status alone), performed significantly better than the latter half with an overall percent accuracy of 77%. Though this cutoff is arbitrary, it still closely reflects the actual 2-week pause in the study due to a logistics issue of sample acquisition that took place in the second half of the study. Another indirect indicator of the chip performances between the two sets is the discordance among observers upon predicting blood types before harmonization. The percent discordance in the first 100 chips is only 13%, while the second set of chips has twice as high the discordance of the first set (**Table 5-4**).

Interestingly, both sets are susceptible to different types of prediction errors. All of the mistyping errors identified in the first set come from false positives in B (n = 2) and RhD (n = 7), but nearly all of the errors in the second set are false negative in A (n = 2), B (n = 16) and RhD (n = 10). These errors are unlikely biased by the samples between the two sets of chips because the blood types in both sets are similarly distributed, with an exception of type-AB/RhD negative samples that are 3-fold higher in the second set (**Table 5-3**). Owing to their higher performance, the first 100 chips were further analyzed for the discrepancies between forward and reverse typing results to investigate the suitability of blood group functionalized polymers in clinical serology and blood typing.

Table 5-3. Distribution of ABO/RhD profiles of blood samples tested in the first 100 chips and last 120 chips.

Blood type	Count	
	Chip 1-100	Chip 101-220
A-NEG	14	13
A-POS	14	14
B-NEG	14	13
B-POS	12	16
O-NEG	13	15
O-POS	15	12
AB-NEG	7	21
AB-POS	11	16
Total	100	120

Table 5-4. Summary of typing performances of the first 100 chips and last 120 chips based on false predictions on A, B and RhD and the overall percent accuracy of the typing results.

Chip number (in chronological order)	Discordance among observers	Total false prediction	A			B			RhD			Percent accuracy	
			FP	FN	Total	FP	FN	Total	FP	FN	Total	ABO	ABO/RhD
1-100	13 (13.0%)	9 (9.0%)	0	0	0	2	0	2	7	0	7	98.0%	91.0%
101-220	32 (26.7%)	28 (23.3%)	0	2	2	0	16	16	3	10	13	85.0%	76.7%
All 220 chips	45 (20.5%)	37 (16.8%)	0	2	2	2	16	18	10	10	20	90.9%	83.2%

Forward and reverse typing discrepancies:

To our knowledge, this is the first use of synthetic blood group trisaccharides conjugated polyacrylamides (PAA) in a blood typing analysis that involves hundreds of human plasma samples. Owing to their synthetic nature that may render themselves antigenically different from naturally occurring ABO blood group antigens, we are interested in comparing the reverse typing results on the multiplexed sensors to the standard reverse typing method performed by the tube test that uses commercial human reference cells. This ad hoc investigation was triggered by conflicting forward and reverse typing results from the same samples that the observers encountered during their blind calls. In order to finalize their predictions, observers were instructed to prioritize forward typing results due to a better fidelity of a forward typing that provides clear, unique cell-binding signals.

The first 100 chips identified previously were selected for this analysis. The performance of PAA-A and PAA-B was assessed by their abilities to provide an accurate binding results for anti-A and anti-B isohemagglutinins in plasma that would in turn allow for a correct prediction of the sample's front blood type. Canonical reverse typing results of type A, B, O and AB samples from the blind analysis agree with results shown during the validation step prior to the analysis (**Figure 5-11** and **5-12**). Namely, the secondary amplification and/or primary binding of plasma on PAA-A and PAA-B probes are specific to the presence of isohemagglutinins in the samples (**Table 5-5**). Note, however, that titer information does not fully correlate with the degree of the secondary amplification responses of the sensors.

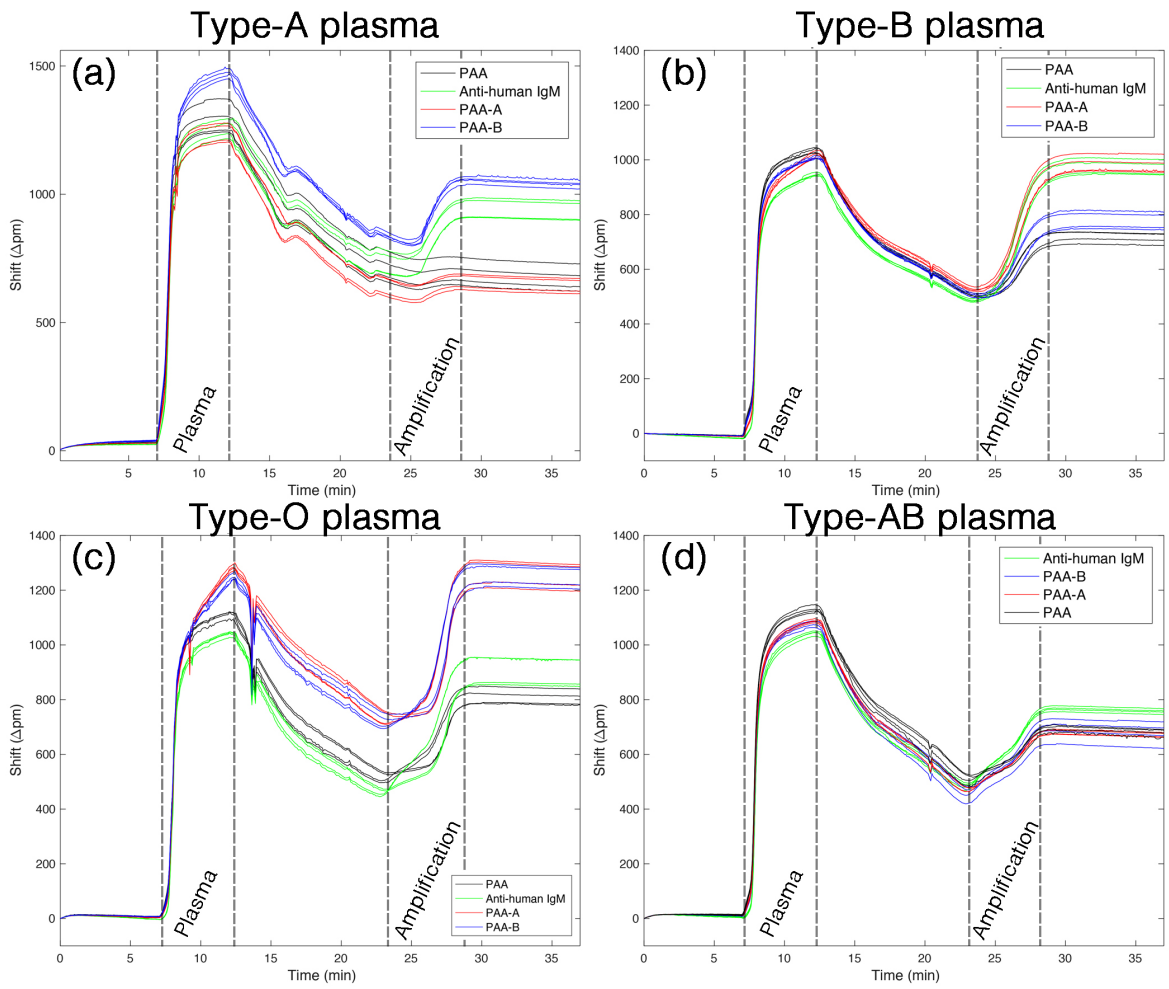

Figure 5-11. Sensorgram of normal raw reverse typing data of type-A (**a**), -B (**b**), -O (**c**) and -AB (**d**) plasma samples. These results provide a clear information of isohemagglutinins present in the samples, allowing for an accurate prediction of the front blood types. Highlighted steps are undiluted plasma and the secondary amplification. Validation of PAA-A and PAA-B step by Immucor antisera is omitted from these sensorgrams. Unlabeled steps are PBS rinses. Note: Raw data from individual sensors are presented here because observers made predictions based on raw data.

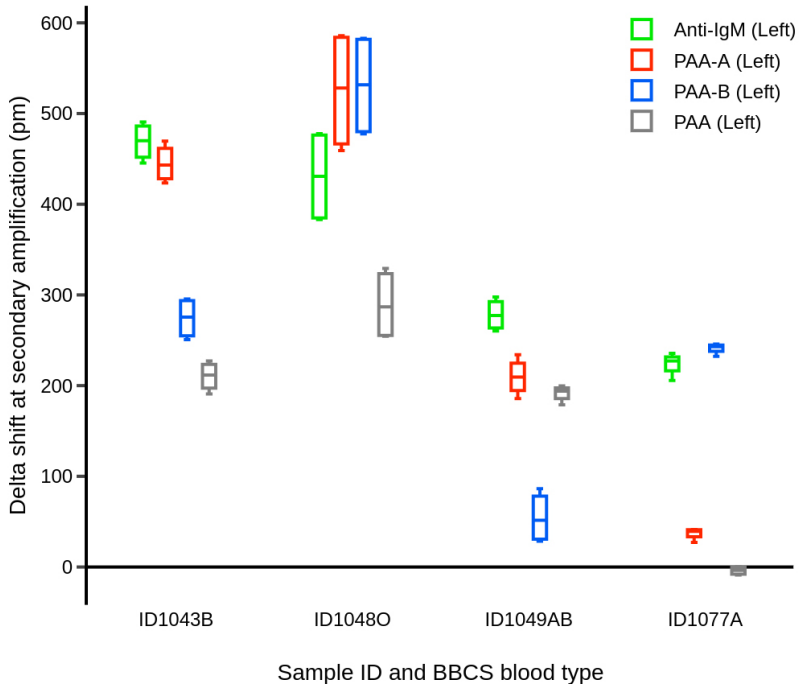

Figure 5-12. The wavelength shifts of sensor probes during the secondary amplification of samples shown in Figure 5-11. The degree of responses shown on this plot is not correlated with titer data.

Table 5-5. Titer information of plasma samples shown in Figure 5-11.

Sample ID	BBCS blood type	Agglutination result	Predicted blood type	Titer information			
				A1 macro	A1 micro	B macro	B micro
1077	A	A2	A	0	0	64	64
1043	B	B	B	32	64	0	0
1048	O	O	O	32	64	4	16
1049	AB	AB	AB	0	0	0	0

Despite the favorable outcomes of the reverse typing of the samples listed above, tube-based reverse typing using human reference cells was able to determine 100% matching blood types to the BBCS database while only 64% (n = 64) of the on-chip reverse typing results were able to match the blood types in BBCS (**Table 5-6**). This disparity in accuracy serves as a solid proof that simplified synthetic blood group antigens do not truly represent the natural structures of blood group antigens that potentially exist in a great structural diversity.[126] The overprediction of blood type AB and underprediction of blood type A suggests that these multivalent polymers

may not efficiently capture anti-B IgM found predominantly in type-A plasma, and thus are not a suitable alternative of naturally occurring blood group antigens for clinical typing. However, a close prediction of type-O blood from on-chip reverse typing results to the BBCS blood types shows that the problem of capturing anti-B might be an isotype-specific issue because type-O plasma is usually predominated with IgG isohemagglutinins.

Table 5-6. Distribution of predicted blood types based on reverse typing results of tube-based agglutination and multiplexed on-chip typing.

Blood Type	BBCS	Predicted front type from reverse typing results	
		Tube test	Chip typing
A	28	28	7
B	26	26	28
O	28	28	33
AB	18	18	32
Sum	100	100	100

Remarks: The results of agglutination test are 100% concordant with the BBCS blood types.

In the analysis of typing result discrepancies, the responsivity of PAA, PAA-A, PAA-B and anti-human IgM were assessed according to the following qualitative characteristics: (1) clear binding observed at both plasma exposure (primary) and secondary amplification steps, (2) clear binding observed at only secondary amplification step and (3) no clear binding observed at both plasma exposure (primary) and secondary amplification steps. This information from PAA-A and PAA-B was used to predict the blood type of a sample while PAA (negative control) and anti-human IgM (positive control) were evaluated to determine whether the assay was performed properly or not. There were 36 chips whose reverse typing results did not match with the sample's corresponding blood types in BBCS. Anti-B antibodies are more mistyped than anti-A based on the results of 17 false negatives where PAA-B responded negatively with type-A and -O plasma when there are only 5 false negatives associated with PAA-A. Nevertheless, PAA-A has an issue

with producing large number of 12 false positives, which are 6-fold higher than PAA-B (**Table 5-7**).

Although the patterns of false negative and false positive responses can manifest themselves differently on the sensorgrams, four plasma samples were selected as examples (**Figure 5-13**) to demonstrate how they could potentially mislead the prediction of blood type when the forward typing data or titer information (**Table 5-8**) are not available. There is one type-A plasma sample (marked * in **Table 5-7**) that showed a strong interaction with PAA-A, but responded negatively with PAA-B, generating a simultaneous false positive for anti-A and false negative for anti-B. Although this could be a result of sample handling error in which a wrong plasma sample was mislabeled and assayed for another sample of a different ABO phenotype, the only type-B sample that was analyzed on the same day as this sample had a different sensor responsivity profile, thus a clerical error may likely not be the cause.

Table 5-7. Summary of typing errors based on the responsivity of PAA-A and PAA-B.

	Typing errors	BBCS	Total
PAA-A	FN	B	5
	FP: Primary and Secondary	A	1*+2
	FP: Secondary	A	8
		AB	1
PAA-B	FN	A	11
		O	1
		O	5
	FP: Primary and secondary	B	1
	FP: Secondary	AB	1
	Grand total		36

Remarks: FN denotes false negative and **FP** denotes false positive. (*****) indicates the sample in which a false negative of PAA-B and a false positive of PAA-A are produced.

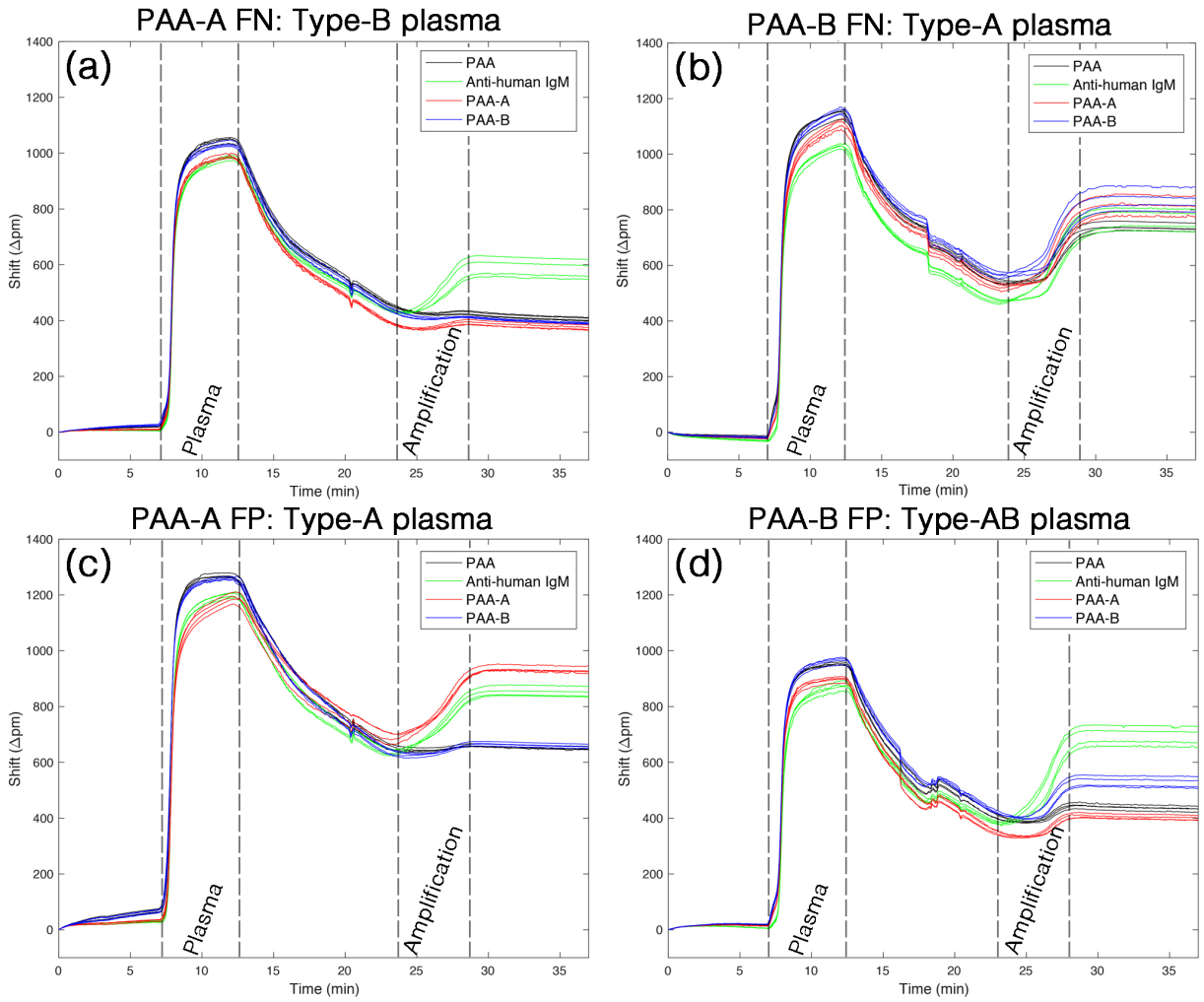

Figure 5-13. Example sensorgrams of misleading reverse typing results: false negative for PAA-A (**a**), false negative for PAA-B (**b**), false positive for PAA-A (**c**) and false positive for PAA-B (**d**). Highlighted steps are undiluted plasma and the secondary amplification. Validation of PAA-A and PAA-B step by Immucor antisera is omitted from these sensorgrams. Unlabeled steps are PBS rinses. Note: Raw data from individual sensors are presented here because observers made predictions based on the raw data.

Table 5-8. Titer information of plasma samples shown in Figure 5-13.

Error type	Sample ID	BBCS blood type	Agglutination result	Predicted blood type	Titer information			
					A1 macro	A1 micro	B macro	B micro
PAA-A FN	1131	B	B	AB	4	16	0	0
PAA-B FN	1045	A	A1	AB	0	0	16	32
PAA-A FP	1119	A	A2	B	0	0	4	16
PAA-B FP	1060	AB	A2B	A	0	0	0	0

5.5 Discussion

5.5.1 Buffer Optimization for Forward Typing on Printed Chip

Although anti-A/anti-mouse IgM mixture has shown no issue regarding its activity when printed on the sensor with the sci-SPOT D1 printing buffer, we wanted to explore how the activity of anti-A in capturing type-A red blood cells was affected by different printing buffers. Anti-A was chosen over anti-B in this experiment due to its higher responsivity to cells, determined empirically on our test platform. Possible degradation of IgM antibodies stored in the acidic condition for an extended period of time was well acknowledged, therefore, the printing facility was strictly instructed to mix the anti-A mixture with test buffers immediately before printing. To our surprise, anti-A printed in a pH-3 glycine buffer consistently elicited higher responses than anti-A printed in sci-SPOT D1 and pH-4.5 acetate buffers. Low-pH buffer, such as glycine, may help facilitate the electrostatic interactions of the capture antibody (pI = 5.5-7.4) to streptavidin (pI = 5) and silicon dioxide layer (pI = 1.7-3.5)[127] in addition to the strong biotin-streptavidin affinity.

In all test buffers, the sensor responses on printed chips are distinct from hand-functionalized chips owing to a much smaller area of surface functionalization (approximately 100 μm per probe), reducing the total number of RBCs that can specifically interact with the sensors. This results in a less degree of cell-binding signals observed on the sensorgrams. A new phenomenon that has only been observed on printed chips is the leap in wavelength shifts produced by some of the sensors. This sudden increase in the absolute shift takes place during a 5-second flow pause to allow a microtiter well to switch on a microplate. The intermission of flow is thought to permit the reorientation of RBCs themselves to bind to the sensors more firmly, hence a rapid, sharp rise in the shift. Once RBCs form a tight contact with the sensors, the signal still persists during a washing step with PBS until a 2% (v/v) RBS-35 detergent is introduced.

5.5.2 Evaluation and Validation of Printed Chips

Twenty printed chips from a test print and a large-scale print were validated to confirm that the chips were functionalized properly. The results from these chips, varying in patterns of response, were also used to train the three independent observers who were assigned to predict the blood types of blind samples. Reagents were printed on every other probe of the sensors to prevent crosstalk and contamination. Unfunctionalized sensors were purposely not being scanned because it would require twice as much time for the laser to raster across all 128 sensors than 64. In reality, the yield of perfectly printed chips was low (less than 250 chips out of 400 chips). Please see Appendix B for criteria for evaluating the physical quality of printed chips. Several sensor chips have spots that were completely missing or partially covering the sensor probes. We carefully selected 220 chips whose coverage of the printed spots was perfect in both reverse and forward typing arrays for a large-scale demonstration of blood typing.

Chips that we used for validation were (1) chips that were test printed before a large-scale print using two old batches of reagents sent previously, and (2) chips from a large-scale print whose only either reverse or forward channel was well-printed. (Note: three batches of reagents were sent to the printing facility. Only the third batch was used for a large-scale print because the first batch was shipped in a temperature that was below the freezing point, while the second batch arrived at the printing facility at room temperature.) Validation of reverse typing channel with commercial Immucor antisera diluted 1:10 in PBS revealed specific binding of anti-A to PAA-A and anti-B to PAA-B, while anti-human IgM probes showed no significant binding of the antisera (mouse IgM).

Interpretation of reverse typing results in general is straightforward, and assessed by comparing the absolute shifts of each functionalized probe during the secondary amplification step to that of PAA. Nevertheless, it is crucial to acknowledge that every plasma sample was different in its antibody repertoire and titers, thus the observed patterns of response can be more

diverse than those recognized in forward typing. **Figure 5-8c** and **d** show consistently high responses of anti-human IgM sensors in plasma from two blood types (AB and O). However, the responses from the same probes tested with B and A plasma samples (**Figure 5-8a** and **b**) are significantly lower compared to the previous two test chips. Although it is possible that these two plasma samples may have a low titer of antibodies overall, the higher secondary amplification shifts of PAA-A and PAA-B have shown otherwise. It is more likely that the antibody spot was no longer functional. Anti-human IgM on the test chips tested with type-A and -B plasma samples was from the first batch of reagents shipped to the printing facility when they were not stored under a proper condition. Anti-human IgM might have gone through a freeze-thaw cycle before it was printed, resulting in low responses after the amplification step. The last two steps in a reverse typing assay use Immucor antisera reagents to validate PAA-A and PAA-B without interfering with the assay. Besides, they revealed how saturated the PAA-A and PAA-B probes were after being occupied with isohemagglutinins and secondary antibody. Antibody-rich type-O plasma often saturated both polymer probes enough such that no binding of antisera were observed. Type-A and -B plasma samples occasionally show different degrees of binding of antisera to PAA-B and PAA-A, respectively, depending on how saturated the polymer-functionalized probes were after plasma exposure.

Interpretation of forward typing performed in Channel 2 of the chip is similar to what has been discussed on hand-spotted chips. Specific cell-binding signals on anti-A and anti-B functionalized probes were still observed, despite anti-B steadily showing a much lower activity on the chip than anti-A based on the overall absolute shift. During the in-line functionalization of anti-RhD cocktail, it can be clearly observed that anti-RhD can bind to both anti-human IgM and anti-glycophorin A functionalized sensors. This has raised a concern that anti-GYPA probes may become partially saturated with anti-RhD. However, our data from RhD negative samples suggest that anti-GYPA probes' ability to detect glycophorin selectively has not been compromised.

However, even if the anti-glycophorin A probe is partially saturated with anti-RhD, the signals are still most likely dominated by glycophorin A. RhD antigen occupies 110,000-202,000 sites on the RBC surface,[72] while the number of glycophorin A is five times more abundant (500,000-900,000 sites).[128] The determination of the sample's RhD status has to take anti-GYPA's signals into account by evaluating which sensor probe produced a higher response overall. It has been observed on our platform that some RhD negative RBC samples could trigger responses that fluctuate with higher frequencies than a typical cell-binding signal from anti-RhD functionalized probes. These transient signals produced by RhD negative RBCs on anti-RhD probes are possibly attributed to the use of RUM-1 in anti-RhD cocktail that may react with other antigens or epitopes on red blood cell surface similar to RhD, whereas clone TH-28 does not exhibit this nonspecific response to the same degree as RUM-1. This agrees with what we have learned earlier on hand-spotted chips that RUM-1 tends to be too sensitive and prone to generating similar false positive signals. However, they were often overcome by the subsequent PBS rinse while true positive signals could still persist. A step-like leap in the wavelength shift during the change of reagent well is a good indicator of a strong positive signal for RhD because it reflects that cells can bind to the chip firmly (**Figure 5-10c**).

5.5.3 Performance of Printed Chips in a Large-Scale Proof of Concept

Multiplexed chips for simultaneous forward and reverse blood typing were tested with 220 blind blood samples to predict the blood types listed in the BBCS and compare the test results with the gold standard tube-based agglutination test. While the tube test was able to provide 100% accurate results in both forward and reverse directions, our on-chip typing assay could determine the samples' blood types with an overall accuracy of 91% and 83% for ABO and ABO/RhD, respectively. With a pause in the interim of the study, we further separated the chips into two sets

using a chronological cutoff that closely reflects this logistics interruption. The first set of chips consists of the first 100 chips used in the study and the remaining 120 chips belong to the second set. Though only weeks apart in storage before their use, the two sets show a drastic difference in their abilities to perform blood typing. With an accuracy of 98% and 91% for ABO and ABO/RhD, respectively, the first 100 chips outperformed the last 120 chips whose overall accuracy only reaches 85% and 77% for ABO and ABO/RhD, respectively. The high rate of false negatives for B and RhD in the second set of chips suggests that the capture antibodies, regardless of the printing buffers, may degrade during storage and therefore fail to produce enough signals for observers to distinguish the positive cell-binding signals from mere noises in the system.

The differences between forward and reverse typing results have been noted among observers during the analysis. This called for another investigation into the discrepancies between forward and reverse typing results that should in theory have been complimentary with each other for ABO blood types. After converted to forward blood types, reverse typing results from the tube test completely matched with the BBCS blood types. However, there are 36 incidences of forward-reverse typing mismatch on samples analyzed on the chips. A bias of reverse typing results from type-A toward type-AB strongly suggests that the commercial multivalent blood group antigens may not efficiently capture anti-B antibodies in various type-A plasma samples, producing a false negative for the anti-B capture, and thereby causing the misinterpretation of a type-A plasma as a type-AB plasma. Upon a closer analysis, this agrees with the breakdowns of typing errors identified in **Table 5-7** where the common error associated with PAA-B is false negative. PAA-A, on the other hand, produced mostly false positives based on its responses at the secondary amplification. In addition, some plasma samples were observed to be reactive to the PAA used as a negative control, further confounding the interpretation of test results. Polymers used in biopharmaceutical applications are often believed to have weak antigenicity to the repertoire of human antibodies; however, antibodies reactive to poly(vinylpyrrolidone) (PVP),[129] and

poly(ethylene) glycol (PEG)[130–132] have been reported in the literature. Thus, it is possible that some donors may develop antibodies against PAA, which is commonly used in the manufacturing of certain consumer products, such as contact lenses. To obviate this problem, we are currently developing a method for glycolipid and glycoprotein extraction of naturally occurring ABO blood group antigens from erythrocyte ghosts with the goal of better representing blood group antigens on the sensors and eliminating the chance for unexpected polymer-reactive antibodies to disturb the readouts.

5.6 Conclusions and Future Directions

The development of a multiplexed platform for blood typing is of great clinical need in point-of-care settings that will have a tremendous value not only in trauma and urgent care, but also in decentralized or remote settings. Here, we have demonstrated the applicability of microring resonator arrays for forward and reverse blood typing of blind blood samples with high accuracy for ABO/RhD. Based on our current analysis, immediate optimization of capture antibodies, particularly anti-RhD capture antibodies in regard to their clonalities and how they are immobilized in flow, has to be done. Despite a room for improvement to be made on the sensing performance, our investigation serves as a basis for the future inroads into the development of a more advanced system for point-of-care use.

5.7 Acknowledgements

I would like to thank Dr. Jill Johnsen, Sophie Schmidt, Sarah Galdzicka and Sarah Ruuska from Bloodworks Northwest for their efforts in sample acquisition, distribution and management. This work could not be completed without collaborative efforts of Kerry Lannert, Dr. Jing Shang and Dr. Adam Munday. This proof-of-concept work is supported by Life Sciences Discovery Fund (LSDF), National Science Foundation (NSF) and Coulter Foundation. I also would like to personally thank the Royal Thai Government for the financial supports throughout my doctoral study.

BIBLIOGRAPHY

1. Rosen, S. The Worldwide Market for IVD Version 9. (2014).
2. Rohr, U.-P. *et al.* The value of in vitro diagnostic testing in medical practice: A status report. *PLoS One* **11,** e0149856 (2016).
3. Market Trends in Lateral Flow Immunoassays | Group T Thesis, Group 1316. at <https://groeptms1316.wordpress.com/2013/04/04/market-trends-in-lateral-flow-immunoassays/>
4. Caliendo, A. M. *et al.* Better tests, better care: improved diagnostics for infectious diseases. *Clin. Infect. Dis.* **57 Suppl 3,** S139-70 (2013).
5. The History of the Pregnancy Test Kit - A Timeline of Pregnancy Testing. at <https://history.nih.gov/exhibits/thinblueline/timeline.html>
6. Woods, A. *Molecular Point-of-care (POC) Markets*. (Kalorama Information, 2018).
7. Schito, M. *et al.* Opportunities and challenges for cost-efficient implementation of new point-of-care diagnostics for HIV and tuberculosis. *J. Infect. Dis.* **205 Suppl 2,** S169-80 (2012).
8. Elder, M. Market Research Report Point of Care Diagnostics. (2012).
9. Peeling, R. W. & Mabey, D. Point-of-care tests for diagnosing infections in the developing world. *Clin. Microbiol. Infect.* **16,** 1062–1069 (2010).
10. St John, A. & Price, C. P. Economic Evidence and Point-of-Care Testing. *Clin Biochem Rev* **34,** 61–74 (2013).
11. Sannes and Associates. Point of Care Diagnostic Tests. (2012).
12. Salazar, E. *The World Market for Molecular Diagnostics*. (Kalorama Information, 2018).
13. Mahieu, L. *et al.* Implementation of a multi-parameter Point-of-Care-blood test analyzer

reduces central laboratory testing and need for blood transfusions in very low birth weight infants. *Clin. Chim. Acta* **413,** 325–330 (2012).

14. Mabey, D., Peeling, R. W., Ustianowski, A. & Perkins, M. D. Diagnostics for the developing world. *Nat. Rev. Microbiol.* **2,** 231–240 (2004).
15. Lafleur, J. P., Jönsson, A., Senkbeil, S. & Kutter, J. P. Recent advances in lab-on-a-chip for biosensing applications. *Biosens. Bioelectron.* **76,** 213–233 (2016).
16. McRae, M. P. *et al.* Cardiac ScoreCard: A diagnostic multivariate index assay system for predicting a spectrum of cardiovascular disease. *Expert Syst. Appl.* **54,** 136–147 (2016).
17. Sayad, A. A. *et al.* A microfluidic lab-on-a-disc integrated loop mediated isothermal amplification for foodborne pathogen detection. *Sensors and Actuators B: Chemical* **227,** 600–609 (2016).
18. Liu, Q. *et al.* The ARTμS: a novel microfluidic CD4+ T-cell enumeration system for monitoring antiretroviral therapy in HIV patients. *Lab Chip* **16,** 506–514 (2016).
19. Mauk, M. *et al.* Miniaturized devices for point of care molecular detection of HIV. *Lab Chip* **17,** 382–394 (2017).
20. MacKenzie, L. E., Barimah, E. K., Jose, G. & Saha, S. P1 Rapid all-optical blood serum assay for heart disease biomarkers. *Heart* (2016).
21. Zhang, J. *et al.* A tunable polarization diversity silicon photonics filter. *Opt. Express* **19,** 13063–13072 (2011).
22. Soref, R. The past, present, and future of silicon photonics. *IEEE J. Select. Topics Quantum Electron.* **12,** 1678–1687 (2006).
23. Vlasov, Y. Silicon Photonics for Next Generation Computing Systems. (2008).
24. Langmuir, I. PROTEIN MONOLAYERS. *Cold Spring Harb. Symp. Quant. Biol.* **6,** 171–189 (1938).
25. Vivien, L. & Pavesi, L. *Handbook of Silicon Photonics*. (CRC Press, 2013).

26. Islam, M. R., Ali, M. M., Lai, M.-H., Lim, K.-S. & Ahmad, H. Chronology of Fabry-Perot interferometer fiber-optic sensors and their applications: a review. *Sensors (Basel)* **14,** 7451–7488 (2014).

27. Murphy, K. A., Gunther, M. F., Vengsarkar, A. M. & Claus, R. O. Quadrature phase-shifted, extrinsic Fabry–Perot optical fiber sensors. *Opt. Lett.* **16,** 273 (1991).

28. Brandenburg, A., Edelhaeuser, R. & Hutter, F. Gas sensor based on an integrated optical interferometer. in *Chemical and Medical Sensors* (ed. Wolfbeis, O. S.) **1510,** 148–159 (SPIE, 1991).

29. Boyd, R. W. & Heebner, J. E. Sensitive disk resonator photonic biosensor. *Appl. Opt.* **40,** 5742 (2001).

30. Chow, E., Grot, A., Mirkarimi, L. W., Sigalas, M. & Girolami, G. Ultracompact biochemical sensor built with two-dimensional photonic crystal microcavity. *Opt. Lett.* **29,** 1093 (2004).

31. Armani, A. M., Kulkarni, R. P., Fraser, S. E., Flagan, R. C. & Vahala, K. J. Label-free, single-molecule detection with optical microcavities. *Science* **317,** 783–787 (2007).

32. Bogaerts, W. *et al.* Silicon microring resonators. *Laser Photon. Rev.* **6,** 47–73 (2012).

33. Estrada, I. A. *et al.* Multiplex detection of pathogen biomarkers in human blood, serum, and saliva using silicon photonic microring resonators. in *Advances in Global Health through Sensing Technologies 2015* (ed. Southern, Š. O.) **9490,** 94900E (SPIE, 2015).

34. Kogelnik, H. in *Guided-Wave Optoelectronics* (ed. Tamir, T.) **26,** 7–88 (Springer Berlin Heidelberg, 1988).

35. Luchansky, M. S. *et al.* Characterization of the evanescent field profile and bound mass sensitivity of a label-free silicon photonic microring resonator biosensing platform. *Biosens. Bioelectron.* **26,** 1283–1291 (2010).

36. Linnet, K. & Kondratovich, M. Partly nonparametric approach for determining the limit of detection. *Clin. Chem.* **50,** 732–740 (2004).

37. Mudumba, S. *et al.* Photonic ring resonance is a versatile platform for performing multiplex immunoassays in real time. *J. Immunol. Methods* **448,** 34–43 (2017).

38. Iqbal, M. *et al.* Label-Free Biosensor Arrays Based on Silicon Ring Resonators and High-Speed Optical Scanning Instrumentation. *IEEE J. Select. Topics Quantum Electron.* **16,** 654–661 (2010).

39. Iqbal, M. *et al.* in *Label-Free Biosensor Methods in Drug Discovery* (ed. Fang, Y.) 133–153 (Springer New York, 2015). doi:10.1007/978-1-4939-2617-6_7

40. Blair, S. & Chen, Y. Resonant-enhanced evanescent-wave fluorescence biosensing with cylindrical optical cavities. *Appl. Opt.* **40,** 570 (2001).

41. Qavi, A. J., Kindt, J. T., Gleeson, M. A. & Bailey, R. C. Anti-DNA:RNA antibodies and silicon photonic microring resonators: increased sensitivity for multiplexed microRNA detection. *Anal. Chem.* **83,** 5949–5956 (2011).

42. Graybill, R. M., Para, C. S. & Bailey, R. C. PCR-Free, Multiplexed Expression Profiling of microRNAs Using Silicon Photonic Microring Resonators. *Anal. Chem.* **88,** 10347–10351 (2016).

43. Cardenosa-Rubio, M. C., Graybill, R. M. & Bailey, R. C. Combining asymmetric PCR-based enzymatic amplification with silicon photonic microring resonators for the detection of lncRNAs from low input human RNA samples. *Analyst* **143,** 1210–1216 (2018).

44. Luchansky, M. S. & Bailey, R. C. Silicon photonic microring resonators for quantitative cytokine detection and T-cell secretion analysis. *Anal. Chem.* **82,** 1975–1981 (2010).

45. Kindt, J. T., Luchansky, M. S., Qavi, A. J., Lee, S.-H. & Bailey, R. C. Subpicogram per milliliter detection of interleukins using silicon photonic microring resonators and an enzymatic signal enhancement strategy. *Anal. Chem.* **85,** 10653–10657 (2013).

46. Luchansky, M. S. & Bailey, R. C. Rapid, multiparameter profiling of cellular secretion using silicon photonic microring resonator arrays. *J. Am. Chem. Soc.* **133,** 20500–20506 (2011).

47. McClellan, M. S., Domier, L. L. & Bailey, R. C. Label-free virus detection using silicon photonic microring resonators. *Biosens. Bioelectron.* **31,** 388–392 (2012).

48. Valera, E., Shia, W. W. & Bailey, R. C. Development and validation of an immunosensor for monocyte chemotactic protein 1 using a silicon photonic microring resonator biosensing platform. *Clin. Biochem.* **49,** 121–126 (2016).

49. Washburn, A. L., Gunn, L. C. & Bailey, R. C. Label-free quantitation of a cancer biomarker in complex media using silicon photonic microring resonators. *Anal. Chem.* **81,** 9499–9506 (2009).

50. Washburn, A. L., Shia, W. W., Lenkeit, K. A., Lee, S.-H. & Bailey, R. C. Multiplexed cancer biomarker detection using chip-integrated silicon photonic sensor arrays. *Analyst* **141,** 5358–5365 (2016).

51. Kirk, J. T. *et al.* Zwitterionic polymer-modified silicon microring resonators for label-free biosensing in undiluted human plasma. *Biosens. Bioelectron.* **42,** 100–105 (2013).

52. Jäger, M., Becherer, T., Bruns, J., Haag, R. & Petermann, K. Antifouling coatings on SOI microring resonators for bio sensing applications. *Sensors and Actuators B: Chemical* **223,** 400–405 (2016).

53. Chae, K. H., Jang, Y. M., Kim, Y. H., Sohn, O.-J. & Rhee, J. I. Anti-fouling epoxy coatings for optical biosensor application based on phosphorylcholine. *Sensors and Actuators B: Chemical* **124,** 153–160 (2007).

54. Vaisocherová, H., Brynda, E. & Homola, J. Functionalizable low-fouling coatings for label-free biosensing in complex biological media: advances and applications. *Anal. Bioanal. Chem.* **407,** 3927–3953 (2015).

55. Akkahat, P., Kiatkamjornwong, S., Yusa, S., Hoven, V. P. & Iwasaki, Y. Development of a novel antifouling platform for biosensing probe immobilization from methacryloyloxyethyl phosphorylcholine-containing copolymer brushes. *Langmuir* **28,** 5872–5881 (2012).

56. Wang, H. *et al.* Amino acid-based anti-fouling functionalization of silica nanoparticles using divinyl sulfone. *Acta Biomater.* **40,** 273–281 (2016).

57. Luchansky, M. S., Washburn, A. L., McClellan, M. S. & Bailey, R. C. Sensitive on-chip detection of a protein biomarker in human serum and plasma over an extended dynamic range using silicon photonic microring resonators and sub-micron beads. *Lab Chip* **11,** 2042–2044 (2011).

58. Sloan, C. D. K., Marty, M. T., Sligar, S. G. & Bailey, R. C. Interfacing lipid bilayer nanodiscs and silicon photonic sensor arrays for multiplexed protein-lipid and protein-membrane protein interaction screening. *Anal. Chem.* **85,** 2970–2976 (2013).

59. Park, M. K. *et al.* Label-free aptamer sensor based on silicon microring resonators. *Sensors and Actuators B: Chemical* **176,** 552–559 (2013).

60. Ghasemi, F. *et al.* Multiplexed detection of lectins using integrated glycan-coated microring resonators. *Biosens. Bioelectron.* **80,** 682–690 (2016).

61. Chalyan, T. *et al.* Aptamer- and Fab'- Functionalized Microring Resonators for Aflatoxin M1 Detection. *IEEE J. Select. Topics Quantum Electron.* **23,** 1–8 (2017).

62. American Red Cross. History of Blood Transfusions. at <http://www.redcrossblood.org/learn-about-blood/blood-transfusions/history-blood-transfusions>

63. American Association of Blood Banks. Highlights of Transfusion Medicine History. at <http://www.aabb.org/tm/Pages/highlights.aspx>

64. Sahoo, A. in *Blood: The Worldwide Market for Blood Products, Blood Testing, Blood Equipment and Synthetic Blood Products* 20 (2014).

65. Storry, J. R. New technologies to replace current blood typing reagents. *Curr Opin Hematol* **14,** 677–681 (2007).

66. Liu, Z., Liu, M., Mercado, T., Illoh, O. & Davey, R. Extended blood group molecular typing

and next-generation sequencing. *Transfus Med Rev* **28,** 177–186 (2014).

67. British Committee for Standards in Haematology *et al.* Guidelines on the management of massive blood loss. *Br. J. Haematol.* **135,** 634–641 (2006).

68. Estcourt, L. J. *et al.* Restrictive versus liberal red blood cell transfusion strategies for people with haematological malignancies treated with intensive chemotherapy or radiotherapy, or both, with or without haematopoietic stem cell support. *Cochrane Database Syst. Rev.* **1,** CD011305 (2017).

69. Mirouse, A. *et al.* Red blood cell transfusion in the resuscitation of septic patients with hematological malignancies. *Ann. Intensive Care* **7,** 62 (2017).

70. Sahoo, A. *Blood: The Worldwide Market for Blood Products, Blood Testing, Blood Equipment and Synthetic Blood Products*. (2014).

71. World Health Organization Blood Transfusion Safety. The Clinical Use of Blood Handbook.

72. Harmening, D. *Modern blood banking & transfusion practices*. (F.A. Davis, 2012).

73. Daniels, G. & Bromilow, I. *Essential guide to blood groups*. (John Wiley & Sons Inc., 2007).

74. Mohandas, N. & Narla, A. Blood group antigens in health and disease. *Curr Opin Hematol* **12,** 135–140 (2005).

75. Dean, L. Blood Groups and Red Cell Antigens. (2005).

76. Giriyan, S. S., Agrawal, A., Bajpai, R. & Nirala, N. K. A1 and A2 Sub-Types of Blood Group “A”: A Reflection of their Prevalence in North Karnataka Region. *J. Clin. Diagn. Res.* **11,** EC40-EC42 (2017).

77. Ranjan, V., Khillan, K. & Sharma, M. Blood group A2B with anti-A1 antibody reacting at 37°C – A case report. *Current Medicine Research and Practice* **6,** 162–163 (2016).

78. Chaudhari, C. N., Misra, R. N. & Nagpal, A. K. Transfusion in Blood Group A2B with Anti

A1 Recipient. *Med J Armed Forces India* **64,** 371–372 (2008).

79. Reid, M. E., Lomas-Francis, C. & Olsson, M. L. *The Blood Group Antigen FactsBook*. (Elsevier/AP, 2012).

80. Lawicki, S., Covin, R. B. & Powers, A. A. The kidd (JK) blood group system. *Transfus Med Rev* **0,** (2016).

81. Fatalities Reported to FDA Following Blood Collection and Transfusion: Annual Summary for Fiscal Year 2008. (2012).

82. Bromilow, I. M. Gel techniques in blood group serology. *Med Lab Sci* **49,** 129–132 (1992).

83. Sauaia, A. *et al.* Epidemiology of trauma deaths: a reassessment. *J. Trauma* **38,** 185–193 (1995).

84. Evans, J. A. *et al.* Epidemiology of traumatic deaths: comprehensive population-based assessment. *World J. Surg.* **34,** 158–163 (2010).

85. Stanworth, S. J. *et al.* Mortality from trauma haemorrhage and opportunities for improvement in transfusion practice. *Br. J. Surg.* **103,** 357–365 (2016).

86. Sakran, J. V., Greer, S. E., Werlin, E. & McCunn, M. Care of the injured worldwide: trauma still the neglected disease of modern society. *Scand J Trauma Resusc Emerg Med* **20,** 64 (2012).

87. Kaur, P., Basu, S., Kaur, G. & Kaur, R. Transfusion protocol in trauma. *J Emerg Trauma Shock* **4,** 103–108 (2011).

88. Tintinalli, J. E., Kelen, G. D., Stapczynski, J. S. & Physicians, A. C. E. *Emergency Medicine: A Comprehensive Study Guide, Sixth edition*. (McGraw-Hill Education, 2003).

89. Schonewille, H., van de Watering, L. M. G., Loomans, D. S. E. & Brand, A. Red blood cell alloantibodies after transfusion: factors influencing incidence and specificity. *Transfusion* **46,** 250–256 (2006).

90. Aysola, A. *et al.* Multi-Center Evaluation of the Automated Immunohematology Instrument,

the ORTHO VISION Analyzer. *Lab Med* **48,** 29–38 (2017).

91. Blakeley, D., Tolliday, B., Colaco, C. & Roser, B. Dry instant blood typing plate for bedside use. *Lancet* **336,** 854–855 (1990).

92. Migeot, V., Ingrand, I., Salmi, L. R. & Ingrand, P. Reliability of bedside ABO testing before transfusion. *Transfusion* **42,** 1348–1355 (2002).

93. ABORhCard Applications and Performance Studies. (2013).

94. Daurat, G. [Yes, we should keep ABO agglutination test within bedside transfusion checks]. *Transfus. Clin. Biol.* **15,** 322–326 (2008).

95. Yeow, N., McLiesh, H., Guan, L., Shen, W. & Garnier, G. Paper-based assay for red blood cell antigen typing by the indirect antiglobulin test. *Anal. Bioanal. Chem.* **408,** 5231–5238 (2016).

96. Songjaroen, T. & Laiwattanapaisal, W. Simultaneous forward and reverse ABO blood group typing using a paper-based device and barcode-like interpretation. *Anal. Chim. Acta* **921,** 67–76 (2016).

97. Noiphung, J. *et al.* A novel paper-based assay for the simultaneous determination of Rh typing and forward and reverse ABO blood groups. *Biosens. Bioelectron.* **67,** 485–489 (2015).

98. Then, W. L., Li, M., McLiesh, H., Shen, W. & Garnier, G. The detection of blood group phenotypes using paper diagnostics. *Vox Sang.* **108,** 186–196 (2015).

99. Yeow, N., McLiesh, H. & Garnier, G. Indirect antiglobulin paper test for red blood cell antigen typing by flow-through method. *Anal. Methods* **7,** 4645–4649 (2015).

100. Khan, M. S., Thouas, G., Shen, W., Whyte, G. & Garnier, G. Paper diagnostic for instantaneous blood typing. *Anal. Chem.* **82,** 4158–4164 (2010).

101. Quinn, J. G. *et al.* Development and application of surface plasmon resonance-based biosensors for the detection of cell-ligand interactions. *Anal. Biochem.* **281,** 135–143

(2000).

102. Houngkamhang, N. *et al.* ABO blood-typing using an antibody array technique based on surface plasmon resonance imaging. *Sensors (Basel)* **13,** 11913–11922 (2013).

103. Quinn, J. G., O'Kennedy, R., Smyth, M., Moulds, J. & Frame, T. Detection of blood group antigens utilising immobilised antibodies and surface plasmon resonance. *J. Immunol. Methods* **206,** 87–96 (1997).

104. Robb, J. S., Roy, D. J., Ghazal, P., Allan, J. & Petrik, J. Development of non-agglutination microarray blood grouping. *Transfus Med* **16,** 119–129 (2006).

105. Pipatpanukul, C. *et al.* Rh blood phenotyping (D, E, e, C, c) microarrays using multichannel surface plasmon resonance imaging. *Biosens. Bioelectron.* **102,** 267–275 (2018).

106. Then, W. L., Aguilar, M.-I. & Garnier, G. Quantitative Detection of Weak D Antigen Variants in Blood Typing using SPR. *Sci. Rep.* **7,** 1616 (2017).

107. Then, W. L., Aguilar, M.-I. & Garnier, G. Quantitative blood group typing using surface plasmon resonance. *Biosens. Bioelectron.* **73,** 79–84 (2015).

108. Ashiba, H. *et al.* Hemagglutination detection for blood typing based on waveguide-mode sensors. *Sensing and Bio-Sensing Research* **3,** 59–64 (2015).

109. Ashiba, H., Fujimaki, M., Awazu, K., Tanaka, T. & Makishima, M. Microfluidic chips for forward blood typing performed with a multichannel waveguide-mode sensor. *Sensing and Bio-Sensing Research* **7,** 121–126 (2016).

110. Ashiba, H. *et al.* Rapid detection of hemagglutination using restrictive microfluidic channels equipped with waveguide-mode sensors. *Jpn. J. Appl. Phys.* **55,** 027002 (2016).

111. Petrik, juraj. Blood Group Antibody Screening. (2010).

112. Kang, T., Lee, S.-J., Kim, Y., Lee, G.-W. & Cho, D.-W. Intelligent micro blood typing system using a fuzzy algorithm. *J. Micromech. Microeng.* **20,** 015024 (2010).

113. Schmidt, S. *et al.* Improving the performance of silicon photonic rings, disks, and Bragg gratings for use in label-free biosensing. in *Biosensing and Nanomedicine VII* (eds. Mohseni, H., Agahi, M. H. & Razeghi, M.) **9166,** 91660M (SPIE, 2014).

114. Kirk, J. T., Lannert, K. W., Ratner, D. M. & Johnsen, J. M. Serologic and phenotypic analysis of blood types via silicon nanophotonics. *Blood* 1565–1565 (2014).

115. Chiang, H. C. & Koshland, M. E. Antigen-induced conformational changes in IgM antibody. I. The role of the antigenic determinant. *J. Biol. Chem.* **254,** 2736–2741 (1979).

116. Feinstein, A. & Munn, E. A. Conformation of the free and antigen-bound IgM antibody molecules. *Nature* **224,** 1307–1309 (1969).

117. Liumbruno, G. *et al.* Recommendations for the transfusion of plasma and platelets. *Blood Transfus.* **7,** 132–150 (2009).

118. Desborough, M. *et al.* Fresh frozen plasma for cardiovascular surgery. *Cochrane Database Syst. Rev.* CD007614 (2015). doi:10.1002/14651858.CD007614.pub2

119. Mannucci, P. M. & Tripodi, A. Liver disease, coagulopathies and transfusion therapy. *Blood Transfus.* **11,** 32–36 (2013).

120. Huber, J. *et al.* Prophylactic plasma transfusion for patients undergoing non-cardiac surgery. *Cochrane Database Syst. Rev.* **2017,** (2017).

121. Pandey, S. & Vyas, G. N. Adverse effects of plasma transfusion. *Transfusion* **52 Suppl 1,** 65S–79S (2012).

122. Domen, R. E., Calero, A. & Keehn, W. H. Acute Hemolytic Transfusion Reaction Due to Anti-A_1. *Lab Med* **19,** 739–740 (1988).

123. Tormey, C. A. & Stack, G. The persistence and evanescence of blood group alloantibodies in men. *Transfusion* **49,** 505–512 (2009).

124. Giblett, E. R. Blood group alloantibodies: an assessment of some laboratory practices. *Transfusion* **17,** 299–308 (1977).

125. Rabe, M., Verdes, D. & Seeger, S. Understanding protein adsorption phenomena at solid surfaces. *Adv Colloid Interface Sci* **162,** 87–106 (2011).

126. de Mattos, L. C. Structural diversity and biological importance of ABO, H, Lewis and secretor histo-blood group carbohydrates. *Rev. Bras. Hematol. Hemoter.* **38,** 331–340 (2016).

127. Chemical Properties of Material Surfaces By Marek Kosmulski (Technical University of Lublin, Lublin, Poland). Surfactant Science Series. Volume 102. Edited by Arthur T. Hubbard (Santa Barbara Science Project, Santa Barbara, CA). Marcel Dekker, Inc.: New York, Basel. 2001. viii + 754 pp. $225.00. ISBN: 0-8247-0560-2. *J. Am. Chem. Soc.* **124,** 1127–1127 (2002).

128. Chasis, J. A. & Mohandas, N. Red blood cell glycophorins. *Blood* **80,** 1869–1879 (1992).

129. Soshee, A., Zürcher, S., Spencer, N. D., Halperin, A. & Nizak, C. General in vitro method to analyze the interactions of synthetic polymers with human antibody repertoires. *Biomacromolecules* **15,** 113–121 (2014).

130. Armstrong, J. K. *et al.* Antibody against poly(ethylene glycol) adversely affects PEG-asparaginase therapy in acute lymphoblastic leukemia patients. *Cancer* **110,** 103–111 (2007).

131. Zhang, P., Sun, F., Liu, S. & Jiang, S. Anti-PEG antibodies in the clinic: Current issues and beyond PEGylation. *J. Control. Release* **244,** 184–193 (2016).

132. Lubich, C. *et al.* The Mystery of Antibodies Against Polyethylene Glycol (PEG) - What do we Know? *Pharm. Res.* **33,** 2239–2249 (2016).

SUMMARY OF PUBLICATIONS AND TALKS

Publications:

1) **Khumwan, P.**, Shang, J., Munday, AD., Kirk, JT., Lannert, KW, Johnsen, JM., and Ratner, DM., “Simultaneous Forward and Reverse Blood Typing on Multiplexed Microring Resonator Arrays.” *(In preparation for submission)*

2) Schmidt, S., et al., “Serologic Phenotyping using Silicon Photonic Biosensors and Capillary Driven Network.” *(In preparation for submission)*

3) Schmidt, S., et al., “Erythrocyte and Serologic Phenotyping using Silicon Photonic Ring Resonators.” *(In preparation for submission)*

4) Kirk, J.T., Hansen, G., **Khumwan, P.**, Lannert, K.W., Johnsen J.M., and Ratner, D.M. "Measuring Anti-A/B Serologies in Human Plasma Using Silicon Photonic Biosensors.". *(In preparation for submission)*

5) Schmidt, S., Flueckiger, J., Wu, W.X., Grist, S., Fard, S.T., Donzella, V., **Khumwan, P.**, et al. "Improving the performance of silicon photonic rings, disks, and Bragg gratings for use in label-free biosensing." SPIE NanoScience+ Engineering, pp. 91660M-91660M. International Society for Optics and Photonics, 2014.

Conference talks:

1) Wende, A.P., **Khumwan, P**., Ratner, D.M., "Combining Silicon Photonics and Machine Learning for the Phenotypic Profiling of Cells." (Talk), Annual Biomedical Engineering Society Conference, Atlanta, Georgia 2018. *(Abstract submitted)*

2) **Khumwan, P**., Wende, A.P., Khaleel, Z., Ratner, D.M., "Optimizing Silicon Photonics for Serologic and Phenotypic Profiling of Blood." (Talk), Annual Biomedical Engineering Society Conference, Phoenix, Arizona 2017.

3) **Khumwan, P**., "Multiplexed Serological Blood Typing on Silicon Photonic Platform." (Talk), Molecular Medicine Capstone Presentation, Molecular Medicine Training Program, University of Washington, 2017.

APPENDIX A

Shipping of Silicon Chips and Reagents Standard Operating Procedure

A.1 Materials and Definitions

A.1.1 Shipping Materials and Consumables

1) The “shipping box” is a container that consists of an interior Styrofoam insulated box with lid, plastic liner bag, and an outer cardboard packaging.
    a) All exterior markings of the package unrelated to the contents or conditions of the current shipment are to be defaced or otherwise permanently covered prior to shipping.
    b) The shipping box must have been tested to maintain the target interior temperature (2°C-10°C) for 36 hours under conditions which reasonably simulate shipping with the packing materials specified in this protocol. The list of shipping boxes may be revised in later versions of this SOP. The list for this version currently includes:
        i) A BloodworksNW Blood Shipping Container 17 x 11 x 11 inch (W x H x D) box lined with 15/16ths inch foam (True Pack) with the following acceptable cooling thermal pack combination:
            (1) 24 Koolit phase change packets (see below) and 12 Ecogel cooling packets (see below)
2) “Cooling packs” for this SOP constitute phase change materials rated 2-8°C. This list may be revised in later versions of this SOP. The list for this version currently includes:
    a) Koolit advanced PCM phase change material packets, typically in strips of 4 (Cold Chain technologies; P/N 732M24+3) (called “Koolit cooling packs” in this SOP)
    b) Ecogel cooling packs (Pelton Shepard; P/N EC-4B-144 or EC-6B-96) (called “Ecogel cooling packs” in this SOP)

3) Gel-Pak 4” Vacuum Release tray (Gel-Pak; P/N VR-44/meshCC-00B-Xn) (called “Gel-Pak” or “Gel-Pak tray” in this SOP)
4) MiniPax desiccant packs (Aldrich; P/N Z163562-100EA)
5) Ambion 0.5 ml microcentrifuge tubes (Ambion; P/N Am12300) (called “microfuge tubes” in this SOP)
6) Parafilm
7) Sharpie (dark color) or similar permanent laboratory marker
8) Packing tape
9) Thermometer with a range which includes -10°C to 24°C
    a) One option is the red mineral spirit-filled General-Purpose Thermometer (VWR; In compliance with accuracy requirements of ANSI-SAMA) or similar
10) Plastic quart size zip top freezer bags (such as Zip-loc or equivalent)
11) Lab tape and/or sticker labels

A.1.2 Silicon Photonic Chips (called “chips” in this SOP)

1) Chips MUST be dry prior to packaging and shipping (room air dried, vacuum dried, etc.).
2) Categories of chips:
    a) A “functionalized chip” is a chip which has had a streptavidin (SA) coating applied.
    b) An “unfunctionalized chip” is a chip which has never been functionalized with SA or any other reagent
    c) A “stripped chip” is a chip which has been previously functionalized and/or tested with laboratory assays undergone chemical stripping or other methods intended to remove most (or all) of material above the original silicon layer of the chip
3) The source of the chips, lots, dates of acquisition, and storage history shall be documented in the shipping log or in a dated laboratory notebook entry referencing the specific shipment. In

the case of functionalized or stripped chips, the histories of those chips, including the experimental dates, reagents used (with lot identifiers), assays run (if relevant), stripping (if relevant), and storage conditions, shall be documented in the laboratory notebook and linked by dates or other unique references to the specific shipment.

A.1.3 Liquid reagents (constitute reagents in liquid solutions included with the shipment)

1) Liquid reagents enter this Shipping SOP in the final buffers and concentrations at which they will be shipped.
2) ALL liquid reagents shipped in this SOP must be compatible with temperatures of 2°C to 10°C
3) The records of liquid reagent sourcing, processing, handling, storage, and final diluent and concentration should be documented in the laboratory notebook and linked by dates or other unique references to the specific shipment.

A.1.4 Shipment Manifest(s) and Shipping Documentation

1) This SOP is for DOMESTIC (U.S.) shipments only. International shipments require a different SOP.
2) The shipping vendor and documentation needed to ship must be identified prior to the ship date.
3) The recipient's name, address, and phone number should be confirmed with the recipient prior to shipping.
4) This shipment must be shipped OVERNIGHT NEXT MORNING on a Monday, Tuesday, Wednesday, or Thursday. The recipient's business must open the following day and the recipient must have been notified to receive the sample.
5) The tracking number must be recorded and provided to the recipient by e-mail (or another method if requested by the recipient).

6) All liquid reagents included in the shipment must appear on the shipment manifest labeled exactly matching the labels on the tubes with volumes recorded.
    a) The shipment manifest should be provided to the recipient separately (e-mail, fax, etc.).
    b) A printed copy of the manifest must be sent with the physical shipment.
    c) A copy of the manifest must be retained for the record.
7) The contents of each shipment must be reviewed for regulated hazards per the UW EH&S Training on “Shipping Hazardous Materials”. It is required that hazards must be appropriately packaged, labeled, and declared with the shipper.

A.1.5 Definition of “4°C spaces”

1) 4°C work spaces:
    a) A 4°C work space includes 4°C environment rooms or 4°C walk-in refrigerators.
    b) Thermometer measures: The temperature of the 4°C work space is measured with a thermometer and recorded in the project laboratory notebook or dated log prior to initiating shipping protocols and again at the time of final packing.
        i) If the measured temperature of the work space is less than 2°C or exceeds 5°C at any time point, the shipping protocol is ABORTED.
            (1) The PI should be notified that the 4°C space is out of temperature range.
    c) Continuous temperature monitoring: If the work space has continuous temperature monitoring, the monitor is also checked prior to beginning work and at the time of packing.
        i) If the temperature of the work space monitor records a temperature less than 2°C or greater than 4.5°C during this protocol, the shipping protocol is ABORTED.
            (1) The PI should be notified that the 4°C space is out of temperature range.

2) 4°C refrigerators:

a) A 4°C refrigerator references plug-in closed refrigeration units, such as upright or under bench refrigerators

b) Thermometer measures: The temperature of the 4°C refrigerator is measured with a thermometer and recorded in the project laboratory notebook or dated log prior to initiating shipping protocols and again at the time of final packing.

i) If the measured temperature of the refrigerator is less than 2°C or exceeds 5°C at any time point, the shipping protocol is ABORTED.

(1) The PI should be notified that the 4°C space is out of temperature range.

c) Continuous temperature monitoring: If the refrigerator has continuous temperature monitoring, the monitor is also checked prior to beginning work and at the time of packing.

i) If the temperature of the refrigerator monitor records a temperature less than 2°C or greater than 5°C during this protocol, the shipping protocol is ABORTED.

(1) The PI should be notified that the 4°C space is out of temperature range.

A.2 Packing and Shipping Protocol

1) At least 36 hours prior to shipping, all packing materials, including the shipping container, are inspected and then stored in a "4°C space" (described above):

a) Shipping box:

i) The shipping box is inspected for evidence of packaging compromise (tears, holes, or other evidence of physical damage). If any part of the shipping box appears compromised by physical damage, the shipping box must be discarded or labeled and otherwise removed from active protocols. Optionally, the box may be retested as described in the Materials above.

ii) The shipping box is placed in a 4°C space with the box top open and styrofoam lid placed separately for at least 36 hours.

b) Cooling packs:

i) Cooling packs are inspected for evidence of physical damage (scrapes or holes in the plastic, evidence of leaks, etc.). If a cooling pack appears compromised by physical damage, it will be disposed of immediately per the manufacturer's instructions.

ii) Koolit cooling packs are laid flat on a surface at 4°C a single layer for at least 36 hours.

iii) Ecogel cooling packs are laid flat on a surface at 4°C a single layer for at least 36 hours.

2) Chips are packaged for shipment as follows:

a) Chips are arranged in a single layer in Gel-Pak trays using clean plastic forceps, up to 96 chips per tray, at room temperature (20°C to 25°C), and the Gel-Pak tray lid is closed per manufacturer's specification.

i) If chips are homogeneous for the whole shipment, no Gel-Pak unique identifier(s) or tray map(s) is/are required.

ii) If chips are mixed by type, pre-treatment, or other condition *within a single* Gel-Pak tray, each Gel-Pak will be labeled with a unique identifier and a map will be generated of the identified Gel-Pak tray chip lay-out to specify each chip individually. The Gel-Pak identifier(s) and map(s) will be included as part of the shipment reagent manifest (see above).

iii) If chips are homogeneous within trays, but mixed by type, pre-treatment, or other condition *between* Gel-Pak trays, each Gel-Pak tray in the shipment will be labeled with a unique identifier and included in the shipment reagent manifest (see above).

iv) The lid of each Gel-Pak tray is labeled as follows:

(1) A label on the top right corner of the Gel-Pak lid with an up arrow and the word “TOP” so that orientation of the chips is clear.

(2) A label in the middle of the lid with the words “Ratner Lab” and “Pack [x] of [y]” where [y] is the total number of Gel-Pak trays an [x] is either “1” or an increasing numeral until [y] is reached (i.e. 1 of 4)

b) Each Gel-Pak tray with chips is placed in an individual zip-top bag containing 1 packet of MiniPax desiccant packs

c) Each zip top bag is backfilled with nitrogen, sealed, and tape applied circumferentially around each bag prior to shipping

d) Each zip top bag is individually labeled with a sticker which reads “Bring to room temperature before opening”.

e) The packaged chips in Gel-Pak trays are either immediately placed at the appropriate layer of a prepared shipping box or are stored in a 4C space prior to shipping

3) Liquid reagents are packaged for shipment as follows:

a) The maximum total time for reagents entering the Shipping SOP to be outside a monitored 4°C space is 30 minutes.

i) The maximum allowable ambient temperature is 25°C (maximum room temperature).

ii) Time spent on wet ice using a thermometer (recording measurements before and after) is excluded as long as the temperature remained less than 4°C.

b) Microfuge tubes are labeled with the reagent identifier and date.

i) Use a permanent laboratory marker and/or

ii) Lab tape/stickers printed with laboratory marker or lab-safe ink

c) The reagent identifier tube labels are cross-referenced with the written manifest and the laboratory notebook (see above).

i) If a code identifier is used on the label, the key with specific reagent details is reviewed in the notebook.

d) Liquid reagents are transferred to the microfuge tubes in the specified volumes per standard laboratory methods.

e) Microfuge tubes are sealed with Parafilm.

f) Labeling, reagents, and volumes are again cross-checked with the written manifest

g) Microfuge tubes are placed in a secondary container, consisting of:

i) zip top plastic bag which is packaged by sealing the bag, rolling the bag for compactness, and tape applied circumferentially around the bag.

h) The packaged tubes are stored at 4°C until shipping.

4) The shipping box is assembled as follows:

a) The temperature of all 4°C containing materials for packing is verified to have been in a 4°C space for more than 36 hours at the time of packing.

i) Temperatures are recorded in the log or notebook

ii) The Koolit packs should be frozen firm to the touch. If they are liquid or slush, they are malfunctioning and/or not at 4°C and the shipping protocol is ABORTED.

b) For the BloodworksNW Blood Shipping Container 17 x 11 x 11 inch (W x H x D) box:

i) 8 Koolit packs are placed lining the bottom of the box to create the first layer

ii) 9 Ecogel packs are placed in the second layer.

iii) 4 Koolit packs are placed in the third layer.

iv) The temperature at the third layer is measured and recorded.

(1) The desired range is 2-4°C

(2) If the temperature measures outside the range of 2-4°C, the shipping protocol is ABORTED.

v) Packaged chips in Gel-Pak trays (see above) and packaged liquid reagents (see above) are placed on top of the third layer of phase change material packets.

vi) The chips and liquid reagents were overlaid with 8 Koolit packs in the fourth layer

vii) 3 Ecogel packs and 4 Koolit packs form the top layers.

viii) Documents to the recipient to be included within the box are placed in plastic sleeves and laid on top.

ix) The foam lid (also stored at 4°C) is placed on the box

x) A paper or label reading “Upon opening please measure the temperature at the location of the reagents” is placed on top of the foam lid

xi) The plastic bag (liner) is sealed with packing tape

xii) The outer cardboard box is sealed with packing tape

xiii) Shipping labels are applied to the box

(1) The tracking number is recorded and sent to the recipient the same day as shipping

xiv) The sealed and labeled shipping box is transferred to the courier or pick up point

xv) The tracking number is used to ensure the package has picked up, is in transit, and is delivered

5) The recipient is to measure the temperature at the level of the reagents upon receipt.

a) If a shipping box is received with contents out of the temperature range (2°C to 10°C), they are to notify the shipper. The shipping box is to be labeled defective and immediately discarded.

6) This protocol may be reversed (with steps appropriate for the contents to be shipped) for the return of chips and/or reagents to the laboratory.

APPENDIX B

Chip Handling Standard Operating Procedure

B.1 Evaluation and Assignment of Chips for Analysis in the LSDF Study.

1) Each sensor chip consists two rows of sensors (**Figure B-1**). The top row performs an indirect typing analysis. The bottom row performs a direct typing analysis.

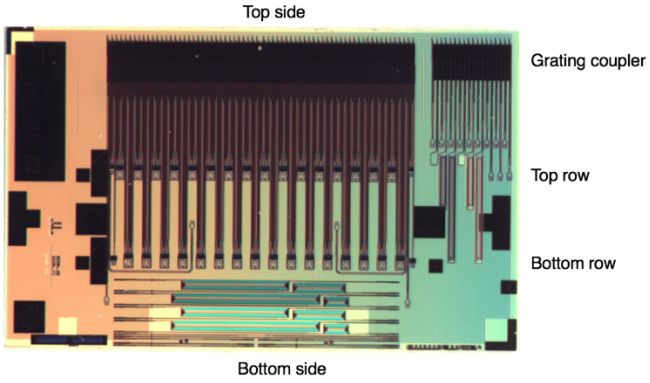

a)

Figure B-14. Micrograph of the sensor chip. The top side of the chip is defined by an array of grating couplers. Sensor devices are offset in the middle part of the chip towards the bottom side. Sensors are divided into two rows which are referred to in this document as the top row and the bottom row based on their relative positions to the top and bottom sides of the chip.

2) Photographs of chips are scored independently by two observers for the quality of reagent spot coverage on each cluster of four sensors based on the following criteria:

   a) Scores for spot coverage on a cluster of four sensor devices is performed for all print targeted clusters. Spot coverage scores fall in six categories

      (1) '1 ring' indicates that a reagent spot only covers one full sensor ring, even if it appears that the spot also covers some portion of other adjacent devices.

      (2) '2 rings' indicates that a reagent spot only covers two full sensor rings, even if it appears that the spot also covers some portion of other adjacent devices.

(3) ‘3 rings’ indicates that a reagent spot only covers three full sensor rings, even if it appears that the spot also covers some portion of the fourth device.

(4) ‘Partial 4’ indicates that a reagent spot covers three full sensor rings, and mostly covers the fourth ring device.

(5) ‘Miss’ indicates that a reagent spot has completely missed a cluster of sensor rings

(6) A reagent spot that covers all four sensor rings completely without leaving any parts exposed receives no scoring by default.

b) Additional notes are made of features observed (apparent merged spots, spot migration, multiply spotted, other artifacts, etc.)

3) Chips are scored for the overall quality based on the following criteria:

a) ‘Perfect’ indicates that all reagent spots fully cover all targeted device clusters.

b) ‘Good’ indicates that all targeted clusters have majority coverage, defined as ‘3 rings’, ‘Partial 4’, or complete coverage.

c) ‘Partial’ indicates that one or more reagent spots classified as ‘Miss’, ‘1 ring’, or ‘2 ring’.

d) ‘Missing’ indicates that the entire chip is missing from the tray or all reagents spots classified as Miss.

4) Scores from two independent observers are compared and harmonized. Images will be inspected again for chips with scores that result in a change of classification in overall quality.

5) Identification of chips for use in blood sample analysis.

a) Chips that are scored ‘perfect’ or ‘good’ receive priority status in indirect and direct blood type testing in the study.

b) Chips that are scored ‘partial’ can be further reviewed for use in study testing or other non-study work. The following combinations of spot coverage scores can be used as follows

i) Single channel (top row or bottom row targeted clusters) meets criteria for ‘perfect’ or ‘good’ determination, but the other row is ‘partial’ or ‘miss’:

(1) Top row ‘perfect’ or ‘good’:

ii) ‘Partial’ chips whose spots in the control reagents are completely absent will not be used for analysis, but can still be used for training purposes. ‘Perfect’ chips are prioritized for running assays over ‘good’ and ‘partial’ chips.

6) Daily, upon receiving blood samples, chips will be assigned to one donor ID per chip. Analysis will be performed in an increasing order of the donor ID number and must be completed by end of day.

B.2 Transfer of Printed Chips from 4oC Spaces to Environment at Room Temperature (between 20^{o}C and 25^{o}C)

1) Chips are stored in the original sealed packaging from the print processing in a 4^{o}C refrigerator (range 3.5-4.5).
2) Transfer the trays containing sensor chips from the 4^{o}C refrigerator to a 4^{o}C cold room. Record the temperature of the cold room upon entering. Cold room should sustain a proper temperature range of 3.7^{o}C - 4.3^{o}C. If the cold room is out of temperature range, the sensor chips are returned to the 4^{o}C refrigerator.
   a) If the time it takes to transfer the trays from a refrigerator to a cold room is more than 5 minutes, store the trays inside a Styrofoam box filled with at least two packages of cooling materials (e.g. Koolit, Ecogel) that have been equilibrated at 4^{o}C for transportation. Measure the temperature on the surface of a sealed tray package in the middle of the box prior to placing the trays in the box. Do not use if the temperature is out of range (2^{o}C to 5^{o}C). Measure the temperature by the same method after removing the trays from the box. If the temperature is out of range (2^{o}C to 5^{o}C), the tray is returned to the 4^{o}C fridge and labeled “do not use, temp”. The maximum time for chip trays to remain in the transfer Styrofoam box is 30 minutes.

3) Inspect the tray packages for tears or evidence of leakage in the sealed plastic bags. If tears or leakage are observed, the tray package bag is not opened and is instead returned to the 4^{o}C refrigerator and labeled “do not use, package”. Determination if the chips are compromised for use in the study will be done outside this protocol by the study team.

4) Lay each of the six sealed packages on the bench inside the cold room in the following order: Tray 1 07/25/2016, Tray 2 07/25/2016, Tray 1 09/22/2016, Tray 2 09/22/2016, Tray 3 09/22/2016 and Tray 4 09/22/2016. Keep the side with label upward.At room temperature, prepare six “Day Vials” for transferring chips between the 4^{o}C cold room and room temperature laboratory:
   a) Insert a MiniPax (Multisorb) absorbent packet inside each of six glass scintillation vials.
   b) Close the vials by twisting the cap clockwise when observing from the top.
   c) Label the vials as follows, “Ratner Day Vial 1”, “Ratner Day Vial 2”, “Ratner Day Vial 3”, “Ratner Day Vial 4”, “Ratner Day Vial 5”, “Ratner Day Vial 6” on their caps and sides.
   d) Set the closed, labeled vials inside the 4^{o}C cold room for at least 30 minutes to allow for temperature to equilibrate.

5) Select the number of chips planned to be run during the working day from the pre-determined list of chips that will be tested in the study. Chips are named based on their position on the tray’s grid and batch. For instance, a “T10 Tr1 Sept” chip is a chip at position 10 out of 96 on the grid, and it belongs to tray 1 of the September batch of chips.
   a) In the lab notebook, designate which chip goes into each numbered Day Vial.
   b) While in the 4^{o}C cold room, cut the top part of a sealed package with a pair of scissors and remove the tray.
   c) Open the lid to the specific day vial. Inspect the color indicator of the MiniPax absorbent beads through a clear strip on the back side of its packet before placing a chip inside the vial. Absorbent beads should maintains light blue color. Discard the packet immediately if

the beads turn pink, and replace it with a new MiniPax packet which has been maintained in the 4°C cold room.

d) Open the tray lid. Using the map of printed chips, identify the position of the chip on the tray, and carefully pick it upward from the tray's surface by using a pair of plastic tweezers and gently place the chip in the day vial (with the functional side facing up). Avoid scratching the chip surface.

   i) If the chip surface is damaged or scratched, close the vial and label "do not use, scratch". Store the vial at 4°C for determination of suitability for use by the study team.

e) Quickly close the Day Vial.

f) Repeat this process for the remainder of the chips that are assigned for daily analysis selected from the open tray.

g) Seal the Day Vial caps with parafilm by stretching the parafilm and wrap it around the edge of a cap. Close the chip tray by placing the lid back to the tray.

h) Insert the tray back to its corresponding plastic package. Make sure that the tray is oriented upward. Store the tray inside a Ziploc bag containing one MiniPax absorbent packet.

i) Place the tray back to its location in the 4°C refrigerator.

6) In the lab notebook, verify the record of which chips are inside which vials and include the date. On a map of printed chips, cross out the chips that have been removed from the tray. Transfer one Day Vial from the 4°C cold room to room temperature for at least 30 minutes prior to analysis. (One vial can only be transferred out from a cold room at a time.)

7) Place the vial on a benchtop and record the ambient temperature in the laboratory notebook.

   a) To prevent condensation on the chip, care should be taken to prevent exposure of chips to the room temperature environment before the chips have fully equilibrated to room temperature in the desiccant-containing "Day Vial."

8) To take the chip out from the “Day vial”:
    a) remove the parafilm
    b) To remove the chip from the vial: uncap the vial and carefully take the chip out of the vial by using a pair of plastic or metal tweezers.
        i) Alternately, the vial can be gently inverted with the lid on to let the chip fall onto the cap, followed by uncapping of the inverted vial.
        ii) During this step, avoid scratching the chip surface to prevent damages. If the chip becomes damaged, place it back in the vial with the desiccant, label the vial “do not use, scratch”, and store at 4^{o}C for assessment by the study team. Note the damage in the laboratory notebook.
    c) Use a pair of plastic or metal tweezers to grab the chip and place it on a clean surface (e.g. Kimwipe, paper towel, etc.).
    d) Close the vial immediately afterward.
9) Return sealed “Day vials” to the cold room following use.

B.3 Preparation of Instrument and Assay

B.3.1 Chip loading, registration

1) Blow dry the chip with filtered compressed house air to eliminate dust or large particles that may adhere to the chip’s surface.
2) Align the chip inside an etched rectangular well in the middle of the chip holder. Make sure that the grating couplers located on the top part of the chip are aligned with the top edge of the well.
3) Rinse the plastic gasket (gasket type 8, IMEC-3) with Milli-Q water and blow dry with a stream of filtered compressed house air.

4) Carefully place the gasket on the top of the chip by aligning the top and bottom holes of the gasket to the top and bottom guides on the chip holder.
5) Press the gasket against the holder to ensure a firm contact between the chip surface and the gasket.
6) Place the Teflon lid to the chip holder and screw the lid tight (10-11 inch ounces) to form a microfluidic assembly.
7) Screw the two inlet ports and two outlet ports to the Teflon lid on its right and left sides, respectively.
8) Place the chip holder on the stage inside the Maverick instrument and secure it in place.
9) Upload the recipe file to M24 software and register the chip. The laser head will be lowered close to the chip assembly during this step. Upon registration, the software will ask users to provide the name of the assay. Name the assay by following this convention <date of testing, chip position inside the tray, tray number, tray batch>, for example, 11292016_T39_Tr1_09222016. Record any unregistered sensor rings. If a target cluster has more than one unregistered sensor ring, the process is stopped.

B.3.2 Sample Preparation for Analysis

Both direct typing and indirect typing are operated on the same recipe that controls the flow rate and the duration of each step. Indirect typing is performed on the top row of the chip while direct typing is performed on the bottom row. Reagents for both assays are prepared in a 96-well plate with one blank row between those designated for indirect and direct typing assays, for instance, if row A is used for indirect typing, row C will be used for direct typing.

1) Sample and reagent preparation:

Notes: Record the time of receipt of blood samples.

All blood samples are stored at 4°C until processing.

a) Compare the DIN of each donor to the sample number labelled on the tube and reconcile this information with the spreadsheet sent to the study team. Label all tubes with the study sample ID number prior to starting.

b) Centrifuge whole blood at 2000xG for 10 minutes at 4°C.

c) Harvest plasma (the top cell-free liquid layer) using a pipette, taking care not to disturb the pellet and placing in a tube with matching ID. Store at 4°C or on wet ice for use in the Indirect assay.

d) Add approximately one plasma volume of CPDA-1 to the cell pellet and mix well by gently pipetting up and down.

e) Centrifuge the resuspended cell pellet at 2000xG for 10 minutes at 4°C.

f) Discard the supernatant and store the cell pellet on wet ice until use in the direct assay.

2) Indirect analysis sample preparation (for chip top row)

Note: all tubes of reagents are kept cold on wet ice during work

Table B-1. Pump recipe of reverse typing.

Well	Reagent	Flow rate (µL/min)	Duration (min)
1	PBS	40	2
1	PBS	20	5
2	Plasma	20	5
3	PBS	20	10
4	Anti-human IgG/M/A	20	5
5	PBS	20	10
6	Immucor A or B	20	5
7	PBS	20	10
8	Immucor B or A	20	5
9	PBS	20	10
10	RBS-35 detergent	40	5
11	Milli-Q	40	10
12	Milli-Q	40	10

a) Transfer 120 µL of undiluted plasma to well 2 of the top row dedicated for indirect typing on a 96-well plate.

b) Prepare a 40 µg/mL anti-human IgG/M/A solution: add 2 µL of anti-human IgG/M/A stock solution (2,400 µg/mL) into 118 µL PBS in well 4.

c) Prepare 1:10 dilution of Anti-A and anti-B Immucor reagents: add 12 µL of Immucor reagent into 108 µL PBS in well 6 and 8. The order of these two reagents will be pre-determined for the study for each run, and must be recorded digitally for the chip/run for downstream analysis.

d) Aliquot 300 µL of 2% (v/v) RBS-35 detergent (Thermo Fisher Scientific) in Milli-Q water to well 10. Aliquot 450 µL of Milli-Q water to well 11 and 12.

e) Aliquot 350 µL of PBS to the rest of wells.

3) Direct typing sample preparation (for chip bottom row):

Table B-2. Pump recipe of forward typing.

Well	Reagent	Flow rate (µL/min)	Duration (min)
1	PBS	40	2
1	PBS	20	5
2	Anti-D cocktail	20	5
3	PBS	20	10
4	RBC	20	5
5	PBS	20	10
6	PBS	20	5
7	PBS	20	10
8	PBS	20	5
9	PBS	20	10
10	RBS-35 detergent	40	5
11	Milli-Q	40	10
12	Milli-Q	40	10

a) Prepare a 1:10 dilution of the cell pellet (packed erythrocytes) in PBS: add 12 µL cell pellet into 108 µL PBS in well 4 of the bottom row dedicated for direct typing on a 96-well plate.

b) Prepare the anti-D antibody reagent: dilute RUM-1 and TH-28 antibody (Millipore) solutions 1:200 in PBS by adding 0.6 µL of each antisera into 118.8 µL PBS in well 2.

c) Aliquot 300 µL of 2% (v/v) RBS-35 detergent (Thermo Fisher Scientific) in Milli-Q water to well 10.

d) Aliquot 450 µL of Milli-Q water to well 11 and 12.

e) Aliquot 350 µL of PBS to the rest of wells.

4) Place the 96-well plate that is filled with reagents on the reagent stage inside the Maverick instrument by aligning the top side of the plate (i.e. side that starts with the letter A) towards the inner side the stage. Upon starting the assay, the robotic controller will raise the stage to the two inlet tubes that are connected to the fluidic assembly. The protocol starts with a two-minute purge of PBS through the system to eliminate air bubbles in the flow channels. Data acquisition will take place after this step and the sensorgram will show two real-time graphs of the top row and the bottom row, accordingly.

5) The assay needs to be aborted if the sensorgram reflects unsteady baseline of PBS, indicating small bubbles inside the flow path that affects signals. In this scenario, the chip assembly needs to be taken out from the stage. The system is required to be manually purged with PBS to remove air bubbles that are trapped inside the flow path on both channels by using a syringe connected to tubing.

6) Once certain that the system is free of bubbles, carefully set the chip assembly back to the stage and secure it. Register the chip again under the same name. Start the assay and observe the initial baseline of PBS.

7) Tubes need to be flushed with PBS after the last assay of the day is finished to prevent sedimentation of cellular materials and clogging.

8) Once the assay is finished, M24 software will create a folder with the same name of chip containing raw data from each individual sensor device on the chip. Unload the chip assembly by unscrewing all inlet and outlet ports. Detach the Teflon lid and the gasket and discard the used chip. Repeat step 10 and 11 for other chips.

9) Upload the data to a cloud storage (Google Drive, Dropbox, etc.) and at least two external hard drives for backup. Data are processed in MATLAB (MathWorks) using an analysis script developed in-house.
10) Tubes need to be flushed with PBS after the last assay of the day is finished to prevent sedimentation of cellular materials and occlusion.